LTKK-TJ--64

LAPPEENRANNAN TEKNILLINEN KORKEAKOULU
LAPPEENRANTA UNIVERSITY OF TECHNOLOGY

TIETEELLISIÄ JULKAISUJA
RESEARCH PAPERS
64

VESA MEURONEN

ASH PARTICLE EROSION ON STEAM BOILER CONVECTIVE SECTION

Lappeenranta
1997

DISCLAIMER

Portions of this document may be illegible electronic image products. Images are produced from the best available original document.

LAPPEENRANNAN TEKNILLINEN KORKEAKOULU
LAPPEENRANTA UNIVERSITY OF TECHNOLOGY

UDK 621.184:
620.19:
662.613

TIETEELLISIÄ JULKAISUJA
RESEARCH PAPERS
64

VESA MEURONEN

ASH PARTICLE EROSION ON STEAM BOILER CONVECTIVE SECTION

Thesis for the degree of Doctor of Technology to be presented with due permission for public examination and criticism in Auditorium 1381 at Lappeenranta University of Technology, Lappeenranta, Finland on the 19th of December, 1997, at noon

Lappeenranta
1997

ISBN 951-764-181-8
ISSN 0356-8210

ERRATUM

p. 37	lines 5 and 6 in text: Table 2.2 must be Table 3.2
p. 38	third chapter, line 8: lignite must be lignine
p. 41	chapter 3, line 4: Radiative must be Radiant
p. 56	Figure 4.8: the nominal velocity 10 m/s must be replaced by nominal velocity 13 m/s
p. 65	Table 5.1 does not include the results of analyses with particle concentration of 375 g/m^3 and flow velocity of 13 m/s
p. 71	second chapter, line 3 in text: 11 must be 10
p. 72	line 2 in text: 312 must be 303
p. 72	second chapter, line 9: Figure 5.5 must be Figure 5.6
p. 73	line 15: Figure 5.6 must be Figure 5.7
p. 77	line 1 and 4: Figure 5.7 must be Figure 5.8
p. 79	line 4: 300° must be 330°
p. 79	second chapter, line 7 in text: Figure 5.8 must be Figure 5.9
p. 82	line 2 in text: rows 6 and 12 must be tubes 6 and 12
p. 83	lines 6 and 10 in text: Figure 5.9 must be Figure 5.10
p. 96	in chapter, Parameters used to explain erosion wear: Velocities w must be Velocities *w*
p. 100	line 2: Table 5.4 must be Table 5.6

Vesa Meuronen

ABSTRACT

Lappeenranta University of Technology
Research Papers 64

Vesa Meuronen
Ash particle erosion on steam boiler convective section
Lappeenranta, 1997.

149 pages, 53 figures, 44 tables
ISBN 951-764-181-8, ISSN 0356-8210 UDK 621.184 : 620.19 : 662.613
Keywords: erosion, wear, steam boiler

In this study, equations for the calculation of erosion wear caused by ash particles on convective heat exchanger tubes of steam boilers are presented. A new, three-dimensional test arrangement was used in the testing of the erosion wear of convective heat exchanger tubes of steam boilers. When using the sleeve-method, three different tube materials and three tube constructions could be tested. New results were obtained from the analyses.

The main mechanisms of erosion wear phenomena and erosion wear as a function of collision conditions and material properties have been studied. Properties of fossil fuels have also been presented. When burning solid fuels, such as pulverized coal and peat in steam boilers, most of the ash is entrained by the flue gas in the furnace. In bubbling and circulating fluidized bed boilers, particle concentration in the flue gas is high because of bed material entrained in the flue gas. Hard particles, such as sharp edged quartz crystals, cause erosion wear when colliding on convective heat exchanger tubes and on the rear wall of the steam boiler. The most important ways to reduce erosion wear in steam boilers is to keep the velocity of the flue gas moderate and prevent channelling of the ash flow in a certain part of the cross section of the flue gas channel, especially near the back wall. One can do this by constructing the boiler with the following components. Screen plates can be used to make the velocity and ash flow distributions more even at the cross-section of the channel. Shield plates and plate type constructions in superheaters can also be used.

Erosion testing was conducted with three types of tube constructions: a one tube row, an in-line tube bank with six tube rows, and a staggered tube bank with six tube rows. Three flow velocities and two particle concentrations were used in the tests, which were carried out at room temperature. Three particle materials were used: quartz, coal ash and peat ash particles. Mass loss, diameter loss and wall thickness loss measurements of the test sleeves were taken. Erosion wear as a function of flow conditions, tube material and tube construction was analysed by single-variable linear regression analysis. In developing the erosion wear calculation equations, multi-variable linear regression analysis was used. In the staggered tube bank, erosion wear had a maximum value in a tube row 2 and a local maximum in row 5. In rows 3, 4 and 6, the erosion rate was low. On the other hand, in the in-line tube bank the minimum erosion rate occurred in tube row 2 and in further rows the erosion had an increasing value, so that in a six row tube bank, the maximum value occurred in row 6.

ACKNOWLEDGEMENTS

I have continued in this work the erosion wear study that was started in my Licentiate Thesis. In this work, a large series of tests were carried out with the purpose of developing erosion calculation equations appropriate for the calculation of erosion wear on the convective heat exchangers of steam boilers when burning solid fuels.

This study was started in Autumn 1994 and without the help and work of very many colleagues this work could not have been done. First of all I am grateful to Lappeenranta University of Technology for supporting this work in the form of a grant and to Professor Reino T. Huovilainen for the idea to study erosion wear and the permission to use the laboratory facilities. I wish to express my thanks to Professor Pertti Sarkomaa for his support and encouragement throughout this work.

Hans Ahlström Laboratory has supported this work by guidance and material supplies. I want to express my thanks to Research Manager Matti Hiltunen, Process Engineer Vesa Jokelainen and Research Engineer Pasi Makkonen.

Perhaps the most important part of this work has been done in the Laboratory for Emission Measurement and Control, LUT, in which many people have been working during the test series. I wish to express special thanks to Laboratory Technician Markku Autio and Project Engineer Kari Ihaksi, Laboratory Engineer Juha-Pekka Lemponen and all the people who have worked with this project. I would also like to thank Graeme Stewart for the proof-reading of this thesis.

Finally, I wish to express my very special thanks to my wife Annika and our daughter Neea for all their support and encouragement during this study and for giving me a pleasant motive to finish the work.

Lappeenranta, November 26th, 1997

Vesa Meuronen

CONTENTS

LIST OF TABLES

LIST OF FIGURES

NOMENCLATURE

A	flow area in the narrowest cross-sectional area of the first row in tube bank, m^2
a	particle material parameter, g/m^2
a_0	particle material parameter without particle concentration, m
a_1	particle material parameter exponent
B	tube material parameter without location parameter, 1/J
B_k	coefficient for non-uniformity of particle concentration distribution, -
B_w	coefficient for non-uniformity of gas velocity distribution, -
b	tube material parameter, 1/(J mm)
b_1	tube material parameter exponent
C	test sleeve location coefficient in x-direction, -
C_d	drag coefficient of a particle, -
c	test sleeve location in x-direction, mm
c_1	exponent of location parameter in x-direction
D	test sleeve location coefficient in y-direction, -
d	test sleeve location in y-direction, mm
d_1	exponent of location parameter in y-direction
d_p	average particle diameter of certain particle size fraction, m
d_u	tube outside diameter, mm
d_p^*	dimensionless particle diameter, -
$E_{\Delta m^*}$	total error in erosion wear calculation, -
E_{x_i}	error of variable x_i
f	relative error, -
g	gravity, 9.81 m/s^2
G_0	proportionality factor, -
G	proportionality factor, -
H	test sleeve location coefficient in z-direction, -
h	test sleeve location in z-direction, mm
h_1	exponent of location parameter in z-direction
K	parameter describing collision probability of particles to tubes, -
k	particle concentration in gas flow, g/m^3
Δm^*	dimensionless mass loss, -

$\frac{\partial(\Delta m^*)}{\partial x_i}$	partial derivate of dimensionless mass loss function
n	number of parameters, -
q_A	erosion mass loss per tube outside area, g/mm^2
q_m	mass flow, kg/s
Re_p	particle Reynolds number, -
R_i	particle reject fraction with sieve opening i, -
R_{i+1}	particle reject fraction with sieve opening i+1, -
s_1	distance of the centre points of two adjacent tubes transverse to the air flow
s_2	distance of the centre points of tubes in two adjacent tube rows in the direction of air flow
Δs	tube wall thickness loss, mm
t	time, h
t_1	time exponent
w	gas velocity in the smallest cross-sectional area of the first row in tube bank, m/s
w_1	flow velocity exponent
w_f	fluidization velocity, m/s
w_{mf}	minimum fluidization velocity, m/s
w_t	terminal velocity of a particle, m/s
w_f^*	dimensionless fluidization velocity, -

Greek letters

α	erosivity coefficient of ash by Kuznetsov, mm s^3/(g h)
β	tube material erosion resistivity coefficient by Kuznetsov, -
Δ	difference (of a value)
η	ash particle collision probability coefficient, -
μ	dynamic viscosity of gas, kg/ms
ρ	density, kg/m^3

Superscripts

*	dimensionless value

Subscripts

A	area
d	particle diameter
f	fluidization
g	gas
i	index
i + 1	index
k	particle concentration
M	tube material
m	mass
Δm	mass loss
m	minimum
p	particle
s	solid
t	terminal
u	tube outside
w	velocity
0	index
1	index
2	index

Others

CA	coal ash
PA	peat ash
Q	quartz

1 INTRODUCTION

1.1 BACKGROUND OF THE STUDY

The burning of fossil fuels plays an important part in electricity and heat production in the world. The fossil fuel resources available are remarkable. The world energy resources in 1993 are evaluated to be sufficient for 44 years for oil and natural gas condensate, 65 years for natural gas, 202 years for coal and anthracite, 339 years for brown coal and 1765 years for peat, by the World Energy Council (1995).

The main sources of energy in Finland in 1994 were oil 26.3 %, industrial refuse 23.3 %, solid import fuels (coal) 13.5 %, fission energy 11.6 %, water power 7.37 %, natural gas 6.82 %, peat 5.28 %, import of electricity 3.79 % and wood 2.15 % of the total energy supply as estimated by Statistics Finland. Solid fuels such as coal, peat, some industrial refuse and wood had a total share of about one-third of the total energy consumption in Finland in 1994.

New techniques like direct solar energy, wind energy, tidal energy and fuel cell energy are developing. The share of the energy production that they will generate will be marginal in the next few decades. It appears that fusion energy production will not become available in the near future. The majority of the energy consumption in the world in the near future has to be satisfied by burning fossil fuels, using fission energy and water power. This, despite their environmental disadvantages such as the Greenhouse Effect, the disposal of nuclear waste, nuclear accidents and large dam constructions with water power.

Solid fossil fuels consist of inherent moisture, mineral matter and burning matter. In large energy production plants, solid fossil fuels are typically burned in a pulverized state. The fuel is ground to a small particle size before burning and is brought to the furnace by the primary air or the flue gas. In a furnace, most of the ash from the mineral matter of the fuel is entrained by the flue gas. This results in a high particle load in the flue gas. In a fluidized bed, burning takes place in an inert material, sand and ash, fluidized by primary air. In both the pulverized fuel burning boilers and fluidized bed boilers, there exist gas flows with high particle loads. In large boilers, high flue gas velocities have to be used to keep the cross-sectional area of the flue gas channels and size of tube banks reasonable and to achieve a high heat transfer rate from the flue gas to the water or steam.

Particulate materials in the flue gas flow cause erosion wear when colliding against heat exchanger tubes or the walls of the channels. In addition to erosion wear, fouling and corrosion can cause problems on heat exchanger tubes. These phenomena are caused mainly by the mineral matter of the fuel. Erosion wear and corrosion can occur simultaneusly and the total damage in the target material is a combination of both phenomena. Fouling and corrosion also occur simultaneusly. Erosion wear and fouling have not been observed in the same place on heat exhanger area (Singer, 1981).

In this study, the focus was on the erosion wear of convective heat exchanger tubes of steam boilers. The term erosion wear, or just erosion, has been used in this study to describe the deterioration of a material caused by colliding ash particles entrained by flue gas. This study was started in the Licentiate Thesis: Flue Gas Side Erosion In a Steam Boiler (in finnish), which was based on literature (Meuronen, 1990). The main part of this study was extensive erosion wear tests which were carried out in the laboratory, and all the conclusions are based on these experiments.

A new, three-dimensional test arrangement was used in the testing of erosion wear on convective heat exchanger tubes. Also, the analysis of the results was conducted three-dimensionally. Using the sleeve-method, it was possible to test three different tube materials in the same flow conditions. New results could be obtained concerning the erosion rate as a function of tube arrangement or tube row number in the in-line or staggered tube bank. New results were also achieved concerning the erosion rate as a function of particle material properties, tube material properties and flow conditions.

1.2 EROSION STUDY DRAWBACKS

To study erosion wear in steam boilers, long test durations are needed to get results with high accuracy. Erosion testing have been done with widely varied test device arrangements. However, erosion wear is highly dependent on particle and target material properties, flow conditions and collision conditions. Erosion wear phenomena in steam boilers depend on many parameters characteristic to the construction of the heat exchangers and particle flow conditions.

There have not been many recent tests describing erosion wear conditions in boilers burning solid fuels. Erosion testing done in earlier decades, for example by Kuznetsov, is not suitable to describe erosion wear in modern pulverized burning boilers or fluidized bed boilers with the fuels, materials,

constructions and flow parameters used. However, the basic correlations of Kuznetsov are valid.

A great amount of measurements is needed to get a valid erosion. Mainly because of large differences in the values of measurements caused by different flow conditions in different parts of the flow channel. Hence, a statistical calculation is needed to handle the mass of measurements and obtain the right correlations. Statistical computer progams offer such tools to handle the great mass of measurements.

1.3 PURPOSE OF EROSION WEAR STUDY

The purpose of this study was to obtain new knowledge about erosion wear in the convective heat exchangers of pulverized burning boilers and fluidized bed boilers when burning solid fuel. The purpose was also to formulate erosion wear by developing erosion wear calculation equations for constructions and flow conditions used normally in the convective heat exchangers of steam boilers. The basic dependencies of erosion wear, such as erosivity of different particle materials, erosiveness of different tube materials and differencies between tube constructions, were studied.

1.4 LIMITATIONS OF THE STUDY

Due to the long duration of the tests, range of test parameters was limited. Testing was done with three tube constructions, three tube materials, two particle concentrations and three flow velocities with particle material quartz sand. Two other particle materials, coal ash and peat ash was tested with one construction, one particle concentration and one flow velocity. The test periods were varied, some test series were composed of several periods and some test series were done as one period with the same total time. The duration of the tests and the amount of tests and test parameters was sufficient for drawing conclusions about erosion wear.

The main measurements used later for analysis were the mass loss measurements of the test sleeves. In addition, losses in diameters and wall thicknesses of the test sleeves at different collision angles were measured. All the tests were conducted at room temperature. Hence, the effect of temperature could not be studied.

2 EROSION AS A PHENOMENA

2.1 DEFINITIONS

The mechanical damage of the target material is influenced by the wear mechanism, conditions in the surroundings and material properties. The main wear mechanisms are ploughing abrasion, polishing abrasion and erosion abrasion. Usually along with these mechanisms, corrosion affects the wear rate of the target material (Siitonen, Mäntylä, Kettunen, 1980).

In ploughing abrasion, wear is caused by objects ploughing into the target surface with a great force and either low or very high velocity. Large particles are removed from the target surface. Polishing abrasion occurs when two moving surfaces have erosive particles between them resulting in local fractures in the surfaces (Siitonen, Mäntylä, Kettunen, 1980).

Erosion abrasion is defined as material removal caused by high velocity particles in liquid or gas flow colliding with a target surface and damaging it. Ash particles entrained by flue gas flow cause erosion abrasion in steam boilers when burning solid fossil fuels. Liquid drops, and in liquid collapsing gas bubbles, also cause erosion abrasion. (Siitonen, Mäntylä, Kettunen, 1980). The erosion abrasion phenomena is called erosion wear or just erosion in this study.

2.2 MAIN MECHANISMS OF EROSION WEAR

Several mechanisms occur in erosion wear depending on process conditions, particle flow density, mass flow and velocity, angle of collision and material properties like toughness and hardness of both the colliding particles and the target material affect the mechanism. Erosion wear consists of several micromechanical phenomena like cutting, elastic and plastic deformation, work-hardening caused by the striking of particles, fracturing, crushing, fatiguing, microscopic cracking and removing of chips. On the target surface smelting can occur. Many of these phenomena occur both in the particles and on the target surface. The components of erosion wear can be combined as three main mechanisms: particles cutting into the target surface, plastic deformation by the forming and removal of platelets, and the removal of material layers by crushing (Levy, 1982; National Materials Advisory Board, 1977).

The damaging of the target surface is a result of a high number of particle collisions. One particle can damage the target surface if it has a kinetic energy high enough to cause plastic deformation on the surface. Generally, a large amount of successive collisions is required to cause damage to the target surface. Under test conditions, erosion wear has an incubation period when no material is removed, an acceleration period with a high material removal rate in relation to the amount of collisions, and a steady state period when the ratio of the mass removed to the mass of particles is constant over a certain time period (Levy, 1982; National Materials Advisory Board, 1977). In Figure 2.1, erosion wear behaviour as a function of time of exposure is presented.

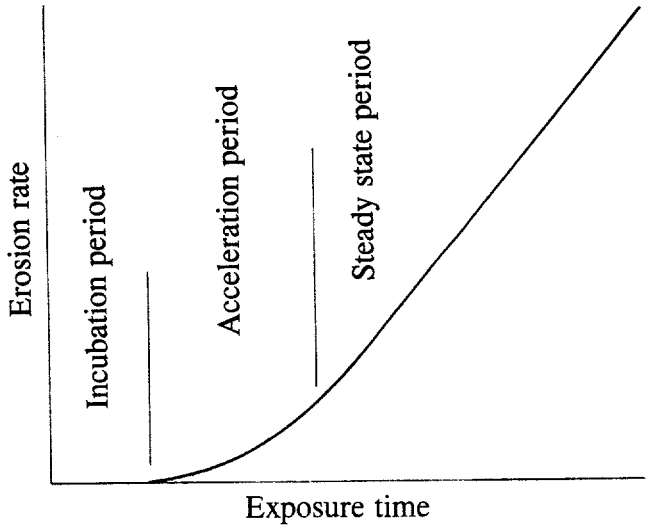

Figure 2.1 Erosion mass loss as a function of time of exposure (National Materials Advisory Board, 1977)

In the cutting mechanism, a single particle behaves like a small tool cutting into the target surface by its kinetic energy. The mechanism can also be described by the terms sinking, ploughing and chipping. The volume of the material loosened is proportional to the length and depth of the furrow (Finnie, 1958; Levy, 1982).

As a result of a single collision, the target material is observed to form a pile around the collision crater. This mechanism is in contradiction with the cutting mechanism, but it explains the different erosion periods in Figure 2.1. In the incubation period, particles collide with the target material resulting in the formation of craters and piles around them, although no material is removed.

When more collisions occur, the piles around the craters form into platelets, which start to be removed. This corresponds to the acceleration period. The material layer below the platelets is work-hardened as a result of the collisions in the initial period. Below the hardened layer is material which has remained unaffected. When the target surface is covered everywhere by craters and platelets and the hardened layer has reached a steady state thickness and hardness, the steady state erosion period begins. It is here that the erosion rate is the highest because of the anvil effect of the hardened material layer. The hardened material layer increases the effects of the collisions on the heated surface which is very susceptible to deformation. The cross section of these layers moves downward when material from the surface is removed (Levy, 1982). The material layers in the cross section of target material is shown in Figure 2.2.

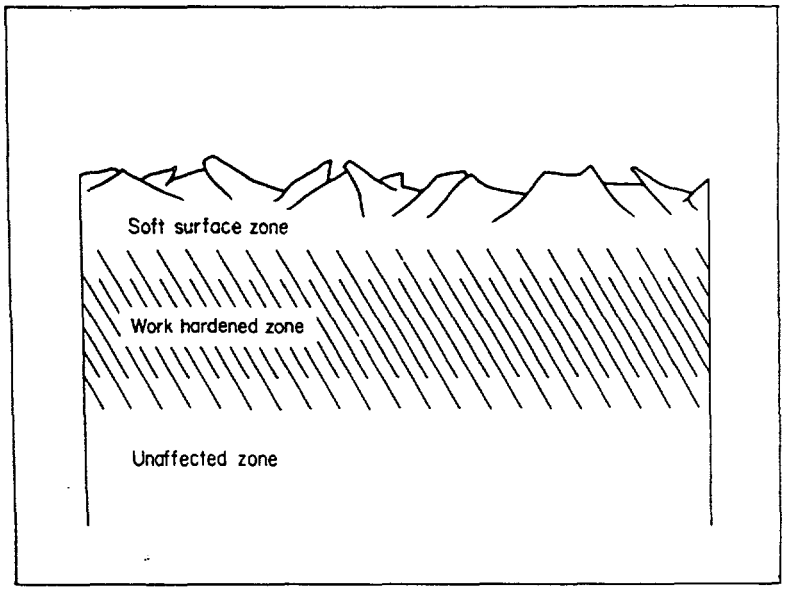

Figure 2.2 Cross-section of target material during erosion (Levy, 1982)

In addition to the mechanisms presented earlier, material layer removal has been observed. Particle collisions result in stress accumulation, cavities and cracking in the material beneath the surface. This leads to crushing of the surface. This mechanism can be compared to fatigue of the material and is the main erosion mechanism in materials consisting of several phases, for example, a phase of hard particles surrounded by a softer phase. The mechanism of layer removal works with the platelet removal mechanism, the

platelets removed are large and thick (Levy, 1982; National Materials Advisory Board, 1977). The critical shear stress areas under the colliding particle, where cavities and crack formation is possible, is presented in Figure 2.3.

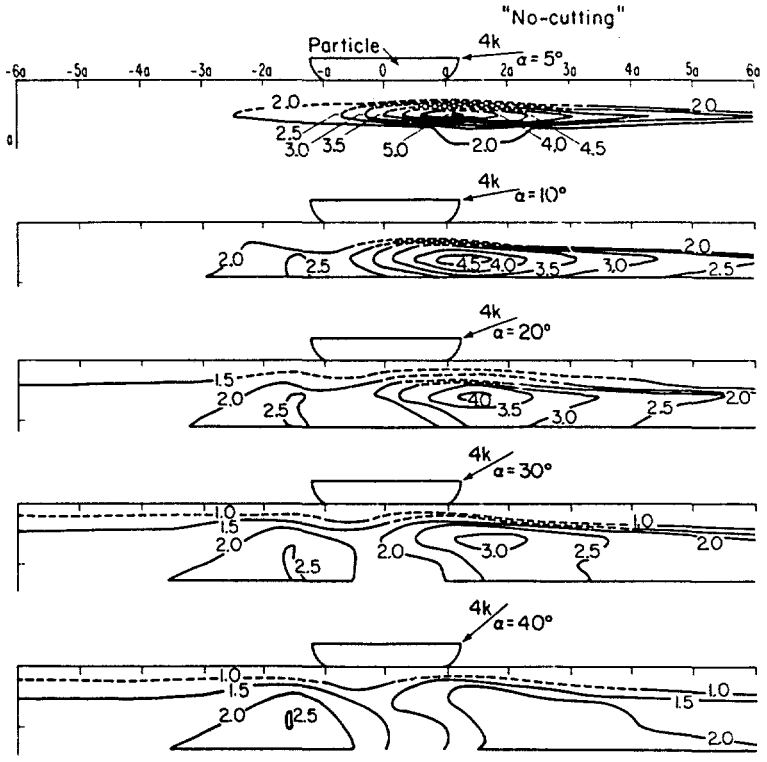

Figure 2.3 Plots of critical shear stress areas under a colliding particle (Levy, 1982)

2.3 EROSION WEAR AS A FUNCTION OF COLLISION CONDITIONS AND MATERIAL PROPERTIES

An increase in the velocity of colliding particles results in an increase of erosion wear rate because of the higher kinetic energy of the particles (Kuznetsov, 1958; Levy, 1982; Raask, 1979). The exponent of the velocity varies between 3.15 and 4.5 (Jianren, Dadong, Kefa, 1989). Figure 2.4 shows the correlation between erosion rate as mg mass loss/g erodent and particle velocity when the target material is Stellite 6B and the particle material is aluminium oxide at a temperature of 760 °C.

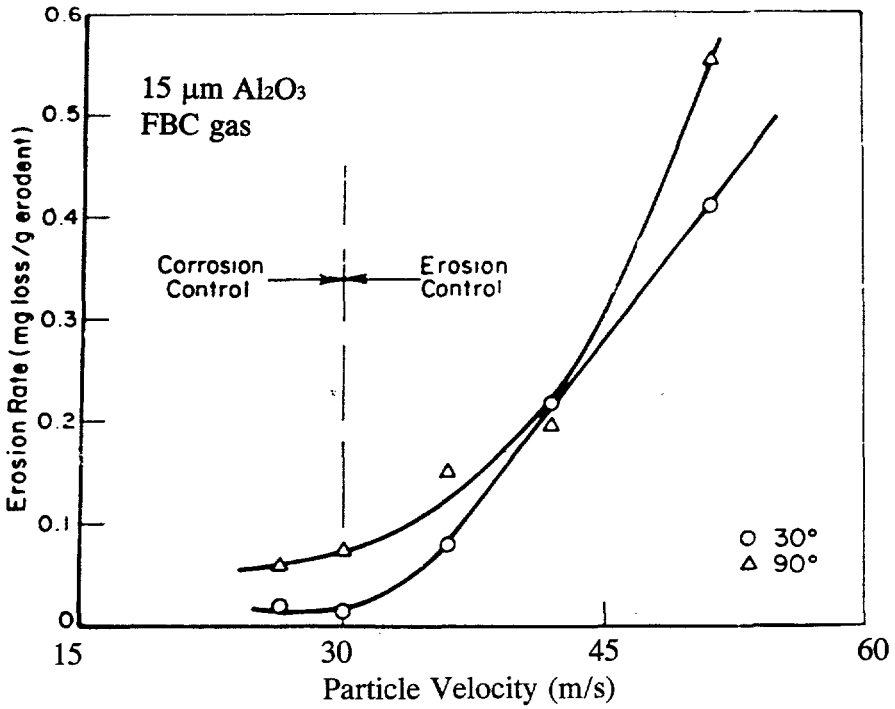

Figure 2.4 Erosion rate (mg loss/g erodent) of Stellite 6B at elevated temperatures as a function of particle velocity at two impingement angles (Levy, 1982)

When the temperature rises, the erosion wear rate can increase or decrease. When temperature increases the toughness of the metal increases, thus resulting in more deformation and less energy concentration and material removal. At high temperatures, the anvil layer of the target material does not become as strong as at lower temperatures, especially with high collision angles between the line of incoming particles and the target surface. On the other hand, less energy is needed to rise the temperature of the metal to the melting point. Above a certain temperature the total strength gets lower and the erosion rate begins to increase. Erosion wear rate of metal alloys decreases generally with high collision angles when the temperature rises. At low collision angles the erosion wear rate of metal alloys increases when temperature rises (Levy, 1982). The erosion rate of stainless steel AISI 310 as a function of temperature at two collision angles is presented in Figure 2.5.

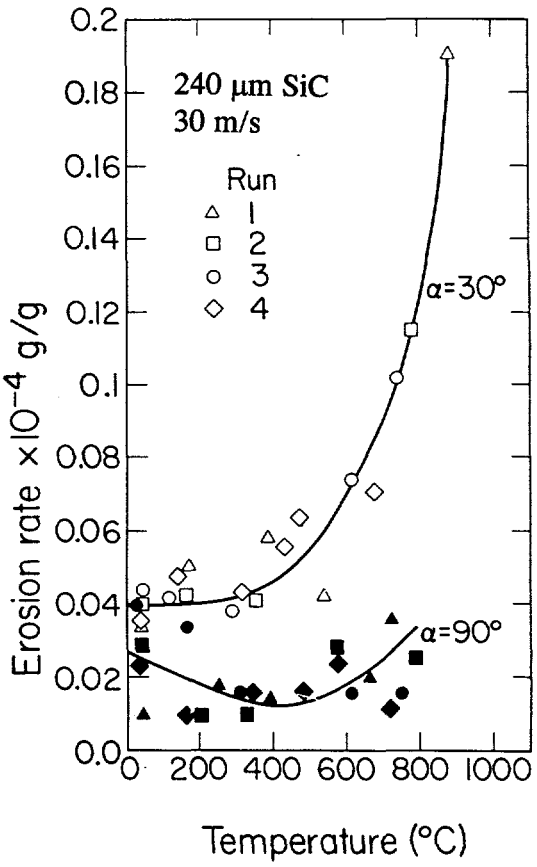

Figure 2.5 Erosion rate (g loss/g erodent) of stainless steel AISI 310 as a function of temperature at two collision angles (Levy, 1982)

The erosion mechanism can be divided into tough erosion and brittle erosion. Tough erosion is characteristic of ductile materials like metals, and brittle erosion is characteristic of hard materials like ceramics. When the collision angle between the line of incoming particles and the target surface is between 0° and 60° the erosion mechanism is mainly cutting and removal of platelets. This mechanism is called tough erosion. When the impingement angle is about 90° the erosion mechanism is crushing of the material which is called brittle erosion. Collision conditions, for example temperature, can change the mechanism between tough and brittle. The erosion mechanism of ceramics can be changed from brittle to tough by rising temperature (National Materials Advisory Board, 1977; Wright, Herchenroeder, 1980). The maximum erosion rate of tough materials like metals occurs at a collision angle of about 20° and for brittle materials such as ceramics at an angle of 90° (Levy, 1982). The

erosion behaviour of aluminium, a ductile material, and aluminium oxide, a brittle material, as a function of collision angle is displayed in Figure 2.6.

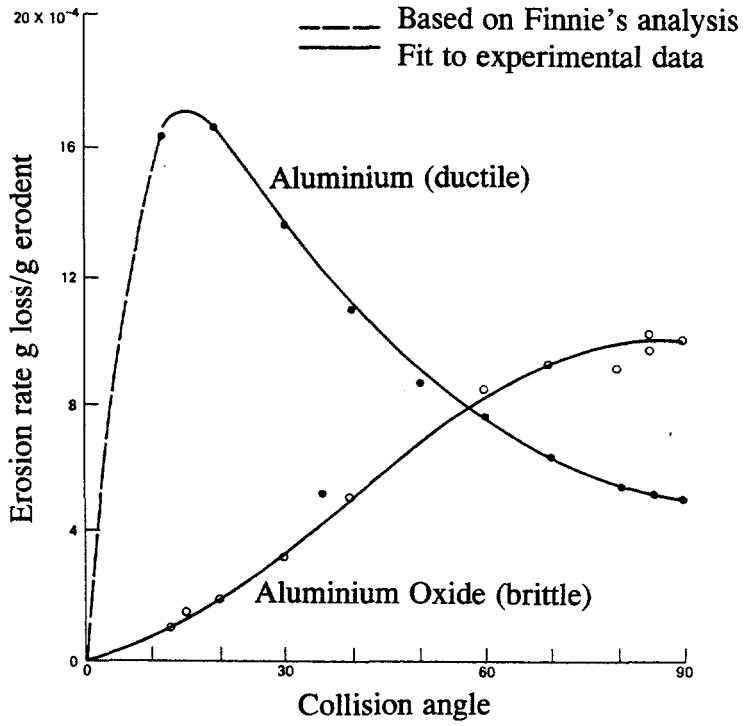

Figure 2.6 Erosion rate (g loss/g erodent) of aluminium and aluminium oxide as a function of collision angle (Sheldon, Finnie, 1966)

The increase of particle concentration in the flow increases erosion rate. The correlation is expected to be linear and erosion rate as a weight loss per unit weight of abrasive particles would remain constant as the concentration of abrasive particles is increased (Wiederhorn, 1975). In Figure 2.7, erosion rate as mg mass loss/g erodent is presented as a function of particle concentration. In this case, the erosion rate is observed to decrease, albeit slowly, when particle concentration is increased. This can be explained by the fact that the increase of erosion rate is controlled by particles rebounding from the surface and the velocity of incoming particles is decreased by the rebounding particles and by particle agglomeration before collision (National Materials Advisory Board, 1977; Wiederhorn, 1975). According to Shida and Fujikawa (1985), the erosion rate as a mass loss per particle concentration should be linear.

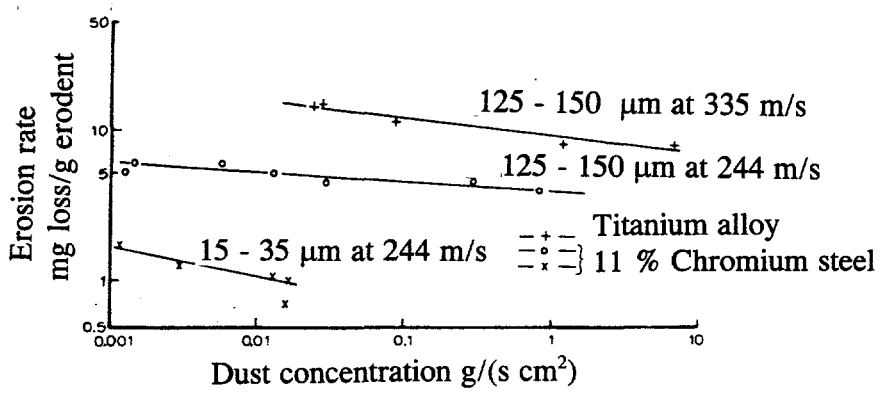

Figure 2.7 Effect of particle concentration on the erosion rate of materials (Finnie, Wolak, Habil, 1967)

The kinetic energy of particles increases when the size of the particles increases. The erosion rate of tough materials, like metal alloys, firstly increases when the particle size increases. When particle size increases above 100 μm, the erosion rate begins to decrease and remains constant. The erosion rate of brittle materials, such as ceramics, increases linearly when particle size increases (Wiederhorn, 1975). In Figure 2.8, the effect of particle size on erosion rate is presented.

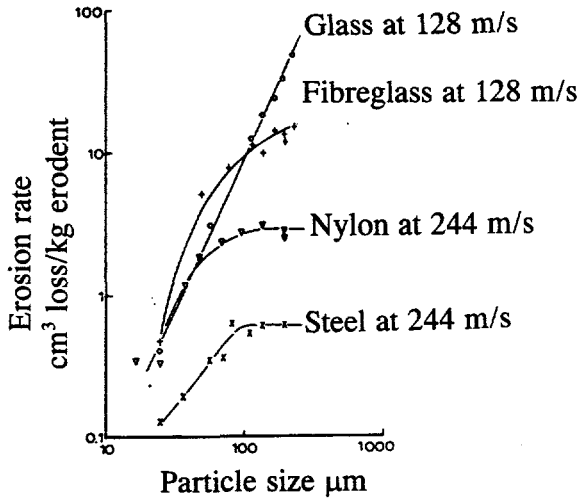

Figure 2.8 Effect of particle size on the erosion rate of materials (Finnie, Wolak, Habil, 1967)

The shape, hardness and possible rotation of particles have an effect on the erosion wear rate. Sharp edged particles cause higher erosion rate than smooth and spherical particles (Raask 1979). Hard particles also cause higher erosion rates. This is because soft particles are often broken up in the collision. The breaking of hard particles results in sharp edged erosive splinters (Levy, 1982; Gat, Tabakoff, 1980; Agarwal, Howes, 1986).

Many properties of the target material influence the erosion wear. The erosion rate of steel alloys increases when hardness increases. Higher toughness causes a lower erosion rate, and higher hardness a higher erosion rate. There is a limit in the increase of toughness where the total strength of the material begins to decrease leading to a higher erosion rate, although the toughness still increases (Levy, 1982; Rao, Buckley, 1984; Agarwal, Howes, 1986). Figure 2.9 shows the erosion rates of stainless steel AISI 304 in the as-wrought and annealed condition. Lower toughness and higher hardness in the as-wrought condition results in a higher erosion rate. However, there is not great differences in erosion durability between the usual boiler steels (Foley, Levy, 1982).

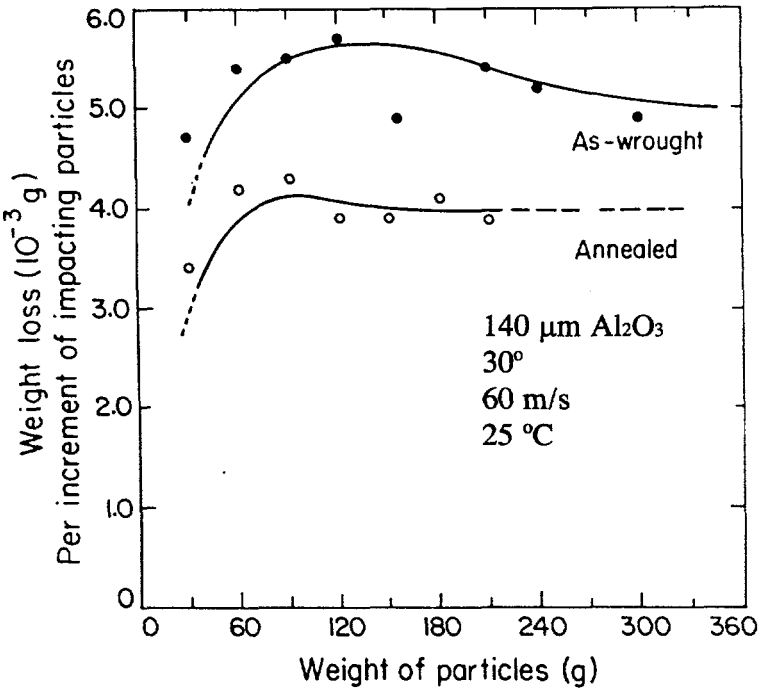

Figure 2.9 Erosion rate of 304 stainless steel in as-wrought and annealed conditions (Foley, Levy, 1982)

2.4 CALCULATION OF EROSION WEAR

2.4.1 GENERAL

Erosion wear has been observed to correlate to several material properties of particles and target material and collision conditions as presented earlier. Erosion formulas are usually based on the kinetic energy of particles and the ability of the target material to absorb the energy of the collision. Erosion wear formulation was widely discussed, and several erosion calculation equations were presented in the Licentiate Thesis of Meuronen, 1990. Hence, only one erosion calculation equation developed especially to calculate the erosion caused by ash particles in staggered tube banks of convective heat exchangers in steam boilers is presented in this study (Kuznetsov, 1958). The disadvantage of Kuznetsov's equation is that the values of the coefficients are approximate and not based on modern tube materials and boiler constructions. Particle erosivity coefficients are presented only for Russian coal ashes.

2.4.2 EROSION CALCULATION EQUATION BY KUZNETSOV

The equation is based on the correlation between erosion rate and kinetic energy of particles. When using particle mass concentration in a gas flow instead of particle mass as a parameter and considering particle and tube material properties, boiler construction types and collision probability of particles by coefficients the equation can be written for a staggered tube bank as

$$q_A = \alpha \cdot \beta \cdot \mathrm{B}_k \cdot k \cdot \eta \cdot (\mathrm{B}_w \cdot w)^3 \cdot t \cdot \rho_{\mathrm{M}} \qquad (2.1)$$

where q_A is the maximum mass loss per tube external area (g/mm^2), α is the erosivity coefficient of ash and includes values of 1.5 and 3 which comes from the maximum erosion rate in row 2 and maximum erosion angle of 30° with respect to the coming flow [mm s^3/(g h)], β is a erosion resistivity coefficient of tube material, 1 for ordinary steel and 0.7 for chrome molybdenium steel, B_k is a coefficient of non-uniformity of particle concentration distribution, k is particle concentration in gas flow (g/m^3), η is a collision probability coefficient of ash particles to the tubes, B_w is a coefficient of non-uniformity of gas velocity distribution, w is gas velocity in the narrowest cross-sectional area of the first row in the tube bank (m/s), t is erosion period (h), and ρ_{M} is density of the tube material (kg/m^3).

The tube wall thickness loss erosion wear rate can be calculated for staggered tube bank from the equation

$$\Delta s = \alpha \cdot \beta \cdot \mathrm{B}_k \cdot k \cdot \eta \cdot (\mathrm{B}_w \cdot w)^3 \cdot t \qquad (2.2)$$

where Δs is the maximum thickness loss of the tube wall (mm).

Ash erosivity coefficients of different Russian coals are presented in Table 2.1. The values of coefficients of non-uniformity of particle concentration and flow velocity distributions are shown in Table 2.2.

Table 2.1 Ash erosivity coefficients (Kuznetsov, 1958)

Coal type	Erosivity coefficient [mm s^3/(g h)]
Donetsk	5.4×10^{-9}
Moscow District	5.4×10^{-9}
Kizelovsk	3.5×10^{-9}
Ekibaztuzsk	9.5×10^{-9}
Tsheljabinsk	4.0×10^{-9}
Bogoslov	2.2×10^{-9}
Volga District	3.0×10^{-9}

Table 2.2 Coefficients of non-uniformity of particle concentration and flow velocity distributions (Kuznetsov, 1958)

Heat Exchanger	Construction	B_k	B_w
Superheater	Pendant	1.2	1.2
Steam Generator	Convective Steam Generator	1.5	2.0
Economizer	Two Pass Construction	1.25	1.2

The probability of an ash particle colliding with the wall of the tube depends on particle size distribution, tube diameter and particle Reynolds number. The probability coefficient is calculated from the formula

$$\eta = \sum \eta_i \cdot (R_i - R_{i+1}) \qquad (2.3)$$

where η_i is the collision probability of particle size fraction between R_i and R_{i+1}, R_i is the reject of the sieve with opening i and R_{i+1} is the reject of the sieve with opening $i+1$.

The collision probability of a certain particle size fraction is shown in Figure 2.10 as a function of parameter K. The parameter K can be calculated from the equation

$$K = \frac{\rho_s \cdot d_p^2 \cdot B_w \cdot w}{\mu_g \cdot d_u} \tag{2.4}$$

where ρ_s is the solid density of particle material, d_p is the average particle diameter of a certain particle size fraction, B_w is a coefficient of non-uniformity of gas velocity distribution, w is the gas velocity in the narrowest cross-sectional area in the tube row, μ_g is the dynamic viscosity of the gas and d_u is tube diameter.

The calculation of the collision probability is presented by N. F. Dergatshev and N. G. Zalogin based on tests in which different sized particles were carried out by a gas flow around a tube with a sticky surface. When studying the particle sizes that gripped to the surface, they observed that the smallest particles did not grip to the surface but were flying around the tube. The collision probability increases when particle size or velocity increases.

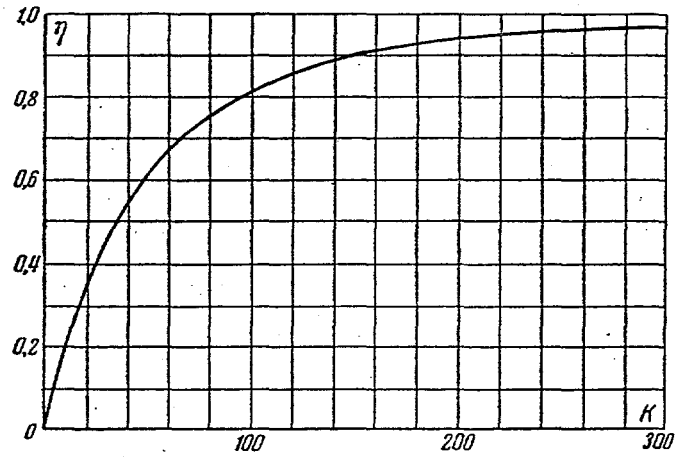

Figure 2.10 Collision probability as a function of parameter K (Kuznetsov, 1958)

3 ASH PARTICLE EROSION WEAR IN STEAM BOILERS

3.1 FOSSIL FUEL PROPERTIES

Solid fossil fuels consist of inherent moisture, mineral matter and burning matter. The inherent moisture comes to the fuel from soil and from air during storage. The mineral matter comes from the minerals of the original plant and from mixing with clay and sand during sedimentation. Minerals can be mixed with the fuel during mining. Solid fuel consists, by proximate analysis of moisture, volatile matter, fixed carbon and ash and by elementary analysis of carbon, hydrogen, nitrogen, oxygen, and sulphur (Singer, 1981). In Table 3.1, typical properties of solid fuels are presented.

Table 3.1 Properties of solid fuels (Moilanen, Nieminen, Alén, 1995)

Property	Wood	Bark	Peat	Coal
Moisture %	30 - 45	40 - 65	40 - 55	10
Mineral matter %	0.4 - 0.5	2 - 3	4 - 7	14
Volatile matter %	84 - 88	70 - 80	65 - 70	29.5
Calorific heat value MJ/kg (calculated as dry basis),	21.0	20	21.6	29.6
Lower heat value MJ/kg (calculated as dry basis)	19.5	19	20.4	28.7
Elementary analysis %, (calculated as dry basis)				
Carbon	48 - 50	51 - 66	50 - 57	76 - 87
Hydrogen	6 - 6.5	5.9 - 8.4	5 - 6.5	3.5 - 5
Nitrogen	0.5 - 2.3	0.3 - 0.8	1 - 2.7	0.8 - 1.2
Oxygen	38 - 42	24.3 - 40.2	30 - 40	2.8 - 11.3
Sulphur	0.05	0.05	<0.2	<0.5
Chlorine	<0.01	<0.01 -0.03	0.03	<0.1
Melting temperatures of mineral matter °C in oxidizing/reducing atmosphere				
Initial deformation temperature	1200/-	1340 - 1405/-	1030 - 1260/ 1000 - 1170	1100 - 1300/ 1000 - 1240
Hemispherical temperature	1250/-	1650/-	1110 - 1355/ 1020 - 1370	1230 - 1415/ 1090 - 1350
Fluid temperature	1275/-	1650/-	1180 - 1480/ 1060 - 1420	1270 - 1450/ 1130 - 1400

The quality of coals mined from different districts varies widely. For example, moisture varies from 0 to 66 mass-%, mineral matter content from 0.7 to 45 mass-% and sulphur content from 0 to 6.5 mass-%. The burning properties and problems caused by mineral matter must be evaluated for each coal by its content (Singer, 1981). In Table 2.2, mass fractions and hardness values of typical coal are presented. It can be seen from Table 2.2 that most of the coal components are soft. Quartz, pyrite, alumina, orthoclase, kyanite, topaz, have high hardness values. From these, only quartz and pyrite contents are significant (Raask, 1983).

Table 3.2 Hardness of coal substance and mineral matter (Raask, 1983)

Constituent	Approx. Fraction, mass-%	Mohs Hardness Number	Vickers Hardness kg/mm^2
Coal Substance	60 - 80	1.5 - 2.5	10 - 70
Quartz	0.5 - 3	7	1200 - 1300
Pyrites	0.5 - 5	6 - 7	1100 - 1300
Alumina	0	9	>1200
Silicates			
Kaolin	2 - 6	2 - 2.5	30 - 40
Illite	1 - 4	2 - 2.5	20 - 35
Muscovite	1 - 4	2 - 2.5	40 - 80
Orthoclase	<0.1	6	700 - 800
Kyanite	<0.1	6 - 7	500 - 2150
Topaz	<0.1	8	1500 - 1700
Carbonates			
Calcite	0.2 - 1.5	3	130 - 170
Magnesite	0.05 - 0.2	4	370 - 520
Siderite	0.1 - 0.5	4	370 - 430

In pulverized firing, the coal is ground and dried in a pulverizer to an average particle size lower than 100 μm before burning. The mineral matter of the coal is very erosive after the pulverizer because of sharp edged mineral particles. Some of the pyrite is extracted from the pulverizer. The amount and content of the mineral matter changes remarkably in the flame because of the loss of combined water from shales, carbon dioxide from carbonates and sulphur dioxide. Original coal has an amount of minerals about 1.1 times the amount of minerals in ash after burning (Wall, Lowe, Wibberley, McC. Stewart, 1979). The smelting temperature of pyrite is below 750 °C, and they experience total physical and chemical change in the coal flame resulting in spherical iron oxide particles that cause less erosion wear than sharp edged particles. Quartz particles are hard, sharp edged, and their smelting

temperature is so high (about 1700 °C) that about 25-50 % of the original quarz particles maintain their erosiveness in the flame (Raask, 1982). Unregular shaped sintered ash particles also cause erosion wear. However, the main cause of erosion wear on heat exchanger surfaces is the quartz particles, and the erosiveness of a certain coal quality can be evaluated as a function of quartz content (Wright, 1987).

Peat is mainly soft, organically dissolved waste that contains mineral matter from 2 to 12 mass-% depending on the location of peat swamp. The majority of minerals in the peat are quartz sand coming from soil. Quartz particles in peat are sharp edged and erosive. In pulverized firing, peat is ground to a small particle size and it is very erosive before burning (Silén, Kettunen, 1984). The minerals in the peat are softened and melted at a lower temperature than most of the coal minerals. This indicates that the mineral particles in peat ash should be more spherical than in coal ashes. However, the burning temperature of peat is lower than that of coals and this causes large quartz particles to remain sharp edged and erosive in the flame.

Mineral matter content of wood is low, ranging from 0.15 to 2.2 mass-% in dry matter and from 0.5 to 2.2 mass-% in dry matter of bark. Because of the low mineral matter content, the erosiveness of wood and bark ash is low (Singer, 1981). The moisture and mineral matter content of fuel oil is low, most of the fuel oil is volatile matter. Natural gas does not contain moisture or solid particles. When burning fuel oil or natural gas, erosion wear does not occur (Singer, 1981; Saviharju, Sjöholm, 1989). Black liquor is a fuel coming from the cellulose mill. Black liquor is composed mainly of lignite from the tree, some unorganic materials, process chemicals and water. The majority of the solid matter in black liquor is sodium (Adams, 1988). Sodium compounds are soft and do not cause erosion wear. The design flow velocities in recovery boilers are from 5 to 20 m/s, which tend to decrease any possible erosion.

3.2 TARGET AREAS OF EROSION WEAR

When burning solid fuels, erosion wear caused by ash particles may occur on the surfaces of superheaters, reheaters, economizers, air heaters and membrane walls. Outside of the boiler, the fuel conveyors, pulverizers, pulverized coal transport tubes and ash conveyors are susceptible to erosion wear caused by minerals of the fuel (Raask, 1979; Wright, 1987). Areas near soot blowers are susceptible to erosion because of high velocity ash and slag particles removed from the tube surfaces causing erosion wear on other tubes. Furnace membrane walls are susceptible to erosion caused by unburned coal

particles in the flame area. Ash or slag pieces dropping off from furnace walls or superheaters cause erosion in the bottom slope of the furnace and on the nose construction of the furnace. In air heaters, local plugging can cause erosion because of high particle velocities on open parts of the flow area (Wright, 1987).

Erosion damage in steam boilers is usually concentrated on a fairly small area. Small levels of damage can be seen as the polishing of an area. More severe erosion damage can be seen as decreased wall thicknesses. Erosion wear occurs in places where there is local turbulence and the velocity of the flue gas is considerably higher than the velocity of the main flow, for example, between the wall and tube bank and in places where by-pass flow is united with the main flow. Even a welding drop can cause turbulence resulting in local erosion (Raask, 1979; Wright, 1987).

Areas in the bends of flue gas channels and areas after the bends are susceptible to erosion wear. The back wall of the rear pass and tube bends next to the back wall suffer especially from erosion wear. When flue gas passes the nose construction of the furnace, it must turn to the flue gas channel. The ash flow separates from the flue gas flow and concentrates near the back wall of the boiler. Most of the ash flow concentrates on the cross-sectional area of one third nearest the back wall. Local velocity and ash flow become high in the area between the back wall and the tube bends of the horizontal tube banks. Erosion wear occurs on front sides of these tube bends and sometimes on wall tubes (Wright, 1987; Mansfeld, Sauermann, Swirski, 1979). The areas most susceptible to erosion wear in a typical pulverized fired steam boiler are presented in Figure 3.1.

Erosion wear is not usually observed in the high temperature heat exchangers in the upper part of the furnace or in the horizontal part of the flue gas channel. In these exhangers, the transverse distances between tubes are high because of high volume flow of flue gas and sticking properties of high temperature ash particles. The flue gas velocity is low, from 3 to 4 m/s. In the rear-pass heat exchanger tube bundles, the transverse distances between tubes are low to get gas velocities appropriate for convective heat exchange and the dimensions of heat exchangers compact. Here, the flue gas velocity is higher, from 10 to 25 m/s. A staggered tube arrangement is observed to be more susceptible to erosion wear than an in-line tube arrangement. The second row in a staggered tube bundle is considered to suffer the most from erosion. However, the maximum erosion row can be deeper in the tube bundle (Wright, 1987; Bratchikov, 1987).

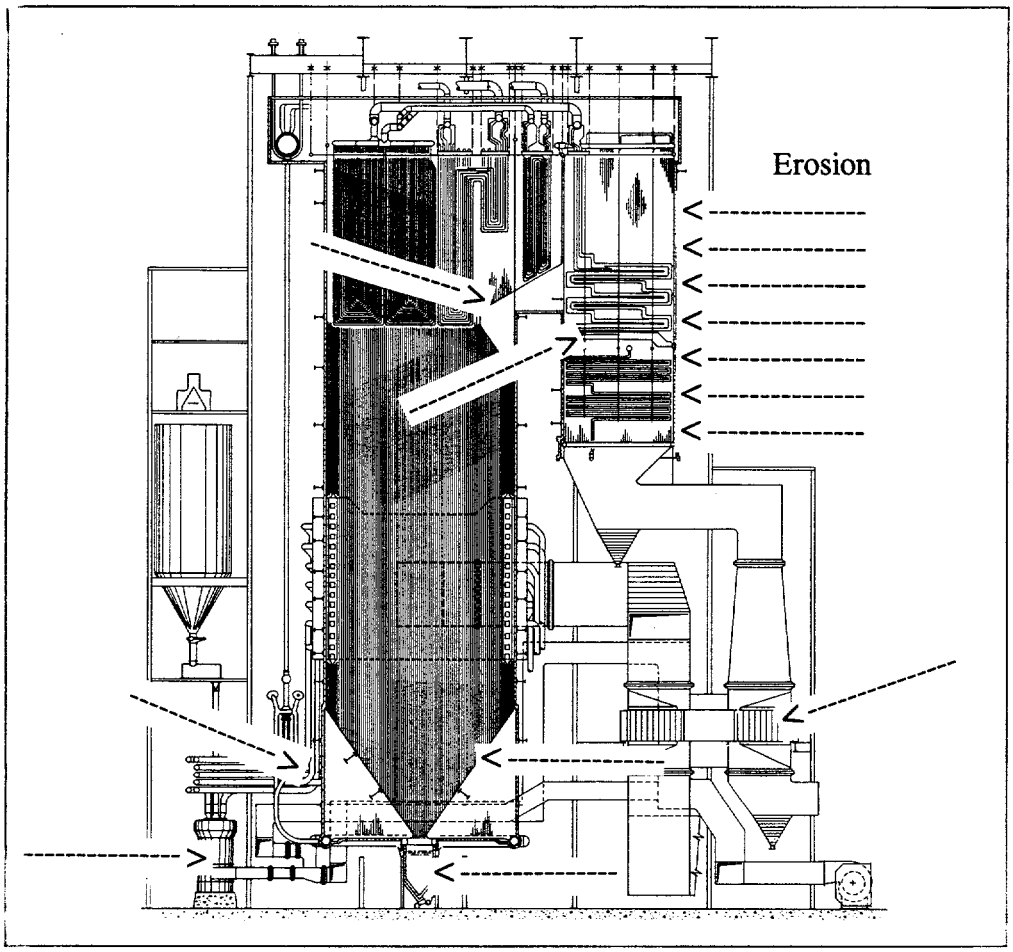

Figure 3.1 Areas most susceptible to erosion wear in pulverized fired steam boiler

Partial plugging of the flue gas channel causes a velocity increase in other parts of the channel or tube bank resulting in high erosion wear. Errors in tube direction caused by heat expansion or installation or tubes with different constructions used to stiffen the tube bank result in high local velocities and high erosion wear (Wright, 1987).

In bubbling bed boilers, erosion wear is high in the bed area in the lower part of the furnace. Heat transfer tubes immersed in the bed are especially susceptible to erosion wear because of the continuous friction of the turbulent flow of bed material. In a circulating fluidized bed boiler there are more parts susceptible to erosion because of higher particle material flow and velocity.

Most of the particle flow is separated from the flue gas in a cyclon and returned to the furnace before the convective heat exchangers. The main areas susceptible to erosion wear are furnace and cyclone walls and radiant superheaters in the upper part of the furnace. Erosion wear in the convective heat exhanger areas of a bubbling bed or circulating fluidized bed boiler is quite similar to the erosion in the convective heat exchanger areas of a pulverized firing boiler (Jansson, 1982).

3.3 DECREASING OF EROSION DAMAGES

Erosion wear can be decreased by changing the fuel to another containing less quartz. The moisture of the fuel is also significant to the level of erosion wear. High moisture causes high volume flow and high velocity of flue gas. Erosion can be decreased by grinding fuel to a smaller particle size resulting in smaller quartz particles. A greater amount of quartz particles is then smelted to spherical in the flame. The amount of erosive minerals in the fuel can be decreased by purification (Raask, 1982; Raask, 1983).

To improve the erosion resistance, the tube material can be changed from low alloyed steel to alloyed Mo- or Cr-steel. However, the differences in erosion durability are small between the usual boiler steels. The thickness of the tube wall can be increased. Radiative heat exchangers can be constructed as plate type, where the velocity of the flue gas is kept low between the plates and the first tubes shield the next. In fluidized bed boilers, radiant heat exchanger tubes with a square cross-sectional area have been used. In convective heat exchangers, the in-line tube construction is considered to be more resistant to erosion than a staggered tube construction because of the shielding effect of previous tubes. A staggered tube bank is more susceptible to be plugged than an in-line tube bank. The bends in the flue gas channels can be smoothened by construction. The cross-sectional areas in tube banks, that have a low resistance for gas flow should be avoided in construction. In areas where by-pass flow is united to the main flow, a sufficient mixing volume should exist (Raask, 1979; Mansfeld, Sauermann, Swirski, 1979).

Erosion wear can be reduced by reducing the average velocity of the flue gas, this also cuts the peak velocities. The peak velocities can be reduced by smoothening the velocity distribution on the cross-sectional area of the flue gas channel by construction. The velocity of the flue gas can be reduced by reducing the excess air rate in burning, reducing flue gas recirculation or, in extreme cases reducing boiler output. High moisture fuel can be dried before

burning so that the volume of flue gas will be lower. Local high velocities can be controlled by steering plates (Levy 1982; Wright, 1987).

In addition to the control of flue gas velocity distributions, particle concentration distributions must be controlled. Areas between walls and tube banks in which high velocities and particle concentrations occur, especially near the rear wall of boiler, can be covered by plates. These plates can however concentrate erosion on the tubes beside them and sometimes the erosion will be concentrated on the middle area of the tube bank upper side. This effect can be minimised by keeping a sufficient distance between the plate and the next tube bank to allow the turbulence to be moderated. Perforated plates and screen plates have been used to allow some flow through the plates and reduce the turning or concentration effect of shield plates (Wright, 1987). In Figures 3.2 and 3.3, erosion reduction methods in the reheater and economizer areas of a steam boiler are presented. In Figure 3.4, the typical installation of a shield plate is presented.

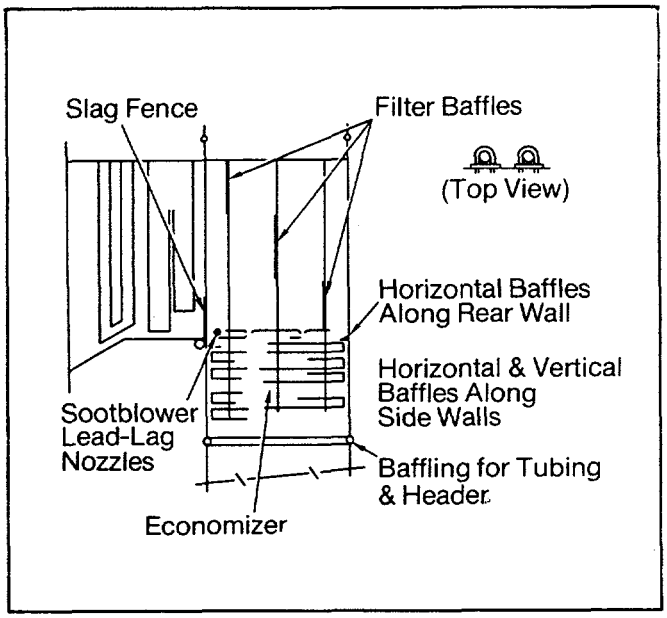

Figure 3.2 Erosion reduction methods in economizer (Singer, 1981)

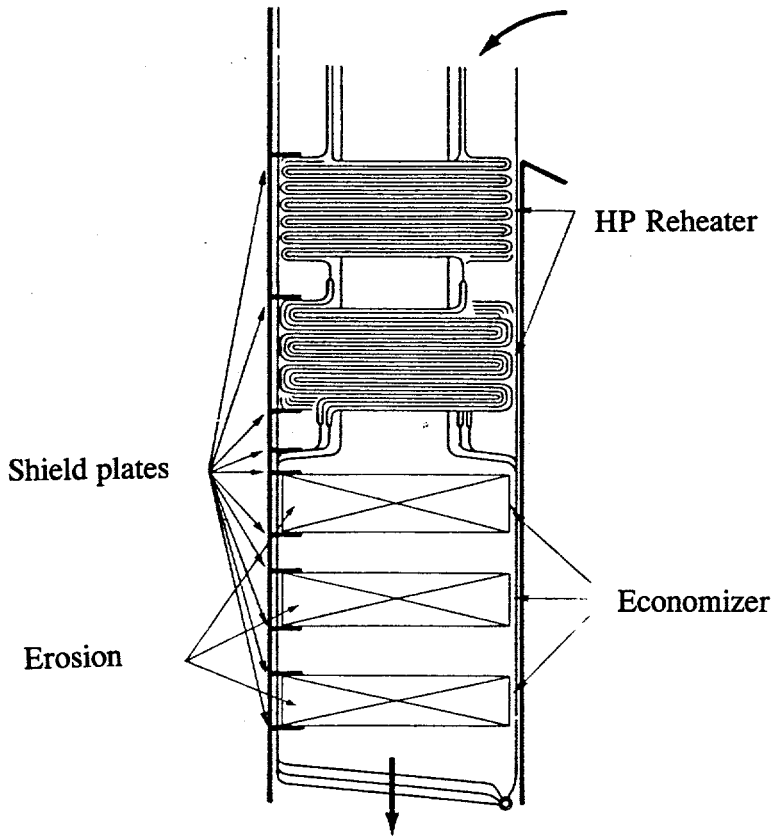

Figure 3.3 Erosion reduction methods in reheater and economizer area (Raask, 1979)

Tube shields curved onto the tube, masonry or filling by welding is used to protect the tubes against erosion wear. Tube shields or masonry have a short life and must be renewed about once a year. Shield welding is slow, highly professionally demanding and an expensive way to protect tubes against erosion and is considered to be a temporary way. Flame spraying and plasma spraying have been used to reduce erosion wear in areas that suffer most from erosion.

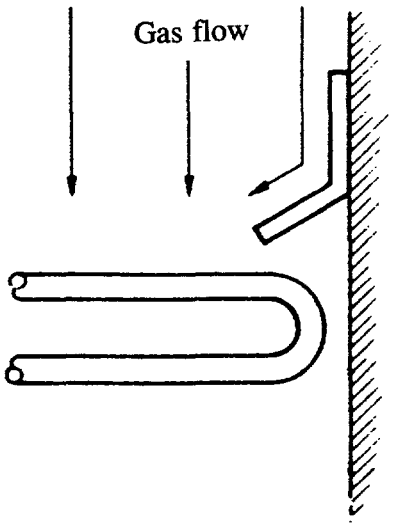

Figure 3.4 Typical installation of a shield plate (Wright, 1987)

In soot blowing, particles removed from the surfaces of tubes can cause erosion wear on the tubes nearby. Water droplets in soot blowing steam can also cause erosion on the tubes. The velocity of the sooting flow should not exceed 100 - 150 m/s depending on the mineral content of the fuel. Soot blowing should be cycled accurately and the order of the blowing in the flue gas channel should be downwards and from front to back (Raask, 1979; Wright, 1987).

4 EROSION TESTING ARRANGEMENTS AND TESTING

4.1 TEST FACILITY

The Test Facility for Emission Measurement and Control in the Department of Energy Technology in Lappeenranta University of Technology was used in this reseach. The test device was connected to the test facility for emission measurement and control, as presented in Figure 4.1. The test device was coupled to the facility with flange joints on the plane 12.0 m. A blower was used to generate the air flow in which erosive particles were injected by a hopper device for the higher particle concentration, and a screw feeder device assisted by pressurised air for the lower particle concentration. The velocity of the air and the mass flow of particles was controlled. The temperature of the flow was about 20 °C in all the tests. The direction of the particle-air suspension flow was upwards through the tube banks in the test device. After the test device, the particles were separated from the air flow by a multicyclone in the tests where the particle material was quartz sand and by a fabric filter and electrostatic precipitator in the tests where the particle material was coal ash or peat ash. Air was transferred to a stack and the particulate material to a hopper. New particulate material was added to the hopper to cover material losses and maintain the erosivity of the particle material.

Figure 4.2 presents the test device in which the test tubes were installed. The test device was constructed from steel plates with conical upper and lower parts to connect it to the flange joints of the test facility riser pipe. The upper conical part could be removed to make the installation of the test tubes possible. The test device was separated by walls into three smaller flow channels, from which the centre channel was used in the tests. The width of the channel was 195 mm, depth 402 mm and height without cones 1650 mm (total height 3208 mm). The other two channels were plugged. Before the tube banks, there were 3.5 hydraulic diameters length of direct flow channel and after the three tube construction, 2.6 hydraulic diameters. After the in-line and staggered tube banks there were 1.5 hydraulic diameters worth of direct flow channel. Three measurement connections were made 154 mm below the tubes in the front wall of the test device.

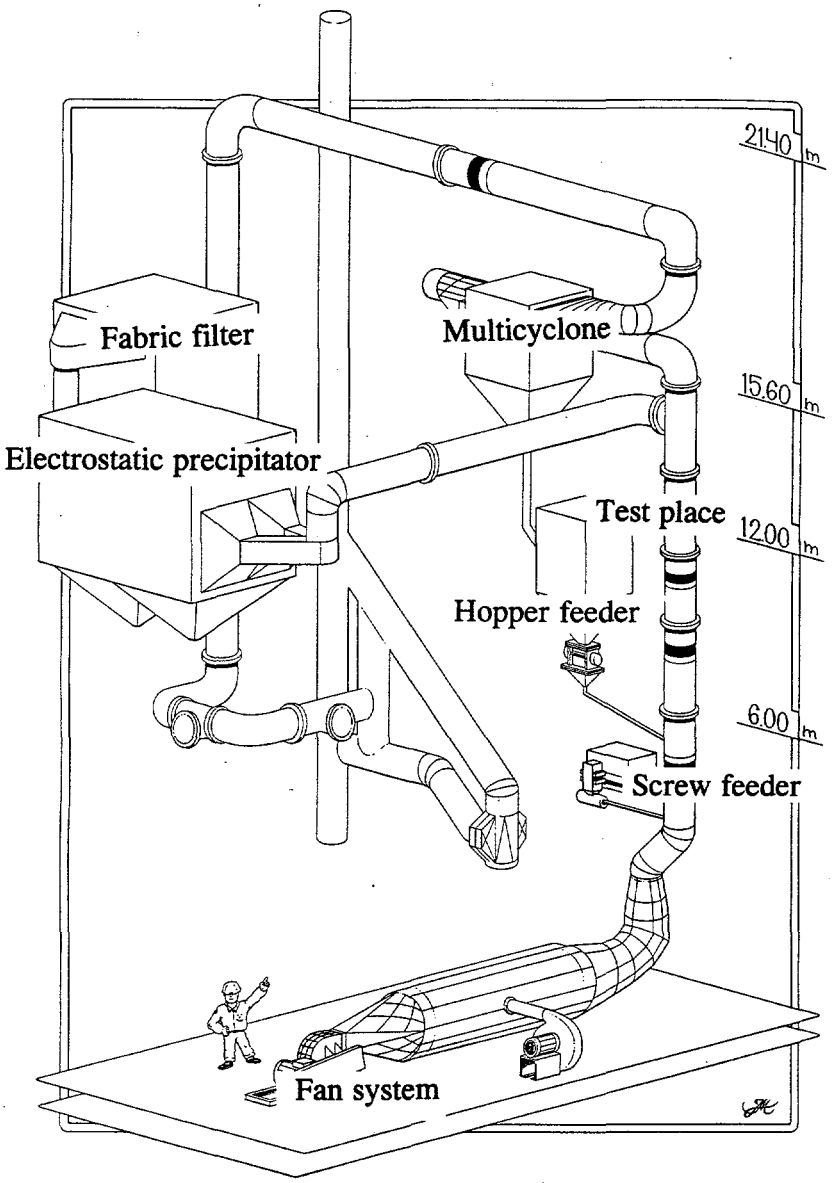

Figure 4.1 Test Facility for Emission Measurement and Control

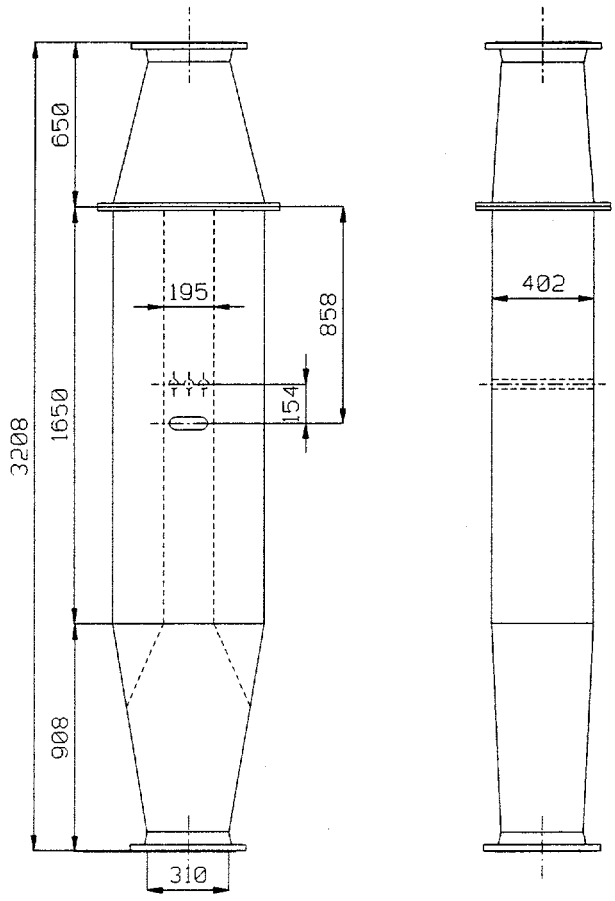

Figure 4.2 Erosion test device with three tube construction

Test tubes were arranged in three different constructions: a construction with one three-tube row, an in-line tube bank with six three-tube rows and a staggered tube bank with three three-tube rows and three two-tube rows. The nominal outer diameter of the tubes was 38 mm and the distance of the centre points of two adjacent tubes transverse to the air flow was 59.0 mm ($s_1 / d_u = 1.55$). The distance of the centre points of tubes in two adjacent tube rows in the direction of air flow was 57.0 mm ($s_2 / d_u = 1.5$). The free space between the side tubes and the wall of the channel was 19.5 mm in three-tube rows and 49.0 mm in two-tube rows.

In Figure 4.3 the three tube construction and horizontal coordination axes is illustrated. In Figure 4.4 the in-line tube bank construction, and in Figure 4.5 the staggered tube bank construction and the vertical location coordinate axis,

is presented. The origin of the horizontal coordinate axes, defined as the x- and y-axis, is the centre-point of the flow channel cross-sectional area. The coordinate of a test sleeve in the x- and y-axis is the distance between the centre-point of the test sleeve and the centre-point of the flow channel. In the vertical direction, defined as the z-axis, the origin is the front side point of the first tube row.

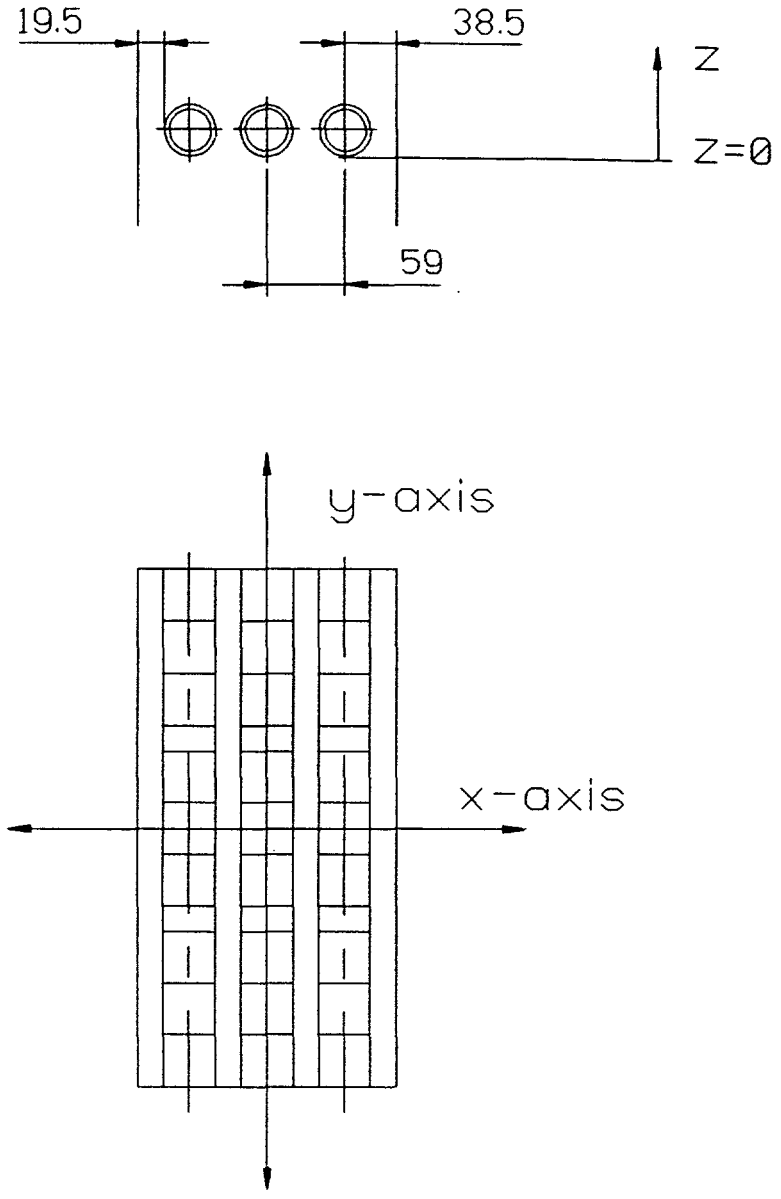

Figure 4.3 Three tube construction

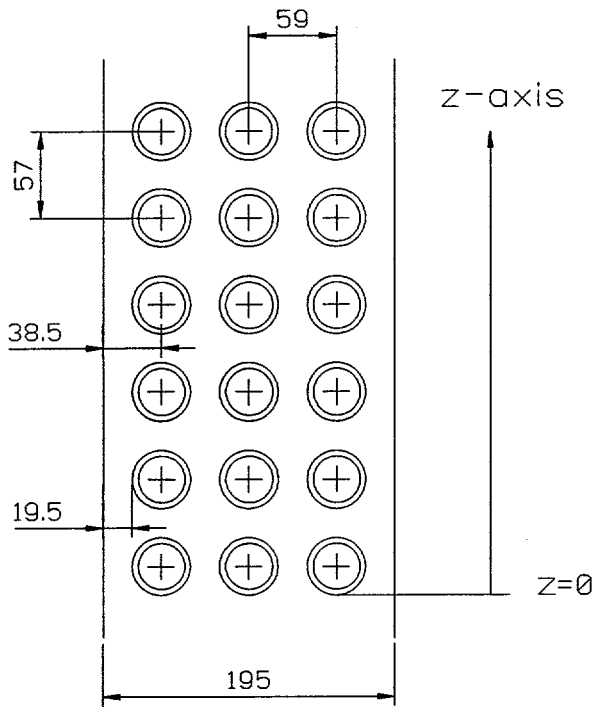

Figure 4.4 In-line tube bank construction

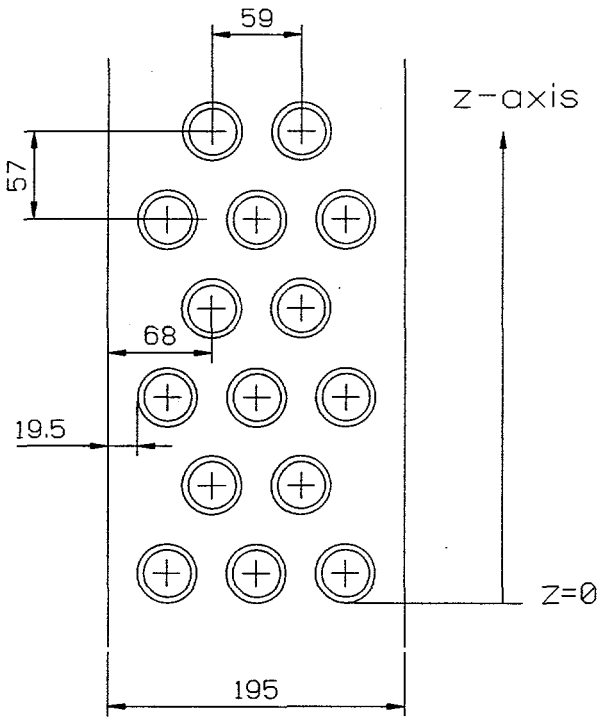

Figure 4.5 Staggered tube bank construction

The test tubes consisted of test sleeves and filling sleeves to keep them in position, and inner solid tubes to give support to the test sleeves and filling sleeves. The inner tubes were fixed at both ends to the walls of the flow channel. Small threaded flanges were welded to the ends of the tubes and one screw at each end of the tube was used to attach the tube to the flow channel. The nominal outer diameter of the inner tubes was 31.8 mm and the material of the inner tubes was St35.8.

The test sleeves were manufactured from tube with a nominal outer diameter of 38 mm. The length of the test sleeves was 40 mm. Three tube materials were used in the test sleeves: St35.8, 15Mo3 and 10CrMo910. Every test tube had nine test sleeves arranged in three groups. In every group, test sleeve materials were arranged in the order St35.8, 15Mo3 and 10CrMo910 from the front wall to the back of the test channel. The first group was located next to the front wall of the flow channel, the second group next to the centre part, and the third group next to the back wall of the flow channel. Filling sleeves

manufactured from tube with a nominal outer diameter of 38 mm and material St35.8 were mounted between the groups. The length of the filling sleeves was 21 mm. One filling sleeve in a test tube was fixed to the inner tube by welding. To prevent rotation, test sleeves were equipped with a node at one end of the sleeve and cavity at the other end to fix them to adjacent sleeves. The order of the test sleeves was the same in every test tube in all the tests. In Figure 4.6, the test assembly of a test tube is presented.

In addition to the test sleeves, tubes (lengths 261 mm and 120 mm) of material St35.8 were manufactured for the three tube construction to test the uniformity of the particle concentration distribution on the cross-sectional area of the flow channel by using painted layers.

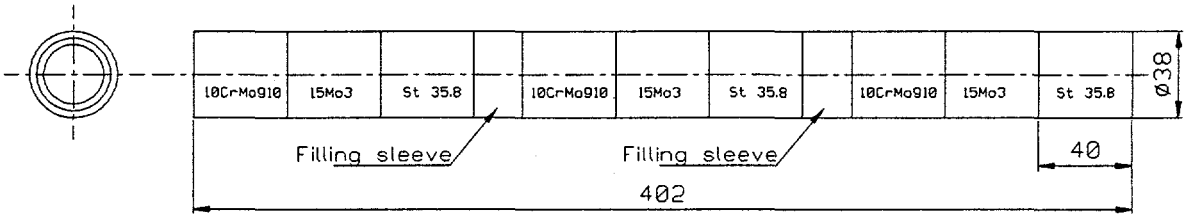

Figure 4.6 Test assembly of a test tube

4.2 MEASUREMENTS

In the tests, three flow velocities and two particle concentrations were used. The actual values of the velocities and particle concentrations were partly determined by the test facility. The minimum useful air velocity proved to be 13 m/s, so it was chosen. Other velocities were 20 m/s and 30 m/s. The velocities were defined as the velocity in the cross-sectional area of the flow channel at the centre-point of the three-tube row. The velocity of the air was measured at the measurement connections and adjusted appropriately.

One low particle concentration was used to describe the particle flow conditions in a pulverized firing boiler, and one high particle concentration to describe conditions in the furnace of a fluidized bed boiler. In addition, sufficiently high erosion wear rates were confirmed by the choice of high particle concentration and high velocity. Particle concentrations used in the tests were 20 g/m^3, which was adjusted by the screw feeder, and 375 g/m^3, which was adjusted by the rotational speed and nominal feeding rate of a

hopper feeder. Particle samples were taken before and after tests and particle size distributions defined by analysis based on the diffraction of laser light. Three particle materials were used: quartz sand, coal ash and peat ash. The temperature of the flow was room temperature, about 20 °C in all tests. The durations of the tests were recorded.

Test sleeves were weighed before and after each test. Before weighing the test sleeves were cleaned with pressurised air. The outer diameters of the test sleeves were measured at angles of 0°, 30°, 60°, 90°, 120° and 150°. The wall thicknesses of the test sleeves were measured at angles of 0°, 30°, 60°, 90°, 120°, 150°, 180°, 210°, 240°, 270°, 300° and 330°. The angle of 90° was defined as the direction of incoming flow. The measuring angles and measuring points of a test sleeve are presented in Figure 4.7. Measurement points were 15 mm from both ends of the test sleeves in the three tube construction. In the in-line and staggered tube banks, only one measuring point 15 mm from the end of the test sleeve was used.

To observe the uniformity of the particle concentration distribution on the cross-sectional area of the flow channel, short tests with painted test tubes were carried out. Yield strengths and toughnesses of samples of the tube materials were defined in laboratory tests.

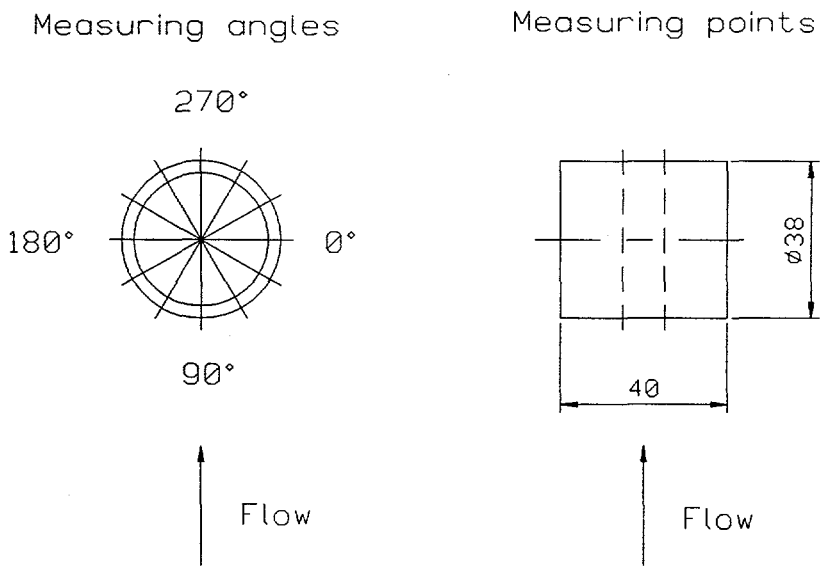

Figure 4.7 Tube diameter and wall thickness measuring angles and measuring points

4.3 EROSION TESTING

4.3.1 TESTING PROGRAMME

The in-line and staggered tube constructions are normally used in steam boiler convective heat exchangers. Typical tube diameters and spacings between the tubes were used in the tests. In addition, erosion wear of a single tube row without the effect of the other rows was studied.

As a reference particle material, quartz sand screened to particle size lower than 0.3 mm was used. Quartz sand is highly erosive and is generally used as a reference material in erosion testing. Quartz is the most erosive component in the mineral matter of coal or peat. All three constructions, two particle concentrations and three velocities were tested with quartz sand as the particle material.

To study the erosivity of coal ash and peat ash with respect to the erosivity of quartz sand, all of the particle materials were tested with the three tube construction. Coal and peat ashes were taken from the hoppers of electrostatic precipitators in power plants. The elementary analyses of coal ash and peat ash used are presented in Appendix A. The silicon contents of coal and peat ashes are 49 and 28 mass percent, respectively. Because of the source of the material, the coal and peat ashes were fly ash that doesn't contain a coarse particle fraction separated in the rear pass hopper of a steam boiler. The proportion of coarse particles is approximately 5 to 10 % of the mass of ash particles entrained from the furnace by the flue gas. However, the fly ashes were considered to describe the erosivity of the respective materials.

Erosion wear tests consisted of 150 hour periods. In some tests, 50 hour periods were used to study the linearity of the measured rates and, in some tests, 300 hour periods were used because of low erosion rates. The testing of the particle materials coal ash and peat ash was difficult because of the accumulation properties of the ashes. The tests were shorter than those for the quartz particle tests. In Table 4.1, the testing programme and the parameters are presented.

Table 4.1 Testing programme

Test No	Tube Construction	Particle Material	Particle Concentration (g/m^3)	Flow Velocity (m/s)	Time (h)
1	Three Tube	Quartz	375	30	50
2	In-line	Quartz	375	30	50
3	Staggered	Quartz	375	30	50
4	Three Tube	Quartz	375	30	50
5	In-line	Quartz	375	30	50
6	Staggered	Quartz	375	30	50
7	Three Tube	Quartz	375	30	50
8	In-line	Quartz	375	30	50
9	Staggered	Quartz	375	30	50
10	Three Tube	Quartz	375	20	50
11, 14, 17	In-line	Quartz	375	20	150
12, 15, 18	Staggered	Quartz	375	20	150
13	Three Tube	Quartz	375	20	50
16	Three Tube	Quartz	375	20	50
19, 22, 25	Three Tube	Quartz	375	13	150
20, 23, 26	In-line	Quartz	375	13	150
21, 24, 27	Staggered	Quartz	375	13	150
28, 31, 34	Three tube	Quarz	20	13	300
29, 32, 35	In-line	Quartz	20	13	300
30, 33, 36	Staggered	Quartz	20	13	300
37, 40, 43	Three Tube	Quartz	20	20	150
38, 41, 44	In-line	Quartz	20	20	150
39, 42, 45	Staggered	Quartz	20	20	150
46, 49, 52	Three Tube	Quartz	20	30	150
47, 50, 53	In-line	Quartz	20	30	150
48, 51, 54	Staggered	Quartz	20	30	150
CA 4	Three Tube	Coal Ash	375	13	10
CA 5	Three Tube	Coal Ash	375	13	10
PA 1	Three Tube	Peat Ash	375	13	50
Q 1	Three Tube	Quartz	375	13	50
Q 2	Three Tube	Quartz	375	13	50
Q 3	Three Tube	Quartz	375	13	50

4.3.2 TESTING

The test sleeves were weighed, and diameters and wall thicknesses measured using a micrometer measuring device. The accuracy of the mass measurements was 0.001 g, and that of the diameter and wall thickness measurements 0.01 mm. When measuring the tube outer diameters and wall thicknesses, a measuring jig was used to assure the location of measuring points to be the

same in different measurements. Test sleeve outer surfaces were as fabricated, and that caused inaccuracy in diameter and wall thickness measurements. The results of tube diameter and wall thickness measurements were used only in analysing erosion wear as a function of collision angle. Tube diameter and tube wall thickness measurements were not done in tests where erosion wear rate was very low.

In the quartz particle tests, the test facility functioned automatically so that the tests continued at nights and weekends. In coal and peat ash tests, the ash accumulated in transport pipes and manual control and maintenance was required to perform the tests. Hence the tests were shorter than the quartz particle tests. Coal and peat ash tests were conducted at a flow velocity of 13 m/s and particle concentration of 375 g/m^3. Five coal ash tests were conducted. The first three tests were rejected because of inaccuracies in the results. Coal ash tests CA 4 and CA 5 were used for analysis. Only one peat ash test (PA 1) was done because of great difficulties caused by the accumulation of ash. Generally, the erosion rate is higher at the first period of testing and gets lower at the subsequent periods. Quartz particle tests Q 1, Q 2 and Q 3 were done with uneroded test sleeves faced towards the particle flow to get reference values for coal and peat ash tests done with uneroded test sleeves.

4.3.3 VELOCITY AND PARTICLE CONCENTRATIONS

Both the air flow velocity distribution and particle concentration distribution on the cross-sectional area of the flow channel influence the local erosion wear. Usually, the flow velocity near the walls is lower than in the centre part of the flow channel. In Figure 4.8, the measured air velocity distributions for the different flow velocities used in the tests with the three tube construction are presented. The velocity measurements were carried out without particles in the flow. In Figure 4.9, the velocity measuring points on the cross-sectional area of the flow channel are illustrated. The co-operation of air velocity and particle concentration distributions was observed by results from tests with painted tubes. On the grounds of these short tests, the distributions were sufficiently flat.

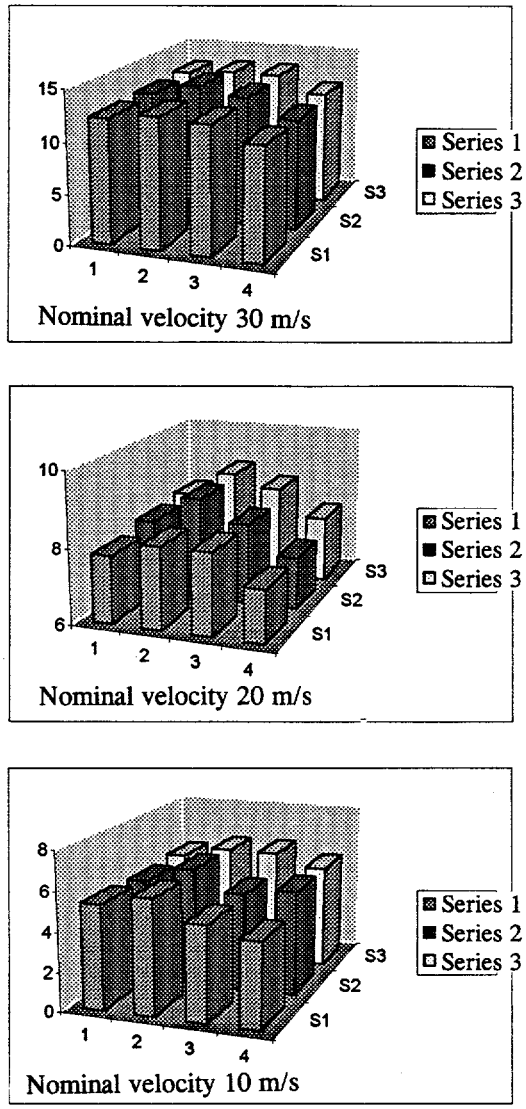

Figure 4.8 The distribution of the free stream velocity before the tube bank, when the nominal velocity of the tube cap is 10, 20 and 30 m/s.

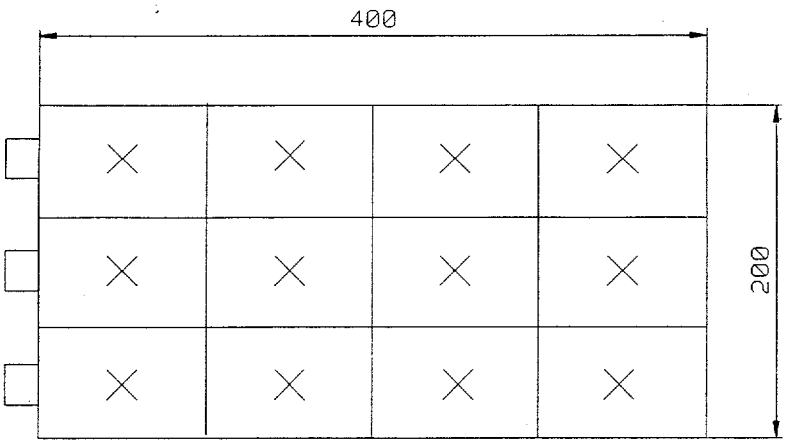

Figure 4.9 Velocity measuring points on the cross-sectional area of the flow channel

The ratio of the gas volume to the total volume in the test channel was 0.9998 with the higher particle concentration and 0.99999 with the lower particle concentration. Hence, the average distance between particles was high compared to the particle diameter, about 10 to 40 times the particle diameter, and the particles in the channel can be treated as being separate. A particle in the air flow is forced upwards by drag and lift forces and downwards by gravity force. When these forces upwards and downwards are balanced the particle has reached the terminal velocity which is defined as the velocity difference between the air velocity and the particle velocity to keep the drag force high enough to keep the particle entrained. Assuming spherical particles, the terminal velocity of a particle can be calculated from the equation of Kay and Nedderman

$$w_t = \left[\frac{4}{3} \cdot d_p \cdot \frac{(\rho_s - \rho_g)}{\rho_g \cdot C_d} \cdot g \right]^{0.5} \qquad (4.1)$$

where w_t is the terminal velocity of the particle,
d_p is the particle diameter,
ρ_s is the solid density of particle material,
ρ_g is the density of air,
C_d is the drag coefficient of the particle, and
g is gravity.

The drag coefficient of a particle can be calculated from the equations

$$C_d = \frac{24}{\mathrm{Re_p}} \tag{4.2}$$

when $\mathrm{Re_p} < 2$ in laminar flow, and from the equation

$$C_d = \frac{24}{\mathrm{Re_p}} \cdot \left(1 + 0.15 \cdot \mathrm{Re_p}^{0.687}\right) \tag{4.3}$$

when $2 < \mathrm{Re_p} < 800$.

When the particle Reynolds number is between 2000 and 200000, the drag coefficient is approximately constant and has a value of 0.44. The particle Reynols number can be calculated from the equation

$$\mathrm{Re_p} = \frac{\rho_g \cdot w_t \cdot d_p}{\mu_g} \tag{4.4}$$

where w_t is the terminal velocity, and
μ_g is the dynamic viscosity of the air flow.

The terminal velocities for particles of different sizes and materials as calculated from equations 4.1 to 4.4 are presented in Table 4.2. Most of the particles used in the tests have sizes ranging from 10 to 300 μm and practically all are smaller than 600 μm. It can be seen from Table 4.2 that in the particle size ranges used in the tests, the terminal velocities are lower than 4.3 m/s for quartz particles, lower than 3.2 m/s for coal ash particles and lower than 2.7 m/s for peat ash particles.

Table 4.2 Terminal velocities for different particles

Particle diameter	Quartz particles	Coal ash particles	Peat ash particles
µm	m/s	m/s	m/s
0.1	4.9×10^{-7}	3.0×10^{-7}	2.4×10^{-7}
1.0	4.9×10^{-5}	3.0×10^{-5}	2.4×10^{-5}
10	4.9×10^{-3}	3.0×10^{-3}	2.4×10^{-3}
100	0.38	0.30	0.24
200	1.0	0.71	0.58
400	2.2	1.6	1.4
800	4.3	3.2	2.7

Air velocities in the riser tube between the feed point of the particle material and the test device and in the flow channel of the test device are presented as a function of nominal testing velocity in Table 4.3. The velocities in the riser tube and flow channel are higher than the terminal velocities of particles used in the tests. A conclusion can thus be drawn that all particle fractions used in the tests are fully entrained by the air flow.

Table 4.3 Air velocities in different parts of the test facility

Test velocity	Riser tube	Flow channel
m/s	m/s	m/s
13	5.5	5.4
20	8.5	8.3
30	13	13

In Figure 4.10, a fluidizing figure is shown in which the dimensionless velocity of the fluidizing element is presented as a function of dimensionless particle diameter (Kunii, Levenspiel, 1991). Dimensionless figures can be calculated from equations

$$d_p^* = d_p \cdot \left[\frac{\rho_g \cdot (\rho_s - \rho_g) \cdot g}{\mu_g^2} \right]^{1/3} \qquad (4.5)$$

$$\text{and} \quad w^* = w \cdot \left[\frac{\rho_g^2}{\mu_g \cdot (\rho_s - \rho_g) \cdot g} \right]^{1/3} \tag{4.6}$$

where d_p^* is dimensionless particle diameter,
d_p is particle diameter,
ρ_g is gas density,
ρ_s is the solid density of particle material,
g is gravity,
μ_g is the dynamic viscosity of the gas,
w^* is the dimensionless fluidization velocity, and
w is the fluidization velocity.

Table 4.4 shows the dimensionless particle diameters for quartz particles, coal ash particles and peat ash particles and in Table 4.5 the dimensionless fluidization velocities are calculated. It can be seen that velocities for all particle sizes and all particle materials are higher than the respective maximum fluidization velocities. This means that all the particles used in tests are fully entrained by the air flow and the particle velocity is close to the velocity of the air flow.

Table 4.4 Dimensionless particle diameters

Particle diameter (μm)	Dimensionless particle diameter	Dimensionless particle diameter	Dimensionless particle diameter
	Quartz	Coal ash	Peat ash
0.1	3.9×10^{-3}	3.3×10^{-3}	3.0×10^{-3}
1.0	3.9×10^{-3}	3.3×10^{-3}	3.0×10^{-3}
10	0.39	0.33	0.30
100	3.9	3.3	3.0
200	7.7	6.6	6.1
400	15	13	12
800	31	26	24

Table 4.5 Dimensionless fluidization velocities

Fluidization velocity in test channel (m/s)	Dimensionless fluidization velocity	Dimensionless fluidization velocity	Dimensionless fluidization velocity
	Quartz	Coal ash	Peat ash
5.4	9.2	11	12
8.3	14	17	18
13	22	26	28

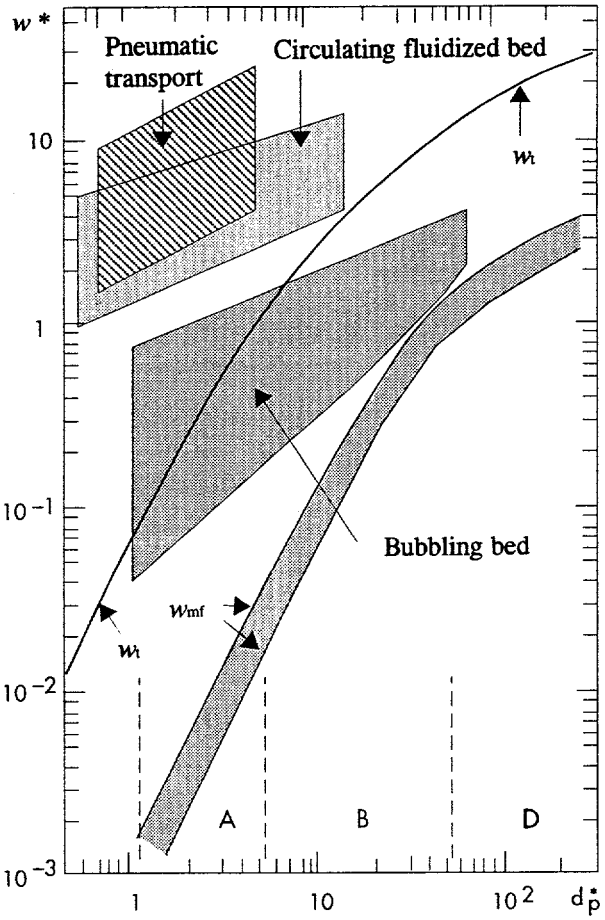

Figure 4.10 Dimensionless fluidization velocity as a function of dimensionless particle diameter (Kunii, Levenspiel, 1991)

5 CONCLUSIONS FROM THE TESTS

5.1 INTRODUCTION

The conclusions from the tests were drawn on the basis of the mass measurements of the test sleeves as far as possible. The mass measurements had superior accuracy compared to the accuracy of test sleeve diameter or wall thickness measurements. The test sleeve diameter and wall thickness measurements were used only when defining erosion rate as a function of collision angle. As the masses, diameters and wall thicknesses of individual test sleeves had different values, percentage values were used in analysing the measurements: test sleeve mass loss divided by the mass of the test sleeve before the tests or test sleeve diameter or wall thickness loss in the test divided by the diameter or wall thickness before the tests.

A linear regression analysis program was used during the analysis of the measurements when the correlation was expected to be linear. If one wants to compare some property to another, for example erosion rate of tube material 15Mo3 or 10CrMo910 to the erosion rate of tube material St35.8, two analyses with one variable were done. The regression coefficient was calculated as the constant term zero, so the regression line goes to the origin. Zero erosion wear rates appeared in the diameter and wall thickness measurements. The regression analysis program used must have all values different from zero. The zero values were replaced by a value of 0.000001 which is practically zero in the range of accuracy used in the tests and analyses. The reliability of the analysis was studied by defining the coefficient of determination and the t-value, which were calculated by the regression analysis program for each case. The coefficient of determination should have as high a value as possible, but lower than 1.0 and the absolute value of t should be higher than two. The reliability of the analyses was also studied by the residual distribution figure drawn by the regression analysis program. The residuals should be distributed randomly as a function of the parameter determined by the analysis. The residual figures of the most important analyses are presented in Appendix B.

5.2 EROSION WEAR AS A FUNCTION OF PARTICLE CONCENTRATION

In the analysis, the erosion rates of the tests with quartz particle concentrations of 375 g/m^3 were compared to the erosion rates of the tests with quartz particle concentrations of 20 g/m^3 on the basis of mass loss measurements in tests with

the three tube construction. The total amount of measurements was 81. The coefficient of determination of the analysis was 0.90 and the t-value of the regression analysis was 36.

As a result of the analysis, the angle coefficient of the regression line became 10. The ratio of the particle concentration 375 g/m^3 to 20 g/m^3 is 19. It is obvious that erosion rate correlates strongly to particle concentration, but the correlation is not linear. The exponent of the particle concentration ratio 19 becomes about 0.8 to obtain the erosion ratio 10. In Figure 5.1, erosion rate ratio (erosion rate at a particle concentration of 375 g/m^3 per erosion rate at a particle concentration of 20 g/m^3) as a function of particle concentration for the results of the regression analysis and for the measurements of test sleeve number 5 is presented.

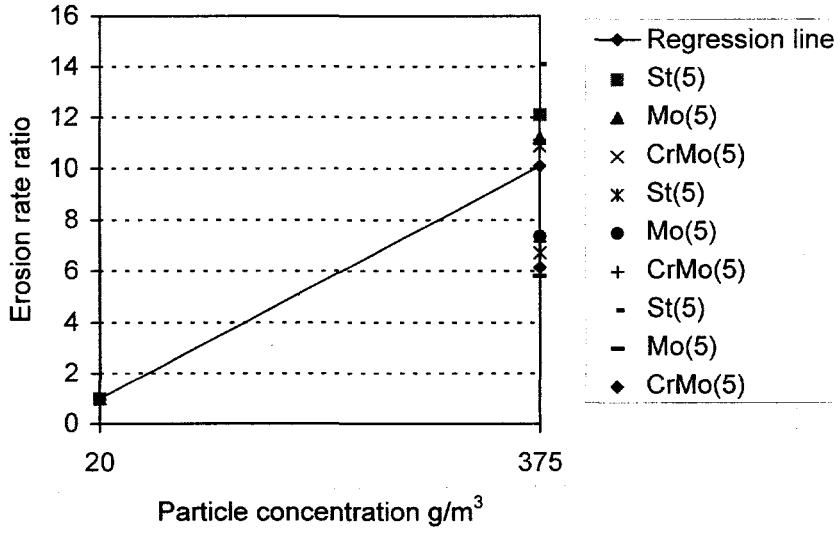

Figure 5.1 Erosion rate ratio as a function of particle concentration

5.3 EROSION WEAR AS A FUNCTION OF PARTICLE VELOCITY

Analyses were carried out with the mass loss measurements of test sleeves in the three tube construction tests with flow velocities of 13 m/s, 20 m/s and 30 m/s and particle concentrations of 20 g/m^3 and 375 g/m^3. The erosion rate in the tests with the velocities 30 m/s and 20 m/s was compared separately to the erosion rate in tests with a velocity of 13 m/s. The total number of measurements in both analyses was 54. The coefficients of determination in the analyses were 0.93 and 0.94, and the t-values 40 and 45, respectively.

As a result of the analyses, the erosion rate coefficient for the flow velocity of 30 m/s compared to the velocity of 13 m/s was 27 and for the velocity of 20 m/s 4.1. Velocity exponents calculated from these values were about 3.9 and 3.3, respectively. The exponent values are in the right range according to literature, but they have some difference. In Figure 5.2, erosion rate per erosion rate at the velocity 13 m/s (erosion rate ratio) as a function of velocity is presented. In Figure 5.2, some measurements of test sleeve number 5 are also presented. The first three measurements are from tests with the higher particle concentration, and the last are from tests with the lower particle concentration.

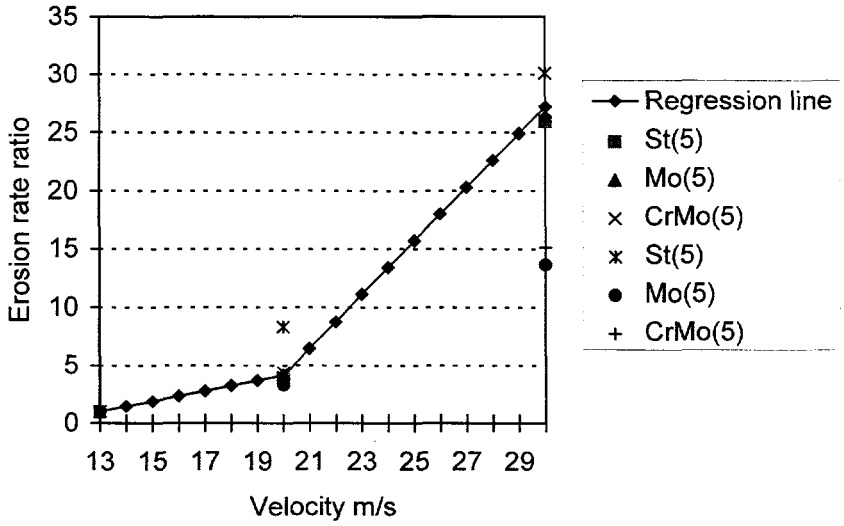

Figure 5.2 Erosion rate ratio as a function of flow velocity

5.4 EROSION WEAR AS A FUNCTION OF TIME

Erosion as a function of time was analysed by regression analysis applied to cumulative mass erosion rates on quartz particle tests with three 50 hour test periods. The analysis was carried out both separately with the mass loss measurements of the three tube construction, in-line tube bank and staggered tube bank, and with all these measurements together. The particle concentration in the tests was 375 g/m^3 and the flow velocity was 30 m/s. The total number of measurements was 27, 162, and 135, and all together 324. The analysis was done separately with mass loss measurements of the three tube construction in tests with a particle concentration of 375 g/m^3 and flow velocity of 20 m/s using test sleeves eroded in earlier tests and with a particle

concentration of 375 g/m^3 and flow velocity of 13 m/s using new test sleeves. The number of measurements in both tests was 27. The results of the analyses are presented in Table 5.1. In all the test series, except 10, 13, 16, new uneroded test sleeves were used. In Figure 5.3 the regression lines of the erosion rate per erosion rate of the first 50 hour period (erosion rate ratio) as a function of time are presented. Some measured values of test sleeve 5 in test series 1, 4, 7; 2, 5, 8 and 3, 6, 9 are also presented.

It can be seen from Table 5.1 and Figure 5.3 that the erosion rate in the quartz particle analyses in the second 50 hour test period is lower than in the first 50 hour period, and in most tests erosion rate in the third 50 hour period is further lower than in the second period. There is not any remarkable difference between the erosion rate in the tests started with the new test sleeves and the tests started with the earlier eroded test sleeves. No incubation or acceleration periods of erosion as presented in Figure 2.1 can be observed. An explanation for this is that even the first 50 hour period describes the steady state erosion period. The exponent of time ranged from 0.8 to 0.9 as calculated from the values of Table 5.1.

Table 5.1 Erosion as a function of time by regression analysis

Test series	Erosion 100 h/ erosion 50 h	Coefficient of determination	t-value	Erosion 150 h/ erosion 50 h	Coefficient of determination	t-value
1, 4, 7	1.7	0.99	230	2.4	0.99	170
2, 5, 8	1.7	0.97	300	2.5	0.94	200
3, 6, 9	1.6	0.93	83	2.5	0.96	120
1 to 9	1.7	0.97	240	2.5	0.98	260
10, 13, 16	1.9	1.00	840	2.6	1.00	560

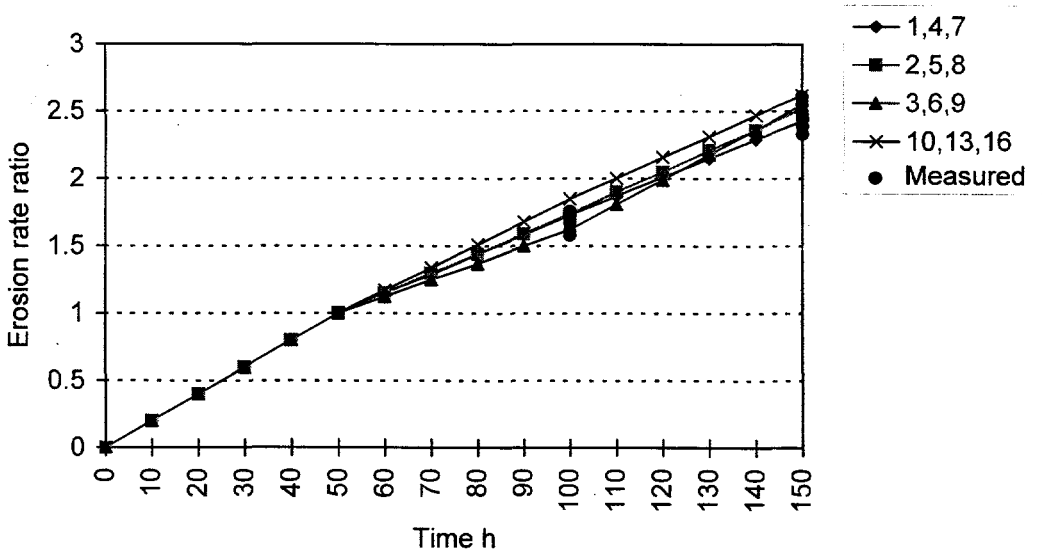

Figure 5.3 Erosion rate ratio as a function of time

5.5 EROSION WEAR AS A FUNCTION OF TUBE ARRANGEMENT

Tests indicated that erosion wear rates are different in different tube constructions and tube rows in tests with the same particle and flow parameters and tube materials. Linear regression analyses were done to evaluate erosion rates in different tube constructions and tube rows. Analyses were based on test sleeve mass loss measurements during the tests.

Two analyses were done to compare the erosion rate of the first row of the in-line tube bank or staggered tube bank to the erosion rate of the three tube construction. The analyses were done with measurements from eight tests with 215 measurements, one measurement point was rejected as fault. The result of the analyses was that the erosion rate in the first row of in-line tube bank is 54 % of the erosion of the three tube construction, and the erosion rate in the first row of the staggered tube bank is 45 % of the erosion rate of the three tube construction. In both analyses, the coefficient of determination was high, 0.98 and 0.95, and the t-values were 150 and 86. A conclusion can be drawn that the erosion rate on the first row of the in-line tube bank or staggered tube bank is about half that for a single three tube row with the same flow conditions.

Six analyses were done to compare the erosion rate of a single row in the staggered tube bank to the erosion rate of a single row in the in-line tube bank. The mass loss of a certain test sleeve in the staggered tube bank was compared to the mass loss of the corresponding test sleeve in the in-line tube bank in a corresponding test. In the staggered tube bank, in two tube rows the average erosion rates of the test sleeves of the left and right tubes were used to describe the erosion rate of the non-existant third centre tube. The analysis matrix consisted of mass loss measurements from eight tests. The total amount of measurements was 215, as above.

The results of the analyses are presented in Table 5.2. The coefficients of determination were high in most analyses, but in the analysis of the fifth row, the coefficient of determination was lower, 0.63. A conclusion can be drawn from the values of Table 5.2 that the erosion rate of the staggered tube bank is lower in the first row and much lower in rows 3 to 6 than the respective erosion rates in the in-line tube bank. Only in row 2 is the erosion rate of the staggered tube bank higher. The staggered tube bank is generally considered to be more erosive than the in-line tube bank because of flow channeling caused by plugging. However, these results indicate that the staggered tube bank has a lower erosion wear rate than the in-line tube bank at all rows but the second. In Figure 5.4 the erosion rate ratio of the staggered tube bank per in-line tube bank as a function of row number is presented.

Table 5.2 Erosion rate of staggered tube bank compared to the erosion rate of in-line tube bank

Row	Erosion rate of staggered tube bank/Erosion rate of in-line tube bank	Coefficient of determination	t-value of the analysis
1	82 %	0.97	120
2	176 %	0.97	120
3	50 %	0.85	51
4	32 %	0.89	60
5	67 %	0.63	27
6	13 %	0.91	65

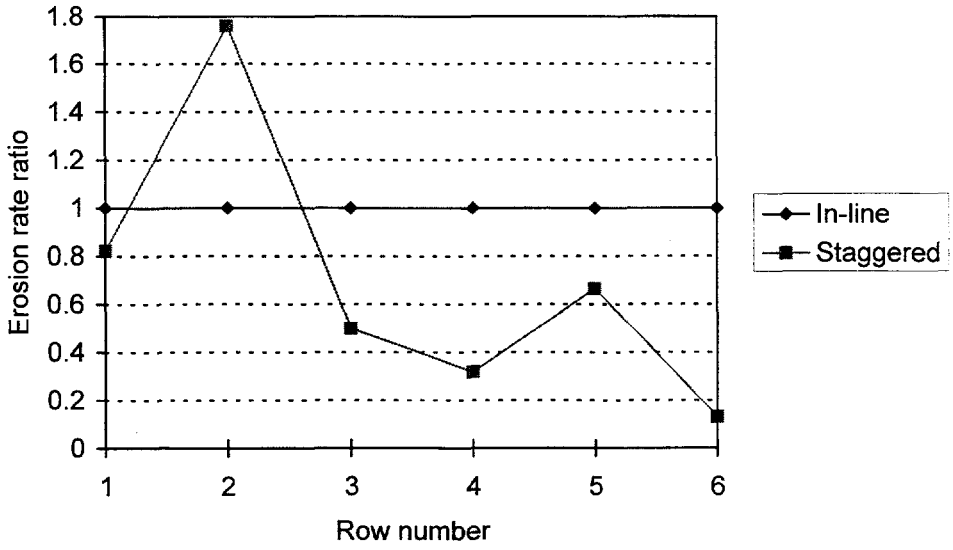

Figure 5.4 Erosion rate ratio as a function of row number

5.6 EROSION WEAR AS A FUNCTION OF ROW LOCATION

Erosion rate as a function of tube row was analysed. The mass loss erosion rate of test sleeves in each row was compared to the average erosion rate. In the in-line tube bank, the regression analysis matrix consisted of mass loss measurements from all eight tests except for one rejected measurement point, the amount of measurements was 215. The coefficient of determination was very high in every analysis. The results of the analyses are presented in Table 5.3.

Table 5.3 Erosion rate coefficients compared to the average erosion rate of all rows in the in-line tube bank

Row	1	2	3	4	5	6
Erosion rate coefficient	0.95	0.62	0.90	1.08	1.17	1.29
Coefficient of determination	0.93	0.98	0.99	0.99	0.99	0.98
t-value of the analysis	73	160	190	200	170	140

From Table 5.3 it can be seen that the erosion rate of the first row is near the average value and decreases in the second row but increases from the second row to the sixth row so that the maximum erosion rate is located at the sixth row. The minor erosion rate of the second row can be explained by the shielding effect of the first row of tubes. However, in the rows from 3 to 6 there must exist growing turbulence and back-flow of particles to explain the growing erosion coefficients. In Table 5.4 are the values of Table 5.3 converted to describe erosion rate in different rows compared to the erosion rate in the first row are presented.

Table 5.4 Erosion rate coefficients compared to erosion rate of the first row in the in-line tube bank

Row	1	2	3	4	5	6
Erosion rate coefficient	1.00	0.65	0.95	1.14	1.24	1.36

In the staggered tube bank, the regression analysis matrix consisted of the measurements of all the eight tests. In the staggered tube bank, there were three tubes in rows 1, 3 and 5, and two tubes in rows 2, 4 and 6. In the regression analysis matrix, there must be the same amount of values in each row. In rows 2, 4 and 6, the third 'middle tube' values were calculated as an average of the left and right tube measurements. The total amount of measurements in the analysis matrix was 216. The coefficients of determination were high in most cases, only in the analysis of row 5 was the coefficient of determination lower, 0.74. The results of the analyses are presented in Table 5.5.

Table 5.5 Erosion rate coefficients compared to the average erosion rate of all rows in the staggered tube bank

Row	1	2	3	4	5	6
Erosion rate coefficient	1.27	1.78	0.76	0.57	1.35	0.27
Coefficient of determination	0.89	0.96	0.97	0.89	0.74	0.89
t-value of the analysis	56	96	120	61	34	59

From the values of Table 5.5 it can be seen that the erosion rate is growing from the first row to the second row, the maximum erosion rate occurs in the

second row. The erosion rate decreases from the third row to fourth and sixth row, but in row 5 there is a local erosion rate maximum value. An explanation for the high erosion rate in the fifth row can be heavy turbulence and back-flow of particles. Kuznetsov (1958) has presented the erosion rate as a function of row location in a staggered tube bank with ten rows. The erosion behaviour is quite different from above. The erosion rate in the first row is lower and in the second row higher than the values in Table 5.5. The erosion rate in the third row is quite the same and in rows higher than 3 the erosion rate is about an average of the whole tube bank. There is not a maximum value in row 5. In Table 5.6 the values from Table 5.5 converted to describe the erosion rate of different rows compared to the erosion rate of the first row is presented.

Table 5.6 Erosion rate coefficients compared to the erosion rate of the first row in the staggered tube bank

Row	1	2	3	4	5	6
Erosion rate coefficient	1.00	1.40	0.60	0.45	1.06	0.22

In Figure 5.5 the values from the Tables 5.4 and 5.6 are illustrated. It can be seen from Figure 5.5 that the erosion rate as a function of row location behaves totally different in the in-line tube bank compared to in the staggered tube bank. The minimum erosion rate occurs in the in-line tube bank in the second row, and in the staggered tube bank in the sixth row. The maximum erosion rate occurs in the in-line tube bank in the sixth row, and possibly further in the tube bank if there were more rows. In the staggered tube bank, the maximum erosion value is in the second row and a local maximum value in the fith row.

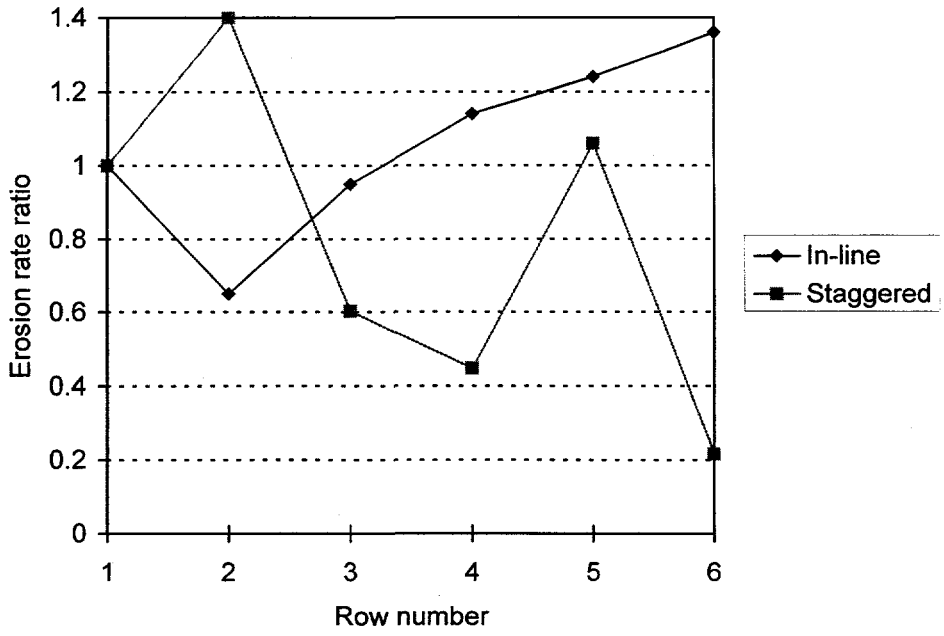

Figure 5.5 Erosion rate ratio as a function of row number in the in-line and staggered tube bank

5.7 EROSION WEAR AS A FUNCTION OF TUBE MATERIAL

Erosion rate depends on the tube material. In these tests, the tube material St35.8 was chosen as a basic material to which two other materials, 15Mo3 and 10CrMo910, were compared to. The percentage mass loss erosion rates of materials 15Mo3 and 10CrMo910 were compared to the percentage erosion rate of material St35.8. Only the test sleeves in the middle part of each test tube were used in the regression analysis matrix because of the non-uniformity of the particle concentration and velocity distributions on the cross-sectional area of the flow channel. The particle concentration and velocity distribution can be considered uniform enough in the middle area of the test channel to verify similar flow conditions, hence, allowing the comparison of test sleeves of different materials.

The analysis matrix contained mass loss measurements of all tube constructions. From the three tube construction tests, there were in the analysis all 11 quartz particle tests, two coal ash particle tests and one peat ash particle test. From the in-line tube bank and staggered tube bank tests, there were 16 quartz particle tests, eight tests in each. In tests that were a part of a

test series with the same flow conditions, the erosion rates were used as cumulative values. The total amount of measurements was 312.

Two analyses were done, one for the erosion rate of material 15Mo3 and another for the erosion rate of material 10CrMo910 and both were compared to the erosion rate of material St35.8. In both analyses, the coefficient of determination was high, 0.99. The t-values of the analyses were both 210. The erosion rate coefficient of material 15Mo3 was 0.95 and the erosion rate coefficient of the material 10CrMo910 was 0.87 compared to the erosion rate of material St35.8. It is generally considered that there are not great differences in the erosion resistivity of the usual tube materials. However, differences such as the above resulted from the tests. In Figure 5.5 the regression lines and some measurements are presented.

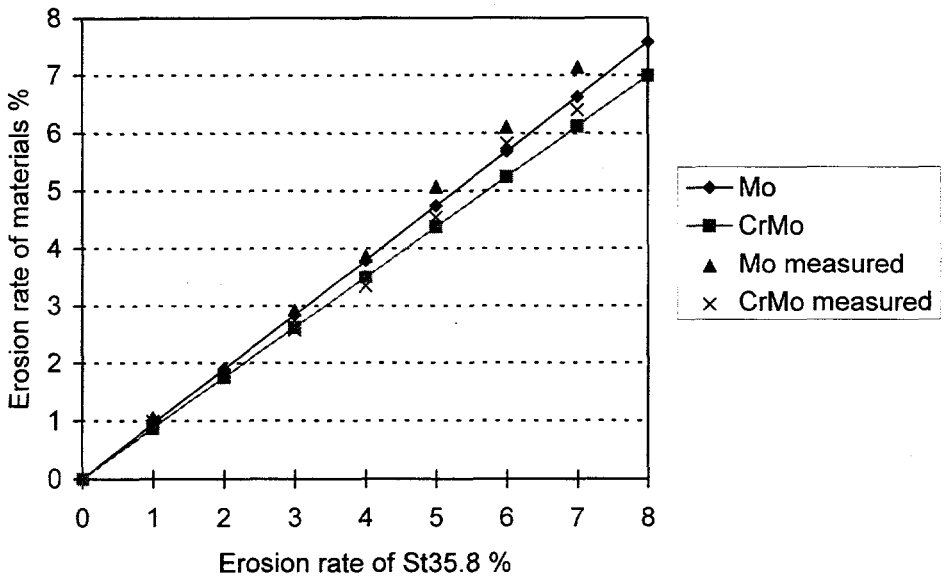

Figure 5.6 Erosion rates of tube materials 15Mo3 and 10CrMo910 compared to the erosion rate of tube material St35.8

5.8 EROSION WEAR AS A FUNCTION OF PARTICLE MATERIAL

Erosion rate as a function of particle material was studied using mass loss measurements from test sleeves in the three tube construction tests. The particle concentration was 375 g/m^3 and flow velocity 13 m/s. New uneroded test sleeves were used in tests to analyse particle material erosivity. Three 50 hour tests were done with quartz particles with new test sleeves. There were

great difficulties in conducting the tests with coal ash and peat ash particles because of plugging of the transport pipes and electrostatic precipitator. Hence, the amount of tests with a particle material of coal ash or peat ash was minimised. One 50 hour test was done with peat ash particles and two 10 hour tests with coal ash particles. The erosion rate in the latter test was so small that no more tests were done with coal ash particles. An attempt was made to use linear regression analyses to define erosion coefficients of different particle materials, but the coefficients of determination were low and a linear correlation could not be formed. An explanation for this may be that the test periods were too short to achieve high enough accuracy in the measurements. Average values of the measurements were used to define the coefficients. Average values of erosion rates of coal ash particles and peat ash particles compared to the erosion rates of quartz particles were 0.11 and 0.12, respectively. Higher erosion rates of coal ash and peat ash were expected because of the considerable silicon content of the ashes. In Figure 5.6, erosion rates of particle materials as a function of erosion rate of quartz are presented.

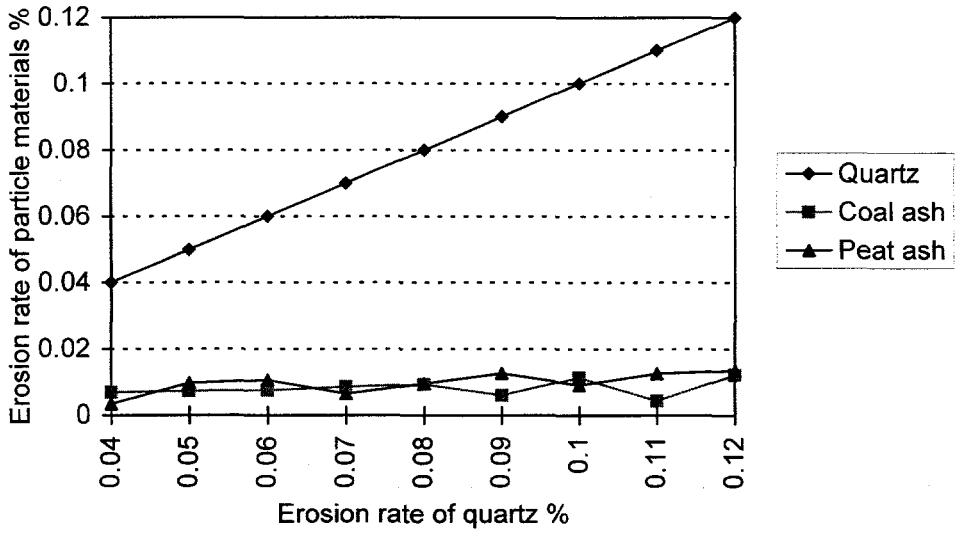

Figure 5.7 Erosion rates of particle materials

5.9 EROSION WEAR AS A FUNCTION OF COLLISION ANGLE

5.9.1 INTRODUCTION

The diameters and wall thicknesses of every test sleeve were measured before and after each test. In the analyses, measurements were calculated as percentage erosion rates. The collision angles were defined such that 90° points down and is facing the incoming particle flow and 0° points to right when standing in front of the test channel. The values of angles are increasing clockwise and measurements were carried out after every 30° angle. In the three tube construction measuring was done at two points in a test sleeve, and in the in-line or staggered tube bank measuring was done at one point in a test sleeve.

Linear regression analysis was used as the analysis method. The purpose of the analyses was to evaluate erosion wear distribution on a test sleeve perimeter. The average erosion rate on the perimeter of a test sleeve was calculated and the erosion rate of each collision angle was compared to the average erosion rate. The analysis matrix was formed so that one test series with the same flow parameters formed one group in the matrix. Exceptions to this were tests with a lower particle concentration. There the erosion rates were so small that all the three test series with different velocities formed one group or two groups. The measurements from the in-line and staggered tube banks were both analysed in one group and the measurements from the three tube construction in two groups. The results of analyses which have a coefficient of determination higher than 0.70 and t-value higher than two have been used. The coefficients of determination and the t-values of the analyses are presented in Appendix C. The figures of residuals of the analyses were plotted, but not presented because of the high number of analyses.

5.9.2 EROSION AS A FUNCTION OF COLLISION ANGLE IN THE THREE TUBE CONSTRUCTION

The three tube construction diameter measurement analysis was done separately for each tube to eliminate differences in the velocity and particle flow distributions. The amount of measurements in the analyses for one tube material was 30, and in the analyses for all materials 90, at every collision angle. In every analysis there were measurements of five quartz particle tests. The number of angles measured was six for the diameter measurements. In Table 5.7 the results of the analyses in the form of erosion rate compared to the average erosion rate on the perimeter of test sleeve are presented. When

standing in front of the test channel, the left-hand side tube is marked as Tube 1, the middle tube as Tube 2 and the right-hand side tube as Tube 3.

Table 5.7 Erosion rate as a function of collision angle in the three tube construction by diameter measurements

Tube		0°	30°	60°	90°	120°	150°
1	St35.8	0.63	0.93	1.1	1.1	1.4	0.94
	15Mo3	0.63	1.0	1.1	1.0	1.3	0.84
	10CrMo910	0.65	1.0	1.2	1.0	1.2	0.88
	All materials	0.64	1.0	1.1	1.1	1.3	0.89
2	St35.8		1.1	1.2	0.92	1.3	0.93
	15Mo3	0.55	1.1	1.2	0.90	1.3	0.87
	10CrMo910	0.58	1.1	1.2	0.99	1.3	0.88
	All materials	0.56	1.1	1.2	0.94	1.3	0.89
3	St35.8	0.65	0.69	1.3	0.96	1.1	1.3
	15Mo3	0.61	0.66	1.2	0.97	1.3	1.3
	10CrMo910	0.63	0.71	1.3	0.98	1.1	1.3
	All materials	0.63	0.69	1.3	0.97	1.2	1.3

In most of the Table 5.7 analyses, the coefficients of determination were high, ranging from 0.80 to 0.99. There are differences between the erosion coefficients of different tubes. They can be explained by differences in the flow distribution on the cross-sectional area of the test channel. It can be seen from Table 5.7 that the erosion coefficients of Tubes 1 and 2 have approximately the same values at different collision angles. However, the behaviour of the erosion coefficient of Tube 3 at angles of 30° and 150° is different. Differences between the values of different tube materials in any one tube is very small.

Test sleeve wall thickness measurements were also analysed separately for each tube and collision angle. The number of measurements was 90 at every angle. The analysis matrix consisted of measurements of 12 angles and five tests. In Table 5.8 the results of the analyses in the form of erosion rate compared to the average erosion rate on the perimeter of a test sleeve are presented.

Table 5.8 Erosion rate as a function of collision angle in the three tube construction by wall thickness measurements

Tube	0°	30°	60°	90°	120°	150°	180°
1	0.96	1.7	2.0	1.9	2.2	1.3	
2		1.9	2.2	1.6	2.3	1.5	
3			2.0	1.8	2.0	2.2	1.2

In the analyses presented in Table 5.8, the coefficients of determination were higher than 0.80 in most of the analyses. All the analyses at angles higher than 180° had low coefficients of determination. It should be noted that the low coefficient of determination usually appeared at angles of 180° to 330° which are at the back-side of the test sleeve with respect to the flow. At these angles erosion rates were low so the accuracy of the measurements was not high enough. In Tables 5.9 and 5.10 the values from Tables 5.7 and 5.8 divided by the value at an angle of 90° are presented.

Table 5.9 Erosion rates at different angles compared to the erosion rate at an angle of 90° by diameter measurements

Tube	0°	30°	60°	90°	120°	150°
1	0.58	0.91	1.0	1.0	1.2	0.81
2	0.60	1.2	1.3	1.0	1.4	0.95
3	0.65	0.71	1.3	1.0	1.2	1.3

Table 5.10 Erosion rates at different angles compared to the erosion rate at an angle of 90° by wall thickness measurements

Tube	0°	30°	60°	90°	120°	150°	180°
1	0.51	0.89	1.1	1.0	1.2	0.68	
2		1.2	1.4	1.0	1.4	0.94	
3			1.1	1.0	1.1	1.2	0.67

It can be seen from Tables 5.9 and 5.10 that the values from the test sleeve wall thickness analyses are a little smaller than the values from the test sleeve diameter analyses. There is erosion wear on the back-side of the tubes, but the erosion rate is small compared to the erosion rate on the front-side of the tubes. The maximum erosion rate occurs at angles of 60° and 120° symmetrically. At angles of 30° and 150° the erosion rate is lower and unsymmetric on the grounds of the values given in Tables 5.7 and 5.8. In

Figure 5.7 the erosion rates in the three tube construction based on the values of Tables 5.7 and 5.8 are presented. In the white areas the erosion rate compared to the average erosion rate is lower than 0.5, in the grey areas from 0.5 to 1.5 and in the black areas 1.5 or higher. It can be seen from Figure 5.7 that the erosion wear is concentrated on the front-side of the test sleeve perimeter facing the coming particle flow. Erosion on the back-side of the test sleeve perimeter is mostly low.

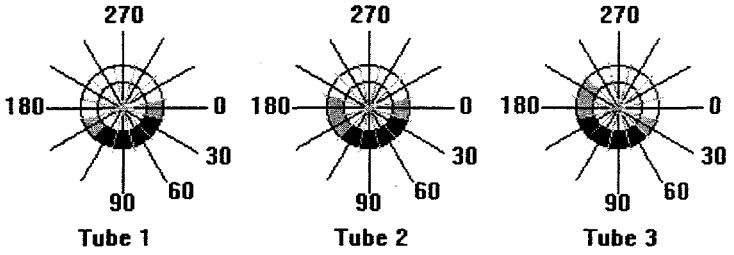

Figure 5.8 Erosion rates at different angles in the three tube construction

5.9.3 EROSION AS A FUNCTION OF COLLISION ANGLE IN THE IN-LINE TUBE BANK

The analysis was carried out separately for each tube at every collision angle. The number of tubes in the in-line tube bank was 18 and the amount of measurements was 36 at every angle. There were four tests and six angles in the diameter measurement analysis. In Table 5.11 the results of the analyses as erosion rate compared to the average erosion rate on the perimeter of a test sleeve are presented. When standing in front of the test channel, the left-hand side tube in the first row is marked as Tube 1, the middle tube as Tube 2, the right-hand side tube as Tube 3, and the left-hand side tube in the second row as Tube 4 and so on.

In most of the Table 5.11 analyses the coefficient of determination was higher than 0.80. It can be seen from Table 5.11 that there are great differencies in erosion rate coefficients in different rows and also in different tubes.

In the wall thickness measurement analyses there were 36 measurements at every collision angle and the number of angles was 12. In Table 5.12 the results of the analyses in the form of erosion rate compared to the average erosion rate on the perimeter of a test sleeve are presented.

Table 5.11 Erosion rate as a function of collision angle in the in-line tube bank by diameter measurements

Tube	0°	30°	60°	90°	120°	150°	Row
1	0.49	0.88	1.3	0.92	1.3	1.1	1
2	0.61	0.88	1.3	0.83	1.3	1.1	
3	0.59	0.84	1.2	0.92	1.3	1.1	
4	1.4	2.1	1.1	0.31		0.80	2
5	1.5	1.4	0.81		0.46	1.5	
6	1.5	0.75			0.85	2.3	
7	1.6	1.7	1.2			1.2	3
8	1.3	1.7	0.70	0.21	0.53	1.5	
9	1.5	1.5	0.79			1.8	
10	1.2	2.4	1.3			0.74	4
11	1.3	2.0	1.3	0.30	0.23	0.83	
12	1.4	2.0	0.90			1.2	
13	1.5	1.9	0.91	0.20	0.22	1.2	5
14	1.2	1.6		0.18	0.72	1.9	
15	1.1	2.3			0.34	1.4	
16	1.5	1.8	0.72	0.19		1.6	6
17	1.3	1.9	1.2	0.31	0.25	1.0	
18	1.1	2.6	0.66		0.32	1.2	

Table 5.12 Erosion rate as a function of collision angle in the in-line tube bank by wall thickness measurements

Tube	0°	30°	60°	90°	120°	150°	180°	Row
1		1.6	2.2	1.5	2.3	1.6		1
2		1.6	2.4	1.3	2.3	1.7	0.67	
3			2.0	1.3	2.3	1.8	0.97	
4	1.2	2.8				1.4		2
5	1.1	2.3			0.97	2.3	1.4	
6		0.94			1.8	3.3	1.5	
7	0.65	2.9				2.3	1.7	3
8	1.6	2.3	1.1		1.1	2.1		
9		2.4				3.4		
10		4.6				1.8	1.3	4
11	0.80	3.3	1.7	0.46		1.8	1.8	
12		3.3		0.43		2.6	1.4	
13	1.2	3.5	1.0			2.5	1.5	5
14	1.5	2.3		0.48		3.1		
15		3.9				2.5		
16		2.9		0.56		3.3		6
17		3.6	1.5			1.9	1.8	
18	2.1	4.2	0.96		0.78	1.8	0.85	

In most of the Table 5.12 analyses the coefficient of determination was low at angles from 210° to 330°, only in the analysis of Tube 13 at an angle of 330° was the coefficient of determination higher than 0.70, the corresponding erosion rate coefficient was 0.36. The angles from 210° to 300° are left out of the table. In Tables 5.13 and 5.14 the values of Tables 5.11 and 5.12 divided by the value at an angle of 90° are presented.

Table 5.13 Erosion rates at different angles compared to the erosion rate at an angle of 90° by diameter measurements

Tube	0°	30°	60°	90°	120°	150°	Row
1	0.53	0.96	1.4	1.0	1.4	1.2	1
2	0.73	1.1	1.6	1.0	1.6	1.3	
3	0.64	0.91	1.3	1.0	1.4	1.2	
4	4.5	6.8	3.5	1.0	0.97	2.6	2
8	6.2	8.1	3.3	1.0	2.5	7.1	3
11	4.3	6.7	4.3	1.0	0.77	2.8	4
13	7.5	9.5	4.6	1.0	1.1	6.0	5
14	6.7	8.9	2.2	1.0	4.0	11	
16	7.9	9.5	3.8	1.0		8.4	6
17	4.2	6.1	3.9	1.0	0.81	3.2	

Table 5.14 Erosion rates at different angles compared to the erosion rate at an angle of 90° by wall thickness measurements

Tube	0°	30°	60°	90°	120°	150°	180°	Row
1		1.1	1.5	1.0	1.5	1.1		1
2		1.2	1.8	1.0	1.8	1.3	0.52	
3			1.5	1.0	1.8	1.4	0.75	
11	1.7	7.2	3.7	1.0		3.9	3.9	4
12		7.7		1.0		6.0	3.3	
14	3.1	4.8		1.0		6.5		5
16		5.2		1.0		5.9		6

It can be seen from Tables 5.13 and 5.14 that the erosion rate on the perimeter of a tube is different in different tube rows. In the first row the erosion rate distribution on the perimeter of a test sleeve is like in the three tube construction, but in other rows where the previous rows have a shielding effect and particle flow directing effect on the next row the erosion rate distribution is different. The erosion rate at angles of 60° and 120° is lower than the maximum erosion rate that occurs at angles of 30° and 150°. In Figure 5.8 the erosion rates in the in-line tube bank based on the values of Tables 5.11 and 5.12 are presented. In the white areas the erosion rate compared to the average

erosion rate is lower than 0.5, in the grey areas from 0.5 to 1.5 and in the black areas 1.5 or higher.

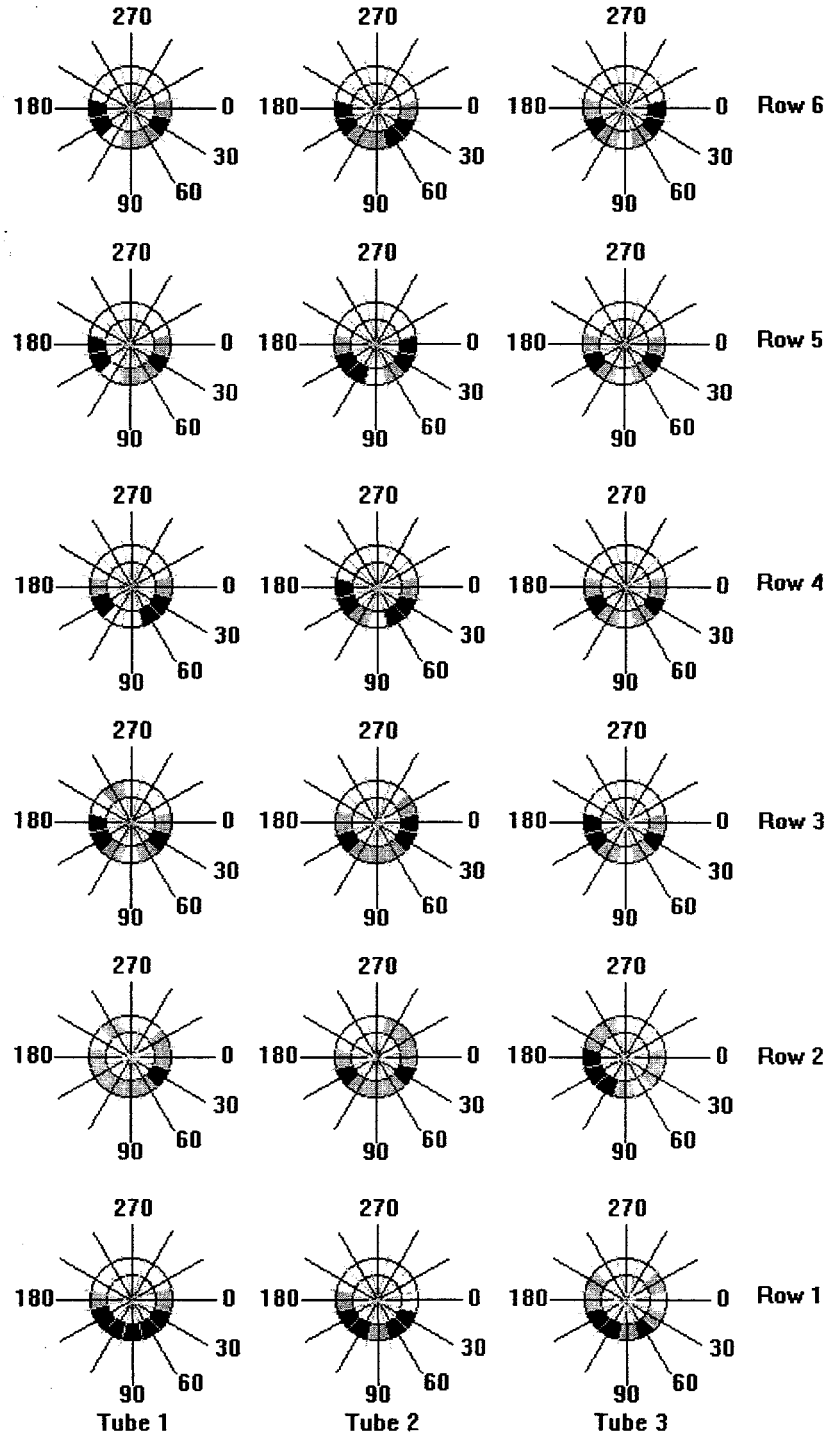

Figure 5.9 Erosion rates at different angles in the in-line tube bank

5.9.4 EROSION AS A FUNCTION OF COLLISION ANGLE IN THE STAGGERED TUBE BANK

Analysis of the staggered tube bank was done separately for each tube at every collision angle. The number of tubes in the staggered tube bank was 15 and the amount of measurements was 36 at every angle. There were four tests and six angles in the diameter measurement analyses. In Table 5.15 the results of the analyses are presented as erosion rate compared to the average erosion on the perimeter of a test sleeve. When standing in front of the test channel the left-hand side tube in the first row is marked as Tube 1, the middle tube as Tube 2, the right-hand side tube as Tube 3, and the left-hand side tube in the second row as Tube 4, and so on. In most of the Table 5.15 analyses the coefficient of determination was high.

Table 5.15 Erosion rate as a function of collision angle in the staggered tube bank by diameter measurements

Tube	0°	30°	60°	90°	120°	150°	Row
1	0.51	1.0	1.3	0.88	1.3	0.91	1
2	0.53	0.96	1.3	0.81	1.4	0.99	
3	0.70	0.71	1.1	0.98	1.1	1.3	
4	0.31	0.37	1.4	2.0	1.6	0.39	2
5	0.29	0.26	1.6	1.9	1.5		
6	1.3	0.60	0.32	0.47	1.4	1.9	3
7	0.54	0.78	1.4	1.3	1.4	0.57	
8	1.2	1.8	1.4		0.40	0.64	
9	0.41	0.42	0.70	1.1	2.2	1.2	4
10			2.1	1.4	0.93		
11	1.2	0.22		0.48	1.7	2.3	5
12	1.2	0.97		0.90	1.1		
13		2.4	2.1	0.65	0.33		
14	0.57		1.2	1.2	1.3		6
15	0.81		1.5	1.1	1.2		

A wall thickness measurement analysis was conducted separately for each tube at every collision angle. In the analysis there were 36 measurements at every angle for one tube. In Table 5.16 the results of the analyses are shown as erosion rate compared to the average erosion rate on the perimeter of a test sleeve.

Table 5.16 Erosion rate as a function of collision angle in the staggered tube bank by wall thickness measurements

Tube	0°	30°	60°	90°	120°	150°	180°	Row
1	0.96	1.8	1.9	1.6	2.2	1.2	0.40	1
2		1.9	2.0	1.5	2.2	1.4		
3			2.1	1.6	1.7	2.3		
4			2.8	3.5				2
5			3.5	3.1	2.2		0.50	
6	1.1		0.61	1.1	2.3	2.3		3
7		1.3	1.9	2.0	1.5			
8		2.6	1.9					
9				1.5	2.3			4
10		1.5	2.9		1.0			
11				1.3	3.2	4.0		5
12		1.4		1.5		1.6		
13		4.4	2.9					
14		1.4		1.6				6
15		1.7	2.0	1.2				

The coefficients of determination in Table 5.16 analyses at angles ranging from 210° to 330° were mostly low. Only at an angle of 330° in rows 6 and 12 was the coefficient of determination higher than 0.70 where the corresponding erosion rate values were 1.0 and 0.89, respectively. The angles higher than 180° were omitted from the table. In Tables 5.17 and 5.18 the values from Tables 5.15 and 5.16 divided by the value at an angle of 90° are presented.

Table 5.17 Erosion rates at different angles compared to the erosion rate at an angle of 90° by diameter measurements

Tube	0°	30°	60°	90°	120°	150°	Row
1	0.58	1.1	1.5	1.0	1.5	1.0	1
2	0.65	1.2	1.6	1.0	1.7	1.2	
3	0.71	0.72	1.1	1.0	1.1	1.3	
4	0.16	0.19	0.7	1.0	0.80	0.20	2
5	0.15	0.14	0.84	1.0	0.79		
6	2.8	1.3	0.68	1.0	3.0	4.0	3
7	0.42	0.60	1.1	1.0	1.1	0.44	
9	0.37	0.38	0.64	1.0	2.0	1.1	4
10			1.5	1.0	0.66		
11	2.5	0.45		1.0	3.5	4.8	5
12	1.3	1.1		1.0	1.2		
13		3.7	3.2	1.0	0.51		
14	0.48		1.0	1.0	1.1		6
15	0.74		1.4	1.0	1.1		

Table 5.18 Erosion rates at different angles compared to the erosion rate at an angle of 90° by wall thickness measurements

Tube	0°	30°	60°	90°	120°	150°	180°	Row
1	0.61	1.1	1.2	1.0	1.4	0.75	0.25	1
2		1.3	1.3	1.0	1.5	0.93		
3			1.3	1.0	1.1	1.4		
4			0.80	1.0				2
5			1.1	1.0	0.71		0.16	
6	1.0		0.55	1.0	2.1	2.1		3
7		0.65	0.95	1.0	0.75			
9				1.0	1.5			4
11				1.0	2.5	3.1		5
12		0.93		1.0		1.1		
14		0.88		1.0				6
15		1.4	1.7	1.0				

It can be seen from Tables 5.17 and 5.18 that the distribution of erosion wear on the perimeter of a test sleeve is different in different rows. In the first row, the erosion rate distribution is similar to in the three tube construction. In the second row, the erosion wear is concentrated at an angle of 90° because of the construction. In rows 3 to 6 there is obviously more turbulence in the flow leading to a high variance in the erosion rates. In Figure 5.9 the erosion rates in the staggered tube bank based on the values of Tables 5.15 and 5.16 are presented. In the white areas the erosion rate compared to the average erosion rate is lower than 0.5, in the grey areas from 0.5 to 1.5 and in the black areas 1.5 or higher. It can be seen from Figure 5.9 that the erosion rate is high at angles of 30°, 60°, 90°, 120° and 150° in most tubes.

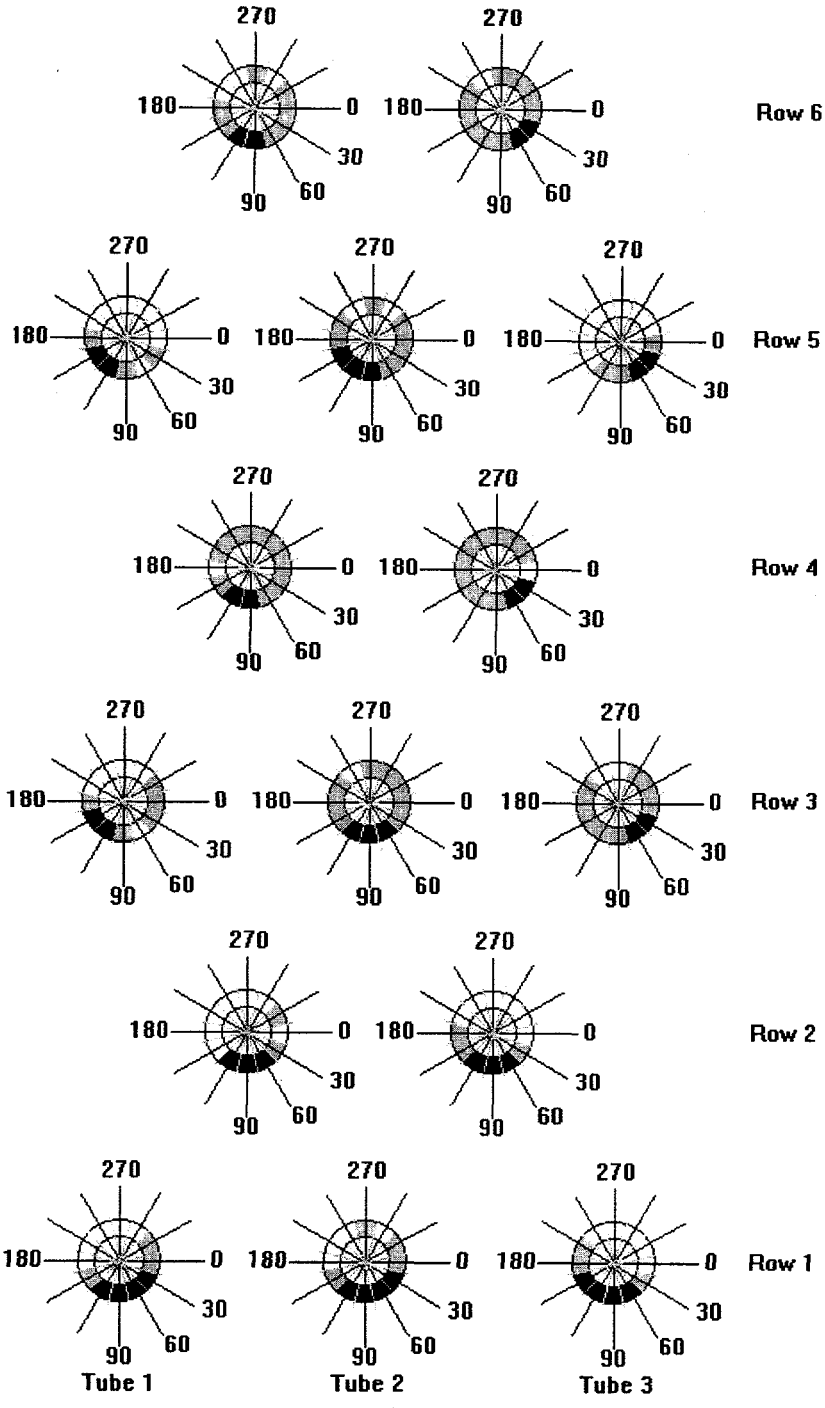

Figure 5.10 Erosion rates at different angles in the staggered tube bank

5.9.5 CONCLUSIONS OF TUBE DIAMETER AND WALL THICKNESS MEASUREMENT ANALYSES

The erosion rate in the first row, on the basis of the previous analyses, acted in the same way at different angles in different tube constructions. The maximum erosion rate occurred on the perimeter of a tube at angles of 60° and 120°. High erosion rates also occurred at angles of 30° and 150°. Erosion rates at angles higher than 180° were mostly rather low.

In the in-line tube bank, the rows from 2 to 6 were shielded by the previous rows, especially at an angle of 90°. The erosion rate was high at angles of 0°, 30°, 150° and 180°. In the second and third row, there also occurred moderate erosion wear at angles higher than 180°. In the staggered tube bank the first row concentrated the particle flow at angles of 60°, 90° and 120° on the second row. In rows 3 to 6 there occurred moderate or high erosion wear at angles of 0° to 180°. In the staggered tube bank, moderate erosion wear occurred at angles higher than 180° in rows 3, 4 and 6.

Erosion rate values varied in the different tubes from 50 % to 140 % in the three tube construction, from 50 % to 950 % in the in-line tube bank, and from 15 % to 480 % in the staggered tube bank compared to the erosion rate at an angle of 90° in the respective tubes. The variation of the erosion rate in different tubes and at different angles was very high.

According to literature the maximum erosion angle in ductile materials occurs at collision angles of from 40° to 60° (whereas from 30° to 50° and 130° to 150° by the definition of this study) with respect to the coming flow in the case of a single tube and the first row tubes of tube banks and between 20° and 40° with respect to the coming flow for the second row tubes in a staggered tube bank (Jianren, Dadong, Kefa, 1989). In a staggered tube bank on the second row the maximum erosion occurs at an angle of 60° with respect to the coming flow (Kuznetsov, 1958). The results of the analyses in this study corresponded to these values for a single tube row, or the first tube row in a tube bank. For the second tube row in a staggered tube bank, the results corresponded to the values presented by Jianren, Dadong and Kefa, but were different from the values presented by Kuznetsov.

6 DETERMINING THE EROSION RATE

6.1 INTRODUCTION

In this chapter, erosion wear calculation equations as a function of material and flow parameters based on erosion test results are developed. This analysis must contain all the parameters studied separately in Chapter 5, where the analysis was done with one variable at a time. The results of the analyses in Chapter 5 can be used as support in formulating erosion as a whole phenomena.

In literature, erosion wear has been found to depend on the properties of the target material, and with metal alloys especially on tensile strength, hardness, and toughness (Levy, 1982; National Materials Advisory Board, 1977). Different combinations have been made from these material properties to describe the energy absorption ability of target material proportional to the erosion resistivity of the material (Rao, Bucley, 1984). The properties of the target material are not enough to explain erosion wear. Particle properties such as particle size distribution, particle hardness and shape and particle mass or particle concentration in the flow correlates to erosion wear (Reid, 1984; Raask, 1979). Obviously the kinetic energy of the particles is proportional to the erosion wear of the target material and the erosion wear rate depends on the velocity of the particles to a power higher than two (Raask, 1979; Jianren, Dadong, Kefa, 1989). In this study, the formulation of erosion wear is based on mass loss measurements of test sleeves. Test sleeve diameter and wall thickness measurements were not used because of their lower accuracy compared to mass loss measurements.

6.2 BASICS OF EROSION WEAR FORMULATION

The formulation of erosion wear in this study is partly based on the equation of Kuznetsov (1958). When one wants to formulate the erosion wear caused by ash particles on steam boiler convection heat exchanger tubes, it is obvious that the erosion wear rate must be proportional to

- particle erosiveness described, for example, by the size, hardness or shape of the particles
- particle mass or particle concentration in the gas flow
- target material properties described, for example, by the strength or toughness of the material

- particle velocity to a power higher than two
- time.

In Kuznetsov's equation as presented in Chapter 2, erosion wear is calculated as wall thickness loss which is proportional to

- erosivity of ash
- target material erosion resistivity coefficient
- a coefficient representing irregularities in particle flow distribution in the cross-sectional area of flow channel
- particle concentration in gas flow
- collision probability of particles
- a coefficient representing irregularities in gas velocity distribution in the cross-sectional area of flow channel
- flow velocity to the power of three
- time.

When starting to develop erosion wear equations, the coefficients in Kuznetsov's equation representing irregularities in particle flow and velocity distributions were left out as they represent local conditions in a certain flow channel or steam boiler type. In the test facility, it was tried to get the particle flow distribution and flow velocity distribution as even as possible on the cross-sectional area of the test channel. The flow velocity distributions in the constructions and flow parameters used in the tests were discussed in Chapter 4. The collision probability of particles in Kuznetsov's equation was taken as part of the parameter describing particle material properties. The exponent of flow velocity was taken as a variable.

Basic parameters describing erosion wear were

- parameter representing erosion properties of particles
- particle concentration in the gas flow
- parameter representing properties of target material
- velocity of gas flow
- time.

Some parameters describing the test facility must be added to these parameters. These were the horizontal and vertical locations of test sleeves in the test channel.

6.3 PROPERTIES OF PARAMETERS USED IN ANALYSES

Particle size, hardness and shape have a large effect on erosion wear. To simplify the study, the average particle diameter was taken to describe particle erosiveness. The particle size distribution was taken into account by the collision probability coefficient calculated by the method of Kuznetsov. As the particle concentration parameter, the particle mass flow fed into the air divided by the air volume flow was taken. It proved useful to combine the particle material parameter and particle concentration into one parameter describing the properties of the particle flow. The collision probability coefficient multiplied by the average particle size multiplied by the particle concentration was taken to describe the particle flow properties in the regression analyses.

Many tube material properties have been found to correlate to erosion wear. These are, for example, hardness, toughness and yield strength. The toughness values of tube materials were measured and the reciprocal of the toughness proved to be an appropriate tube material parameter. Because of the asymmetrics in the location of test sleeves of a certain material, the horizontal location parameter was combined with the tube material parameter in the regression analyses.

The velocity at the centre-line of the first tube row in the test channel was taken as the velocity parameter of the air flow. Velocity and particle mass flow distributions were taken into account by the horizontal location parameters. The test periods used in tests were taken as time parameter. The test results that were part of a test series with the same flow parameters were taken as cumulative in the regression analyses.

6.4 ADAPTATION OF MULTI-VARIABLE LINEAR REGRESSION ANALYSIS

6.4.1 INTRODUCTION

Linear regression analysis was adapted separately on the different tube constructions: three tube construction, in-line tube bank and staggered tube bank. The purpose of the use of regression analyses was to define erosion calculation equations composed of parameters with a high correlation to erosion wear. The reliability of the analysis was studied by the coefficient of determination which should have a value as high as possible, but lower than 1.00, and by the t-value as an absolute value of the parameters. The absolute

value of t should be higher than two. Also, the figures of the residuals of the parameters were drawn by the program and are presented in Appendix B.

The process used in the analyses was to do the first analysis with all the parameters included, and then leave out in the second analysis the parameters with low absolute values of t. In the final analysis, the coefficient of determination should be high and the absolute values of t for all the parameters higher than two.

6.4.2 EROSION WEAR EQUATION

Erosion wear can be formulated in general as

$$\Delta m^* \approx a^{a_1} \cdot b^{b_1} \cdot w^{w_1} \cdot c^{c_1} \cdot d^{d_1} \cdot h^{h_1} \cdot t^{t_1} \tag{6.1}$$

where Δm^* is dimensionless test sleeve mass loss,
a is particle material parameter,
b is tube material parameter,
w is air flow velocity,
c is test sleeve location in the x-direction,
d is test sleeve location in the y-direction,
h is test sleeve location in the z-direction,
t is time,
a_1 is particle material exponent,
b_1 is tube material exponent,
w_1 is air flow velocity exponent,
c_1 is exponent of test sleeve location in the x-direction,
d_1 is exponent of test sleeve location in the y-direction,
h_1 is exponent of test sleeve location in the z-direction, and
t_1 is time exponent.

When a proportionality factor G_0 is defined, the equation can be written as

$$\Delta m^* = G_0 \cdot a^{a_1} \cdot b^{b_1} \cdot w^{w_1} \cdot c^{c_1} \cdot d^{d_1} \cdot h^{h_1} \cdot t^{t_1} \tag{6.2}$$

6.4.3 LINEARISATION OF THE EQUATION

Equation 6.2 can be linearised by taking a logarithm on both sides of the equation. Erosion wear as a function of each parameter should be a continuing function and not have local minimum or maximum values. On the basis of the observations in Chapter 5, erosion wear can be considered as continuing as a function of every parameter. Erosion wear has local minimum and maximum values as a function of parameter h in different tube rows as presented in Figure 5.5. Erosion wear as a function of vertical location can be linearised by reducing the erosion wear of the tube rows to the erosion wear of the first row using the erosion coefficients defined in Tables 5.4 and 5.6.

The equation 6.2 can be written as

$$\ln\left(\Delta m^*\right) = \ln\left(\mathrm{G}_0 \cdot a^{a_1} \cdot b^{b_1} \cdot w^{w_1} \cdot c^{c_1} \cdot d^{d_1} \cdot h^{h_1} \cdot t^{t_1}\right) \tag{6.3}$$

$$\Leftrightarrow \ln\left(\Delta m^*\right) = \ln \mathrm{G}_0 + \ln a^{a_1} + \ln b^{b_1} + \ln w^{w_1} + \ln c^{c_1} + \ln d^{d_1} + \ln h^{h_1} + \ln t^{t_1} \tag{6.4}$$

$$\Leftrightarrow \ln(\Delta m^*) = \ln \mathrm{G}_0 + a_1 \cdot \ln a + b_1 \cdot \ln b + w_1 \cdot \ln w + c_1 \cdot \ln c + d_1 \cdot \ln d + h_1 \cdot \ln h + t_1 \cdot \ln t \tag{6.5}$$

This equation is linear and linear regression analysis can be adapted to find the values of coefficients. The results of the linear regression analysis are presented in the form

$$\Delta m^* = e^{\ln \mathrm{G}_0} \cdot a^{a_1} \cdot b^{b_1} \cdot w^{w_1} \cdot c^{c_1} \cdot d^{d_1} \cdot h^{h_1} \cdot t^{t_1} \tag{6.6}$$

When defining $\mathrm{G} = e^{\ln \mathrm{G}_0}$, equation 6.6 can be re-written as

$$\Delta m^* = \mathrm{G} \cdot a^{a_1} \cdot b^{b_1} \cdot w^{w_1} \cdot c^{c_1} \cdot d^{d_1} \cdot h^{h_1} \cdot t^{t_1} \tag{6.7}$$

6.4.4 COLLISION PROBABILITY COEFFICIENT OF PARTICLES

The collision probability coefficients of particles were calculated by the method presented by Dergatshev and Zalogin. The collision probability coefficient is a function of parameter K, as presented in Chapter 2. The parameter K was calculated for one particle size fraction at a time and as a function of K the collision probability coefficient for a certain particle size fraction was given by Figure 2.10. The collision probability coefficient for the whole particle material was calculated from the Equation 2.3.

The parameters needed to calculate the collision probability coefficients were:

- Density of the particle material, quartz 1600 kg/m^3, coal ash 1000 kg/m^3 and peat ash 775 kg/m^3.
- Particle size fractions, 10 %, 25 %, 50 %, 75 %, and 90 % of the volume of the sample.
- Air velocity at the centre-line of the tube row, 30 m/s, 20 m/s and 13 m/s for three tube rows and 20.4 m/s, 13.6 m/s and 8.8 m/s for two tube rows.
- Dynamic viscosity of air at temperature +20 °C, 18.0 x 10^{-6} kg/ms.
- Test sleeve nominal outer diameter 38 mm.

In Table 6.1, particle size volume fractions and average particle diameters in different tests or test series are presented. One analysed particle size distribution was used to represent the particle size distribution in a certain test or test series. In Table 6.2, calculated collision probability coefficients for different particle size fractions and the collision probability coefficient for the whole particle material are presented. The average particle sizes of the fractions are used in calculating the collision probabilities of particle fractions 10 to 25 %, 25 to 50 %, 50 to 75 % and 75 to 90 %. The particle size values of Table 6.1 were used in the calculation of collision probabilities of particle fractions 0 to 10 % and 90 to 100 %. In the tests or test series with the staggered tube bank, the latter of the values is the collision probability in two tube rows.

Table 6.1 Particle size volume fractions and average particle diameters

Test series	Fraction 10 %, Maximum Particle Size	Fraction 25 %, Maximum Particle Size	Fraction 50 %, Maximum Particle Size	Fraction 75 %, Maximum Particle Size	Fraction 90 %, Maximum Particle Size	Average particle size
	μm	μm	μm	μm	μm	μm
1	98.00	128.8	172.4	235.1	319.8	192.1
4	105.8	143.0	199.7	283.6	376.2	221.4
7	105.8	143.0	199.7	283.6	376.2	221.4
2	54.05	94.16	142.6	209.0	301.7	162.3
5	57.73	93.29	133.8	184.7	249.0	146.1
8	54.91	96.32	146.1	211.3	290.9	161.1
3	55.70	91.22	137.9	205.1	307.8	161.6
6	56.34	83.95	118.3	162.3	217.4	130.1
9	52.73	90.92	139.2	206.5	309.1	162.0
10	96.92	128.5	175.0	243.4	331.9	197.0
13	107.7	142.4	196.0	275.4	375.0	220.2
16	79.86	118.4	168.7	239.6	326.4	186.8
11, 14, 17	54.41	103.2	164.0	244.6	344.2	183.6
12, 15, 18	54.41	103.2	164.0	244.6	344.2	183.6
19, 22, 25	61.52	100.1	148.9	217.0	308.2	168.1
20, 23, 26	60.88	97.97	144.5	212.2	316.3	168.5
21, 24, 27	61.52	100.1	148.9	217.0	308.2	168.1
28, 31, 34	64.27	114.3	166.7	235.7	321.6	181.1
29, 32, 35	122.9	155.4	205.9	276.1	353.6	223.6
30, 33, 36	62.38	113.9	164.4	224.3	292.1	172.0
37, 40, 43	58.87	109.3	159.0	220.1	295.2	170.0
38, 41, 44	68.01	113.2	158.2	213.1	279.6	167.2
39, 42, 45	73.72	118.9	166.7	227.3	301.2	178.4
46, 49, 52	73.72	118.9	166.7	227.3	301.2	178.4
47, 50, 53	60.06	98.09	137.0	183.0	237.8	145.0
48, 51, 54	60.85	103.7	145.0	192.4	247.6	151.7
CA 4, 5	2.141	6.325	17.70	50.90	99.22	39.38
PA 1	2.071	6.743	18.94	48.62	112.6	41.90
Q 1	38.78	73.20	116.2	171.1	232.5	127.9
Q 2	32.69	69.35	123.8	189.7	262.1	137.7
Q 3	62.49	107.0	181.2	280.2	369.4	200.4

Table 6.2 Collision probability coefficients

Test series	Fraction 0 - 10 %	Fraction 10 - 25 %	Fraction 25 - 50 %	Fraction 50 - 75 %	Fraction 75 - 90 %	Fraction 90 - 100 %	Total
1	0.98	0.98	0.98	0.98	0.98	0.98	0.980
4	0.98	0.98	0.98	0.98	0.98	0.98	0.980
7	0.98	0.98	0.98	0.98	0.98	0.98	0.980
2	0.95	0.97	0.98	0.98	0.98	0.98	0.976
5	0.96	0.98	0.98	0.98	0.98	0.98	0.978
8	0.95	0.98	0.98	0.98	0.98	0.98	0.977
3	0.95/0.90	0.97/0.96	0.98/0.98	0.98/0.98	0.98/0.98	0.98/0.98	0.976/0.969
6	0.95/0.90	0.97/0.96	0.98/0.98	0.98/0.98	0.98/0.98	0.98/0.98	0.976/0.969
9	0.94/0.87	0.97/0.96	0.98/0.98	0.98/0.98	0.98/0.98	0.98/0.98	0.975/0.966
10	0.98	0.98	0.98	0.98	0.98	0.98	0.980
13	0.98	0.98	0.98	0.98	0.98	0.98	0.980
16	0.97	0.98	0.98	0.98	0.98	0.98	0.979
11,14,17	0.89	0.96	0.98	0.98	0.98	0.98	0.968
12,15,18	0.89/0.79	0.96/0.94	0.98/0.98	0.98/0.98	0.98/0.98	0.98/0.98	0.968/0.955
19,22,25	0.85	0.94	0.98	0.98	0.98	0.98	0.961
20,23,26	0.85	0.94	0.98	0.98	0.98	0.98	0.961
21,24,27	0.85/0.74	0.94/0.88	0.98/0.97	0.98/0.98	0.98/0.98	0.98/0.98	0.961/0.939
28,31,34	0.87	0.96	0.98	0.98	0.98	0.98	0.966
29,32,35	0.98	0.98	0.98	0.98	0.98	0.98	0.980
30,33,36	0.85/0.76	0.96/0.92	0.98/0.98	0.98/0.98	0.98/0.98	0.98/0.98	0.964/0.949
37,40,43	0.92	0.97	0.98	0.98	0.98	0.98	0.973
38,41,44	0.95	0.97	0.98	0.98	0.98	0.98	0.976
39,42,45	0.96/0.51	0.98/0.97	0.98/0.98	0.98/0.98	0.98/0.98	0.98/0.98	0.978/0.932
46,49,52	0.97	0.98	0.98	0.98	0.98	0.98	0.979
47,50,53	0.96	0.98	0.98	0.98	0.98	0.98	0.978
48,51,54	0.96/0.93	0.98/0.97	0.98/0.98	0.98/0.98	0.98/0.98	0.98/0.98	0.978/0.974
CA 4,5	0	0.01	0.06	0.38	0.83	0.94	0.330
PA 1	0	0.01	0.04	0.32	0.80	0.94	0.304
Q 1	0.59	0.80	0.97	0.98	0.98	0.98	0.912
Q 2	0.49	0.75	0.97	0.98	0.98	0.98	0.894
Q 3	0.85	0.95	0.98	0.98	0.98	0.98	0.963

It can be seen from Table 6.2 that for quartz particles, in most fractions, the collision probability coefficients are high. This is caused by the large particle size of quartz. For coal and peat ash particles the collision probability coefficients are lower because of the smaller particle size.

6.4.5 ANALYSIS OF THREE TUBE CONSTRUCTION

The analysis matrix consisted of the test series done with the three tube construction, 16 tests with 27 measurements in each test. Erosion wear rate was analysed as the relative mass loss value of a test sleeve (test sleeve mass loss divided by test sleeve mass before the test as a percentage value).

Parameters used to explain erosion wear:

- Particle material property *a* was the collision probability coefficient times the average particle diameter times the particle concentration, 375 g/m^3 or 20 g/m^3. When the unit of the particle diameter is in m, the unit of the particle material parameter is g/m^2.

- Tube material property *b* was 1/(test sleeve material toughness times the test sleeve location in y-direction). Test sleeve material toughness values were measured as the strike energy needed to bend test rods (Charpy V impact test). The values were 9.8 J for St35.8, 10.1 J for 15Mo3 and 10.8 J for 10CrMo910. The units of the tube material parameter are 1/(J mm).

- Velocities *w* were 30 m/s, 20 m/s and 13 m/s.

- Test sleeve locations *c*, in x-direction, were 59 mm, 1 mm and 59 mm. Test sleeve location *c* is the distance between the test sleeve centre-point and the centre-point of the test channel. As a location coordinate of the middle of the test sleeves, 1 mm was used instead of 0 mm because the value 0 can't be used in the regression analysis.

- Test sleeve locations *d*, in y-direction, were 181 mm, 141 mm, 101 mm, 40 mm, 1 mm, 40 mm, 101 mm, 141 mm and 181 mm. Test sleeve location *d* is the distance between the test sleeve centre-point and centre-point of the channel. As a location coordinate of the middle of the test sleeves, 1 mm instead of 0 mm was used because the value 0 can't be used in the regression analysis.

- Time periods *t* in the tests were 10 h, 20 h, 50 h, 100 h, 150 h and 300 h.

Linear regression analysis was carried out including all the above parameters. As the test sleeves were not placed symmetrically in the y-direction in the test facility and symmetric location coordinates was used, the location parameter *d*

was taken into the tube material parameter. There is a correlation between tube material parameter b and the location parameter d. The results of the first analysis are presented in Table 6.3.

Table 6.3 Results of regression analysis for three tube construction with all parameters included

Coefficient of determination 0.92		
Parameter	Coefficient	t-value
Constant	-12.0076	-7.6
Particle material, ln(a)	0.687	33
Tube material, ln(b)	-0.0701	-0.10
Velocity, ln(w)	3.67	44
Location in x-direction, ln(c)	-0.0118	-0.84
Location in y-direction, ln(d)	-0.162	-0.24
Time, ln(t)	0.553	17

It can be seen from Table 6.3 that the coefficient of determination is high. The absolute values of t of the parameters tube material, location c and location d are lower than two. When trying to maintain the tube material parameter in the analysis, the location parameters c and d were left out in the next analysis, the results of which are presented in Table 6.4.

Table 6.4 Final results of regression analysis for three tube construction

Coefficient of determination 0.92		
Parameter	Coefficient	t-value
Constant	-11.6657	-38
Particle material, ln(a)	0.687	33
Tube material, ln(b)	0.0915	5.2
Velocity, ln(w)	3.67	44
Time, ln(t)	0.553	17

The dimensionless mass loss of a test sleeve becomes

$$\Delta m^* = e^{-11.6657} \cdot a^{0.687} \cdot b^{0.0915} \cdot w^{3.67} \cdot t^{0.553} \cdot 6.60 \cdot 10^{-3} \cdot \frac{s^{2.93}}{kg^{0.596} \cdot m^{2.02}} \tag{6.8}$$

$$\Rightarrow \Delta m^* = 5.67 \cdot 10^{-8} \cdot a^{0.687} \cdot b^{0.0915} \cdot w^{3.67} \cdot t^{0.553} \cdot \frac{s^{2.93}}{kg^{0.596} \cdot m^{2.02}} \qquad (6.9)$$

The coefficient of determination and the absolute values of t of all the parameters in the analysis of Table 6.4 are high. An equation for the calculation of erosion wear in the three tube construction has been achieved.

6.4.6 ANALYSIS OF IN-LINE TUBE BANK

The regression analysis matrix consisted of all the test series done with the in-line tube bank, 8 tests with 162 measurements in each test. The erosion wear rate was analysed as the relative mass loss of a test sleeve (test sleeve mass loss divided by test sleeve mass before the test as a percentage value).

Parameters used to explain erosion wear:

- Particle material property *a* was the collision probability coefficient times the average particle diameter times the particle concentration, 375 g/m^3 or 20 g/m^3. When the units of the particle diameter is in m, the units of the particle material parameter is g/m^2. Only quartz particles were used in the tests.

- Tube material property *b* was 1/(test sleeve material toughness times the test sleeve location in the y-direction). Test sleeve material toughness values were measured as the strike energy needed to bend test rods (Charpy V impact test). The values were 9.8 J for St35.8, 10.1 J for 15Mo3 and 10.8 J for 10CrMo910. The units of the tube material parameter are 1/(J mm).

- Velocities w were 30 m/s, 20 m/s and 13 m/s.

- Test sleeve locations *c*, in the x-direction, were 59 mm, 1 mm and 59 mm. Test sleeve location *c* is the distance between the test sleeve centre-point and the centre-point of the test channel. As a location coordinate of the middle of the test sleeves, 1 mm instead of 0 mm was used because the value 0 can't be used in the regression analysis.

- Test sleeve locations d, in the y-direction, were 181 mm, 141 mm, 101 mm, 40 mm, 1 mm, 40 mm, 101 mm, 141 mm and 181 mm. Test sleeve location d is the distance between the test sleeve centre-point and centre-point of the channel. As the location coordinate of the middle of the test sleeves, 1 mm was used instead of 0 mm because the value 0 can't be used in the regression analysis.

- The location parameter coefficient h, in the z-direction, was 1 for the first row, 1/0.650 for the second row, 1/0.949 for the third row, 1/1.14 for the fourth row, 1/1.24 for the fifth row and 1/1.36 for the sixth row. Erosion rates in different tube rows were reduced to the erosion rate of the first row by the coefficients of Table 5.4.

- Time periods t used in the tests were 50 h, 100 h, 150 h and 300 h.

Linear regression analysis was done including all the above parameters. The location parameter in the y-direction was combined with the tube material parameter on the same reason as in three tube construction analysis. In Table 6.5 the results of the analysis are presented.

Table 6.5 Results of regression analysis for in-line tube bank with all parameters included

Coefficient of determination 0.88		
Parameter	Coefficient	t-value
Constant	-10.2805	-11
Particle material, ln(a)	0.609	48
Tube material, ln(b)	0.782	2.1
Velocity, ln(w)	3.44	61
Location in x-direction, ln(c)	0.00321	1.6
Location in y-direction, ln(d)	0.775	2.1
Location in z-direction, ln(h)	-0.977	-15
Time, ln(t)	0.577	12

In Table 6.5 the coefficient of determination is high and only the absolute value of t for parameter c is lower than two. The results of the analysis without parameter c are presented in Table 6.6.

Table 6.6 Results of regression analysis for in-line tube bank

Coefficient of determination 0.88		
Parameter	Coefficient	t-value
Constant	-10.2788	-11
Particle material, ln(a)	0.609	48
Tube material, ln(b)	0.783	2.1
Velocity, ln(w)	3.44	61
Location in y-direction, ln(d)	0.776	2.1
Location in z-direction, ln(h)	-0.956	-15
Time, ln(t)	0.577	12

In Table 6.6 all absolute values of t are higher than two. The tube material parameter b and location parameter d correlate with each other because of the definition of the tube material parameter. When trying to maintain the tube material parameter, the location parameter d was left out of the analysis. The results of the analysis are presented in Table 6.7.

Table 6.7 Final results of regression analysis for in-line tube bank

Coefficient of determination 0.87		
Parameter	Coefficient	t-value
Constant	-12.0793	-34
Particle material, ln(a)	0.609	48
Tube material, ln(b)	0.00795	2.6
Velocity, ln(w)	3.44	60
Location in z-direction, ln(h)	-0.955	-15
Time, ln(t)	0.577	12

It can be seen from the Table 6.7 that the coefficient of determination has remained almost as high as in previous analyses and the absolute values of t of all parameters are high. Hence, an equation for calculating the erosion wear in an in-line tube bank has been achieved.

The dimensionless mass loss of a test sleeve comes from the analysis of the Table 6.7 as

$$\Delta m^* = 3.20 \cdot 10^{-8} \cdot a^{0.609} \cdot b^{0.00795} \cdot w^{3.44} \cdot h^{-0.955} \cdot t^{0.577} \cdot \frac{\mathrm{s}^{2.85}}{\mathrm{kg}^{0.601} \cdot \mathrm{m}^{2.20}} \tag{6.10}$$

6.4.7 ANALYSIS OF STAGGERED TUBE BANK

The regression analysis matrix consisted of all the test series done with the staggered tube bank, 8 tests with 135 measurements in each test. Erosion wear rate was analysed as the relative mass loss of a test sleeve (test sleeve mass loss divided by test sleeve mass before the test as a percentage value).

Parameters used to explain erosion wear:

- Particle material property a was the collision probability coefficient times the average particle diameter times the particle concentration, 375 g/m^3 or 20 g/m^3. When the units of particle diameter is in m, the units of the particle material parameter is g/m^2. Only quartz particles were used in the tests.

- Tube material property b was 1/(test sleeve material toughness times the test sleeve location in the y-direction). Test sleeve material toughness values were measured as the strike energy needed to bend test rods (Charpy V impact test). The values were 9.8 J for St35.8, 10.1 J for 15Mo3 and 10.8 J for 10CrMo910. The units of tube material parameter are 1/(J mm).

- Velocities w were 30 m/s, 20 m/s and 13 m/s.

- Test sleeve locations c, in the x-direction, were 59 mm, 1 mm and 59 mm for three tube rows and 29,5 mm and 29,5 mm for two tube rows. The test sleeve location c is the distance between the test sleeve centre-point and the centre-point of the test channel. As the location coordinate of the middle of the test sleeves, 1 mm was used instead of 0 mm because the value 0 can't be used in the regression analysis.

- Test sleeve locations d, in the y-direction, were 181 mm, 141 mm, 101 mm, 40 mm, 1 mm, 40 mm, 101 mm, 141 mm and 181 mm. Test sleeve location d is the distance between the test sleeve centre-point and the centre-point of the channel. As the location coordinate of the middle of the test sleeves, 1 mm instead of 0 mm was used because the value 0 can't be used in the regression analysis.

- The location parameter h, in the z-direction, was 1 for the first row, 1/1.40 for the second row, 1/0.602 for the third row, 1/0.448 for the fourth row, 1/1.06 for the fifth row and 1/0.216 for the sixth row.

Erosion rates in different tube rows were reduced to the erosion rate of the first row by the coefficients listed in Table 5.4.

- Time periods t used in the tests were 50 h, 100 h, 150 h and 300 h.

Linear regression analysis was done including all the above parameters. The location parameter in the y-direction was taken into the tube material parameter for the same reason as in the three tube construction analysis. In Table 6.8 the results of the first analysis are presented.

Table 6.8 Results of regression analysis for staggered tube bank with all parameters included

Coefficient of determination 0.85		
Parameter	Coefficient	t-value
Constant	-12.8081	-11
Particle material, ln(a)	0.522	33
Tube material, ln(b)	-0.0502	-0.11
Velocity, ln(w)	3.30	47
Location in x-direction, ln(c)	0.199	17
Location in y-direction, ln(d)	-0.0919	-0.20
Location in z-direction, ln(h)	-0.967	-31
Time, ln(t)	0.600	10

In Table 6.8 the coefficient of determination is high and the absolute values of t are only lower than two for the tube material parameter b and location parameter d. It is obvious that the tube material parameter should be kept in the analysis and in the next analysis, presented in Table 6.9, the location parameter d is omitted.

Table 6.9 Results of regression analysis for staggered tube bank

Coefficient of determination 0.85		
Parameter	Coefficient	t-value
Constant	-12.5961	-28
Particle material, ln(a)	0.522	33
Tube material, ln(b)	0.0414	3.5
Velocity, ln(w)	3.30	47
Location in x-direction, ln(c)	0.199	16
Location in z-direction, ln(h)	-0.967	-31
Time, ln(t)	0.600	10

In the Table 6.9, the coefficient of determination is the same as in the previous analysis and the absolute values of t of all parameters are higher than two. The result of the analysis is satisfactory. However, another analysis without parameter c was carried out. The results are presented in Table 6.10.

Table 6.10 Results of regression analysis for staggered tube bank without horizontal location parameters

Coefficient of determination 0.81		
Parameter	Coefficient	t-value
Constant	-12.0158	-24
Particle material, ln(a)	0.521	29
Tube material, ln(b)	0.0414	3.1
Velocity, ln(w)	3.30	42
Location in z-direction, ln(h)	-0.918	-26
Time, ln(t)	0.599	8.9

In Table 6.10 the coefficient of determination is lower than in previous tables because the location parameter c was left out. A better correlation is achieved in Table 6.9.

The dimensionless mass loss of the test sleeve comes from the analysis shown in Table 6.9 as

$$\Delta m^* = 2.72 \cdot 10^{-8} \cdot a^{0.522} \cdot b^{0.0414} \cdot w^{3.30} \cdot c^{0.199} \cdot h^{-0.967} \cdot t^{0.600} \cdot \frac{s^{2.62}}{kg^{0.481} \cdot m^{2.33}} \tag{6.11}$$

7 RESULTS AND DISCUSSION

7.1 CONCLUSIONS OF THE ANALYSES

In Table 7.1 the exponents of the erosion wear calculation equations given in Chapter 6 are presented for all tube constructions. The exponents for particle material, velocity and time are in the same range. The exponents relating to location in the z-direction have almost the same values, and near unity, as expected due to the definition of the parameter. The tube material parameter has greater differences, the value of the exponent in the in-line tube bank is low compared to the values in other constructions. The location parameter c exists only in the staggered tube bank and the value of the exponent indicates that in the staggered tube bank the erosion wear rate is higher near the side walls of the test channel than in the middle area of the channel. Observations from the measurements confirm this. In the first row, erosion rates of the test sleeves in the middle tube are higher than erosion rates in the side tubes. However, in the third and fifth row, the erosion rates of the test sleeves in the middle tube are much lower than in the side tubes.

The effect of parameter c can be expressed as a location coefficient C. The value of C is 1.00 for the middle tube and 2.25 for the side rows of the three tube row and 1.96 for both tubes of the two tube row. In the analyses of Chapter 6, the location parameter d was connected to the tube material parameter b. When defining tube material parameter B without the location parameter d, the coefficient D is taken into the equations. In Table 7.2 the coefficient D as a function of location parameter d is presented. It can be seen from the values of Table 7.2 that the distribution of the velocity and particle mass flow in the y-direction is the flattest in the in-line tube bank and has a large variance in the three tube construction.

Table 7.1 Exponents of calculation equations

Exponents	Three tube construction	In-line tube bank	Staggered tube bank
Particle material, a_1	0.687	0.609	0.522
Tube material, b_1	0.0915	0.00795	0.0414
Velocity, w_1	3.67	3.44	3.30
Location in x-direction, c_1			0.199
Location in z-direction, h_1		-0.955	-0.967
Time, t_1	0.553	0.577	0.600

Table 7.2 Location coefficients in the y-direction, D

Location parameter d (mm)	Three tube construction	In-line tube bank	Staggered tube bank
1	1.00	1.00	1.00
40	0.71	0.97	0.86
101	0.66	0.96	0.83
141	0.64	0.96	0.82
181	0.62	0.96	0.81

Erosion wear rate as a function of the vertical location parameter h was linearized by reducing the erosion rates of tube rows two to six to the erosion rate of the first row by using the coefficients determined in Chapter 5. In Table 7.3, the vertical location coefficient H as a function of tube row in the in-line and staggered tube banks, as calculated from the values of Table 7.1, is presented.

Table 7.3 Vertical location coefficients, H

Configuration	Tube Row 1	Tube Row 2	Tube Row 3	Tube Row 4	Tube Row 5	Tube Row 6
In-line tube bank	1.00	0.66	0.95	1.13	1.23	1.34
Staggered tube bank	1.00	1.38	0.61	0.46	1.06	0.23

The dimensionless mass loss erosion rate of a test sleeve can be written in general form for the three tube construction as

$$\Delta m^* = 1.07 \cdot 10^{-7} \cdot a^{0.687} \cdot B^{0.0915} \cdot w^{3.67} \cdot t^{0.553} \cdot \mathrm{D} \cdot \frac{\mathrm{s}^{2.93}}{\mathrm{kg}^{0.596} \cdot \mathrm{m}^{2.11}} \tag{7.1}$$

for the in-line tube bank as

$$\Delta m^* = 3.38 \cdot 10^{-8} \cdot a^{0.609} \cdot B^{0.00795} \cdot w^{3.44} \cdot t^{0.577} \cdot \mathrm{D} \cdot \mathrm{H} \cdot \frac{\mathrm{s}^{2.85}}{\mathrm{kg}^{0.601} \cdot \mathrm{m}^{2.21}} \tag{7.2}$$

and for the staggered tube bank as

$$\Delta m^* = 9.16 \cdot 10^{-9} \cdot a^{0.522} \cdot B^{0.0414} \cdot w^{3.30} \cdot t^{0.600} \cdot \mathrm{C} \cdot \mathrm{D} \cdot \mathrm{H} \cdot \frac{\mathrm{s}^{2.62}}{\mathrm{kg}^{0.481} \cdot \mathrm{m}^{2.17}} \tag{7.3}$$

Erosion wear rate as mass loss per tube area (g/m^2) can be calculated for the three tube construction from the equation

$$q_A = 2.31 \cdot 10^{-6} \cdot a^{0.687} \cdot B^{0.0915} \cdot w^{3.67} \cdot t^{0.553} \cdot \mathrm{D} \cdot \frac{\mathrm{s}^{2.93}}{\mathrm{kg}^{-0.404} \cdot \mathrm{m}^{4.11}} \tag{7.4}$$

for the in-line tube bank from the equation

$$q_A = 7.30 \cdot 10^{-7} \cdot a^{0.609} \cdot B^{0.00795} \cdot w^{3.44} \cdot t^{0.577} \cdot \mathrm{D} \cdot \mathrm{H} \cdot \frac{\mathrm{s}^{2.85}}{\mathrm{kg}^{-0.399} \cdot \mathrm{m}^{4.21}} \tag{7.5}$$

and for the staggered tube bank from the equation

$$q_A = 1.98 \cdot 10^{-7} \cdot a^{0.522} \cdot B^{0.0414} \cdot w^{3.30} \cdot t^{0.600} \cdot \mathrm{C} \cdot \mathrm{D} \cdot \mathrm{H} \cdot \frac{\mathrm{s}^{2.62}}{\mathrm{kg}^{-0.519} \cdot \mathrm{m}^{4.17}} \tag{7.6}$$

In Chapter 5 the erosion wear rate as a function of one parameter at a time was analysed. Erosion wear rate as a function of particle concentration, which was assumed to be linear, was studied. As a result of the analysis, the erosion rate of a particle concentration of 375 g/m^3 compared to the erosion rate of a particle concentration of 20 g/m^3 was 10. When assuming the correlation to be exponential, the value of the exponent is approximately 0.8. In the calculation equations, the value of the exponent of particle material, which includes the particle concentration parameter, varies from a value of 0.687 in the three tube construction to a value of 0.522 in the staggered tube bank. The decrease in the magnitude of the exponent can be explained by the fact that the intensity of the particle flow turbulence increases in rows higher than one in the in-line and staggered tube bank. Hence, the local particle concentration in the tube bank has values of large variations and the erosion rate is proportional to a concentration parameter exponent lower than one.

As a result of the analyses of erosion rate as a function of flow velocity, it was found that erosion rate correlates to velocity to the power of 3.9 when comparing the erosion rate in a velocity of 30 m/s to the erosion rate in a velocity of 13 m/s, and 3.3 when comparing the erosion rate in a velocity of 20 m/s to that in a velocity of 13 m/s. In equations 7.1 to 7.3 the velocity exponents are 3.67, 3.44 and 3.30. Based on literature, a conclusion can be drawn that these values are in the right range.

In Table 7.4 some values of erosion wear as a function of time from Table 5.1 and the same values as calculated from equations 7.1 to 7.3 are presented. When the correlation between erosion rate and time is assumed to be exponential, the value of the exponent becomes 0.8. In equations 7.1 to 7.3 the value of the exponent of time varies from 0.553 in the three tube construction to 0.600 in the staggered tube bank.

Table 7.4 Erosion as a function of time

Test series	Erosion 100 h/ Erosion 50 h from Table 5.1	Erosion 150 h/ Erosion 50 h from Table 5.1	Erosion 100 h/ Erosion 50 h as calculated	Erosion 150 h/ Erosion 50 h as calculated
1,4,7	1.7	2.4	1.5	1.8
2,5,8	1.7	2.5	1.5	1.9
3,6,9	1.6	2.5	1.5	1.9

Erosion rate as a function of tube material was analysed in Chapter 5.7 with a result that the erosion rate of 15Mo3 compared to the erosion rate of St35.8 is 0.95, and the erosion rate of CrMo910 compared to that of St35.8 is 0.87. In all the calculation equations, the exponent of the tube material parameter b is very low and so the effect of the tube material on erosion rate is very low. Differences such as those calculated in Chapter 5.7 are not obtained from the equations. A reason for this is obviously the location correlation of the test sleeve in the test channel. A conclusion can be drawn that the values of analyses in Chapter 5.7 give the right ratio between the erosivity of tube materials.

The erosiveness of each particle material was calculated in Chapter 5.8 with a result that the erosion rate of coal ash particles compared to the erosion rate of quartz particles is 0.12 and the erosion rate of peat ash particles compared to that of quartz particles is 0.11. When calculated from equation 7.1, both values are 0.22. The reason for the differences in the particle erosiveness results is the low number of coal ash or peat ash tests and the short test periods.

New results for the erosion rate of different tube bank constructions were obtained in this study. In Figure 5.5, the behaviour of the erosion rate as a function of tube row number was presented. Erosion rate in the in-line tube bank has a minimum value in row 2, and after that the erosion rate increases slowly in the subsequent rows of the tube bank. The minimum value of tube row 2 can be explained by the shielding effect of the first row. In the in-line tube bank, the shielding effect of the previus rows can be observed in all row numbers from row 2 to 6. Erosion wear occurs mostly on the sides of the tubes, as can be seen from Figure 5.9. The increase in the erosion rate in the subsequent rows can be explained by the growing intensity of the gas and particle flow turbulence. The collisions of the particles with the tubes cause particles to rebound and decelerate in directions different from the direction of the main gas flow. Particles are also decelerated by interparticle collisions. The particle flow is separated from the gas flow, and there occurs high intensity local turbulence of the particle flow. Large eddies are developed causing a high erosion rate. Also, the downward flow of particles, which occurs especially near the walls, assists in the development of eddies.

In the staggered tube bank, the erosion rate has a maximum value in tube row 2 and a local maximum in row 5. The high erosion rate of row 2 can be explained by the construction, the particle flow is directed towards row 2 from the tube gaps of the first row, see Figure 5.10. The gas flow and the particle flow are separated because of the high momentum of the particles which cause them to keep their direction and not to follow the gas around the tubes. Particles collide with the front-side of the tubes of row 2 and their velocity is quickly decelerated, and when rebounding from the tubes, the velocity of some particles is even negative with respect to the coming flow. The incoming particles are decelerated because of collisions with the rebounding particles. The low erosion rates in rows 3 and 4 can be explained by the low velocity of particles, they haven't yet been accelerated to a velocity high enough to cause a high erosion rate. They have a low momentum and most particles are following the gas flow around the tubes. In tube row 5, the particles have been accelerated to a higher velocity and they cause the high erosion rate found in that row. Due to the high number of particle collisions and rebounds in row 5, the velocity of the particles is again low in row 6. The intensity of turbulence is growing in the areas of rows 3 and 4 and large-eddies in the particle flow are generated. The downward flow of particles near the walls of the test channel assists the generation of eddies. The velocity and direction of the gas flow and particle flow are separated in the area of row 2 and united again before row 5 and again separated in the area of row 5. It can be expected that if there were more tube rows, more maximum erosion rate values would occur, for example, in rows 8 and 11 with the tube diameter and spacings used

in this study. The frequency of the erosion maximum values is expected to be different with other tube diameters and tube spacings.

Another interesting result in these analyses is that the erosion rate of the staggered tube bank is considerably lower than that of the in-line tube bank in all the rows but the second. The erosion rate of the second row in the staggered tube bank is about 180 % compared to the erosion rate in the in-line tube bank. The staggered tube bank is generally considered to have a higher erosion rate than the in-line tube bank because of flow channelling caused by plugging. From this study a conclusion can be drawn that if the staggered tube bank is kept unplugged by soot blowing, this type of construction can also be used when burning solid fuels when the high erosion rate of the second row is controlled.

When comparing the erosion rate of the first row in the in-line tube bank and in the staggered tube bank to the erosion rate of the three tube construction, the result was that the erosion rate in the first row of the in-line and the staggered tube banks was 54 % and 45 % of the erosion rate in the three tube construction, respectively. This indicates that the higher flow resistance and intensity of the turbulence in both the tube banks have a reducing influence on the erosion rate of the first row.

7.2 COMPARISON OF CALCULATED EROSION RATE TO MEASURED

In Figure 7.1, the calculated percentage erosion mass loss is presented as a function of particle material parameter a, in Figure 7.2 as a function of tube material parameter B, and in Figure 7.3 as a function of velocity for the three tube construction, all with the flow values of test number 1. Measured values are not plotted in these figures. In Figure 7.1, erosion mass loss as a function of particle material for test sleeves in the middle part of the flow channel (test sleeve number 5) are plotted. The erosion rate of the material 15Mo3 is higher than the others. This is because of the location of the test sleeve of this material in the middle point of the test channel, whereas the test sleeves of the other two materials were placed beside it. For example, the value of the particle material parameter in test 1 was about 0.07 g/m^2 and in tests CA 4 and PA 1 it was 0.005 g/m^2. In Figure 7.2, the erosion rate of the test sleeves in the middle part of the test channel (test sleeve number 5) is almost linear as a function of tube material parameter B. The values of the tube material parameters were 0.102 1/J for St35.8, 0.099 1/J for 15Mo3 and 0.093 1/J for 10CrMo910. In Figure 7.3, the erosion rate of the test sleeve of material

15Mo3 is higher than the others for the same reason as in Figure 7.1. The velocities used in the tests were 13 m/s, 20 m/s and 30 m/s. It can be seen from Figures 7.1 to 7.3 that the erosion wear rate as a function of these parameters behaves in such a way as is expected.

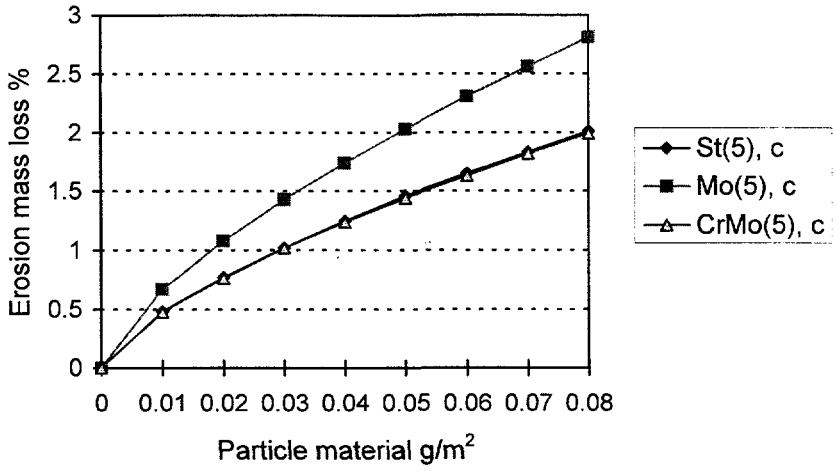

Figure 7.1 Erosion rate as a function of particle material parameter

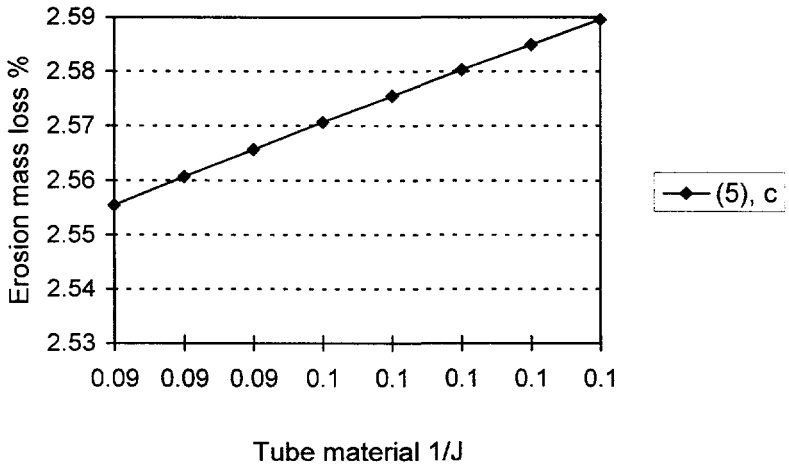

Figure 7.2 Erosion rate as a function of tube material parameter

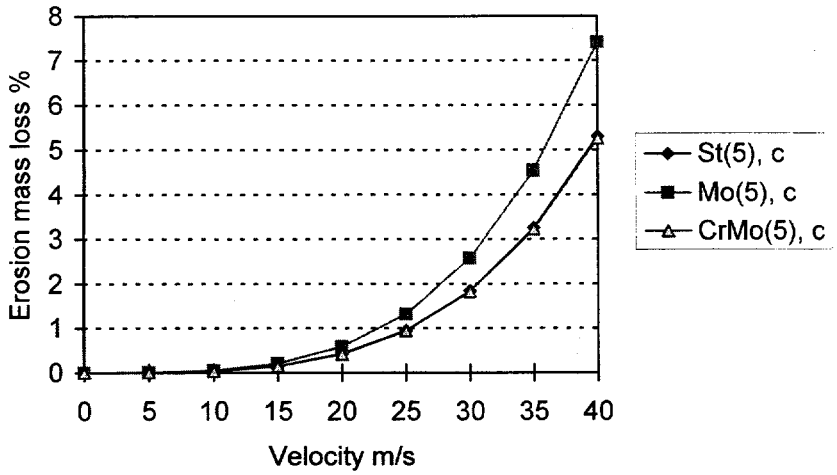

Figure 7.3 Erosion rate as a function of velocity

In Figure 7.4 percentage mass losses of the test sleeves in the middle part of the flow channel (number 14 in the first row) in the in-line tube bank is presented as a function of tube row number in test number 2. In Figures 7.5 to 7.7 the percentage mass losses of the test sleeves in the diagonal location from the left to right and front to back walls (numbers 64, 68 and 72 in the first row and 73, 77 and 78 in the second row) in the staggered tube bank as a function of tube row number in test 3 are presented. It can be seen from Figure 7.4 that the measured and calculated values are close to each other in the in-line tube bank, whereas in the staggered tube bank there are great differences, especially in the sleeves near the front wall, see Figure 7.5.

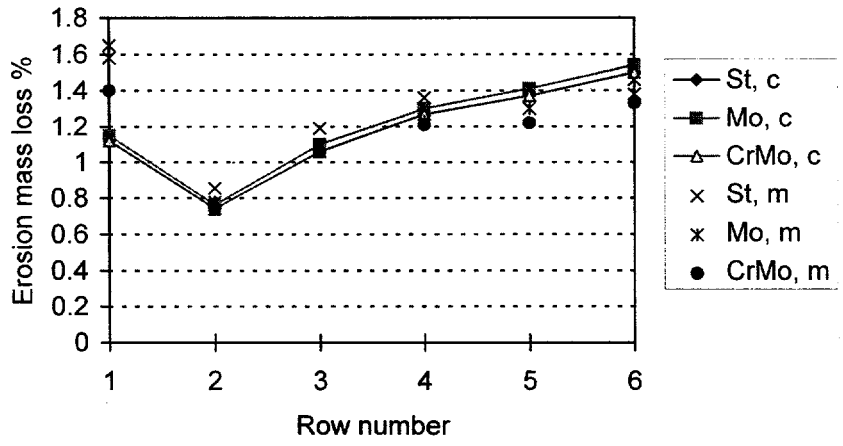

Figure 7.4 Calculated, c, and measured, m, erosion rates as a function of row number in in-line tube bank

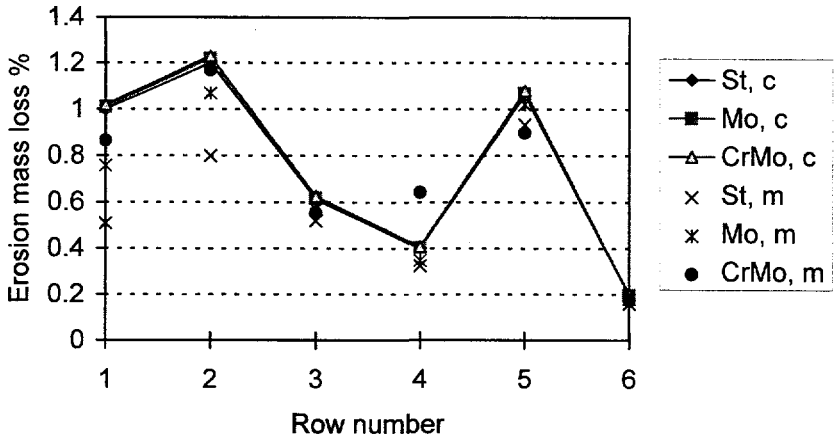

Figure 7.5 Calculated, c, and measured, m, erosion rates as a function of row number in staggered tube bank, test sleeves near the front wall

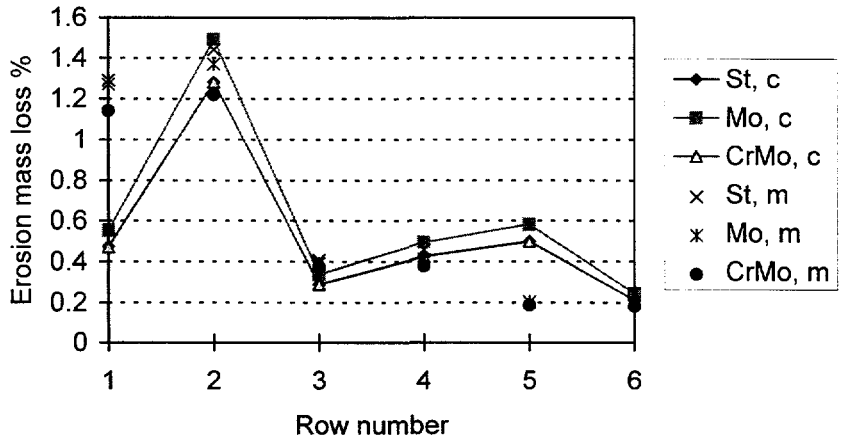

Figure 7.6 Calculated, c, and measured, m, erosion rates as a function of row number in staggered tube bank, test sleeves in middle part of the channel

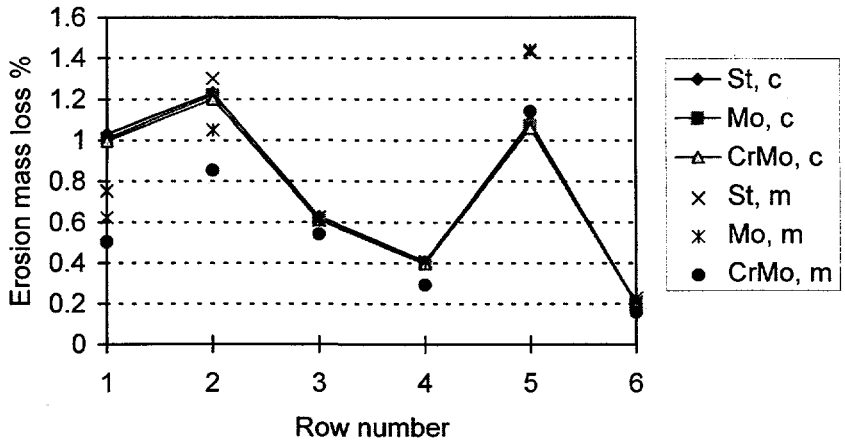

Figure 7.7 Calculated, c, and measured, m, erosion rates as a function of row number in staggered tube bank, test sleeves near the back wall

In Figure 7.8, the percentage mass losses of test sleeves 1, 5 and 9 of material St35.8 are presented as a function of time in the form of the calculated and measured values from the test series 1, 4, 7. The values were calculated using the particle material parameter from test 1. The test sleeves numbered 1 were located at the left side and near the front wall of the test channel, and the test sleeves numbered 9 at the right side and near the back wall of the test channel. Test sleeves numbered 5 were located in the middle area of the test channel. It can be seen that the erosion rate per unit time decreases as time increases. However, the value of the particle material parameter is different in different tests. In Figure 7.9 the same values are plotted using the particle material parameter of each test. It can be seen from Figure 7.9 that the calculated and measured values are closer to each other than in Figure 7.8. The general presentation form of Figure 7.9 is used in all the following figures in this chapter.

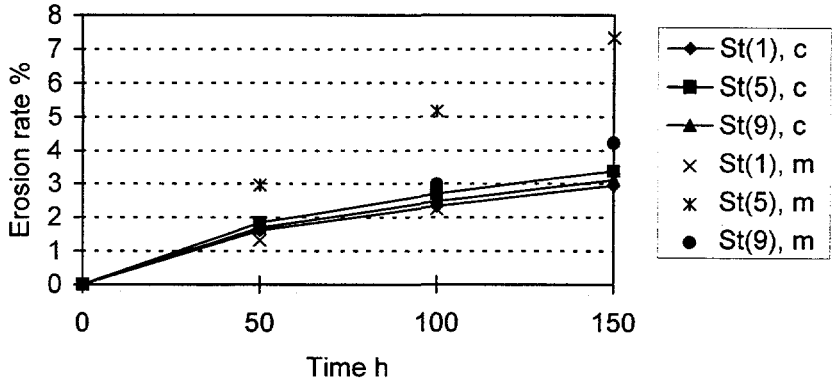

Figure 7.8 Calculated, c, and measured, m, erosion rates as a function of time in test series 1, 4, 7 for tube material St35.8, one particle material parameter

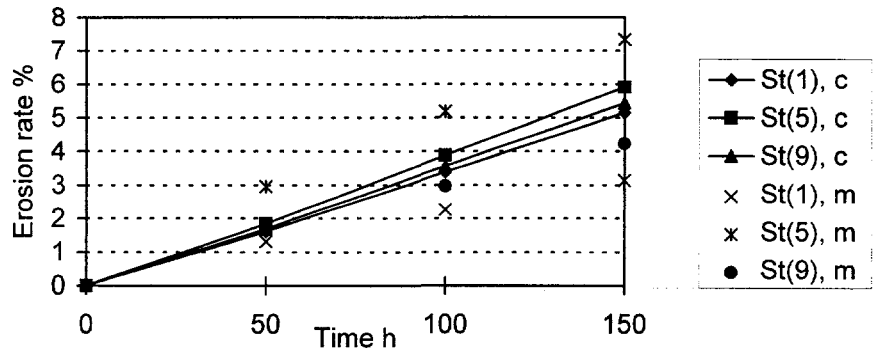

Figure 7.9 Calculated, c, and measured, m, erosion rates as a function of time in test series 1, 4, 7 for tube material St35.8

In Figures 7.10 and 7.11, the percentage erosion mass losses of test sleeves 1, 5 and 9 are presented for materials 15Mo3 and CrMo910 in the test series 1, 4, 7. In Figure 7.12, the percentage mass losses of the test sleeves numbered 5 of different materials are plotted in the same figure. The erosion rate of test sleeve number 5 is higher than the erosion rates of test sleeves numbers 1 and 9 because of the location of the test sleeve.

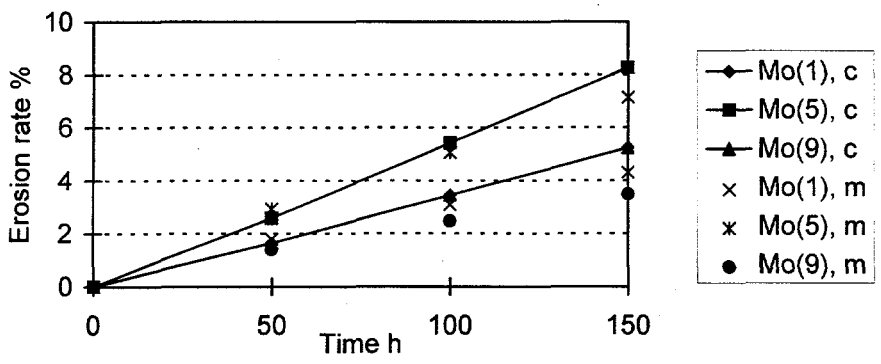

Figure 7.10 Calculated, c, and measured, m, erosion rates in test series 1, 4, 7 for tube material 15Mo3

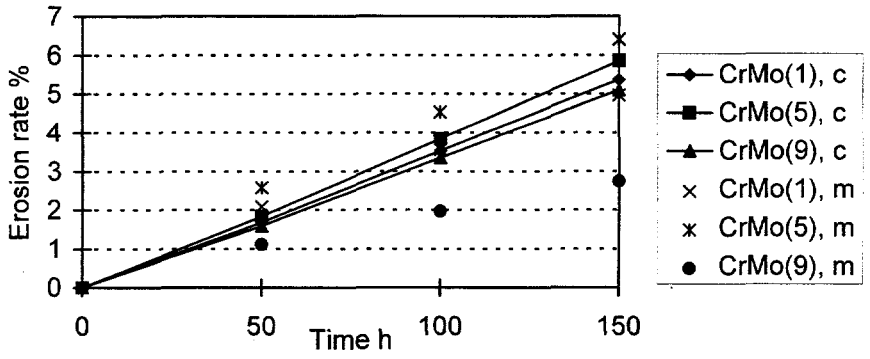

Figure 7.11 Calculated, c, and measured, m, erosion rates in test series 1, 4, 7 for tube material 10CrMo910

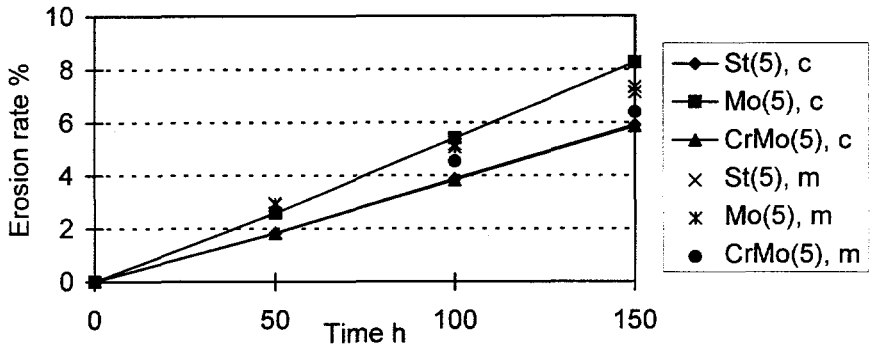

Figure 7.12 Calculated, c, and measured, m, erosion rates in test series 1, 4, 7 for the test sleeve number 5

In Figures 7.13 to 7.15 the percentage erosion mass losses of the test sleeves numbered 5 are presented for different tube materials in the test series 10, 13, 16; Quartz 1, 2, 3 and Coal ash 4, 5.

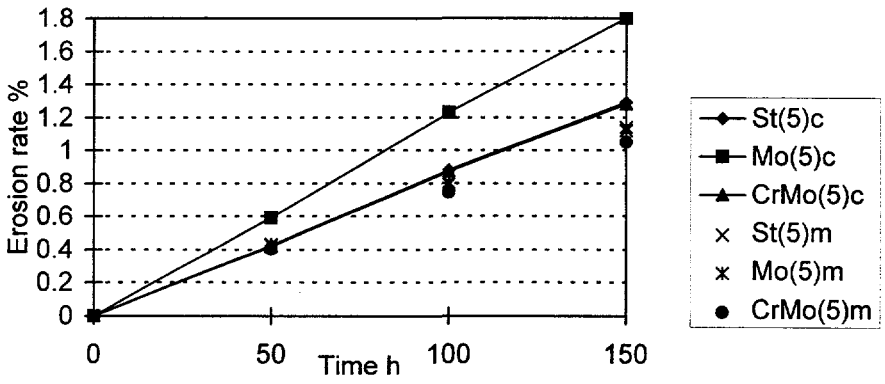

Figure 7.13 Calculated, c, and measured, m, erosion rates in test series 10, 13, 16 for the test sleeve number 5

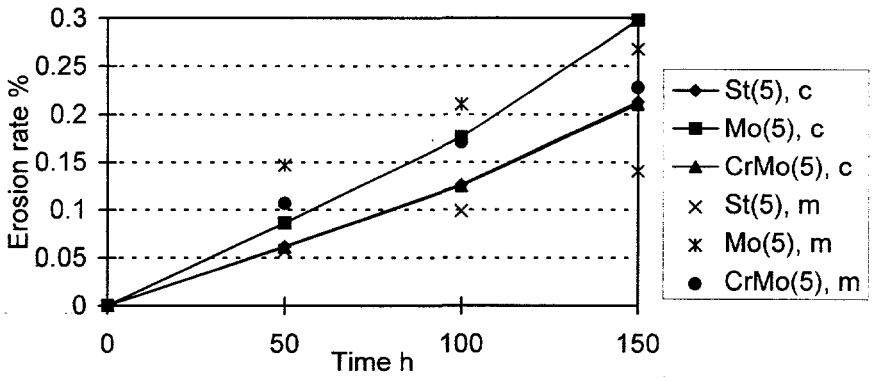

Figure 7.14 Calculated, c, and measured, m, erosion rates in test series Q 1, 2, 3 for the test sleeve number 5

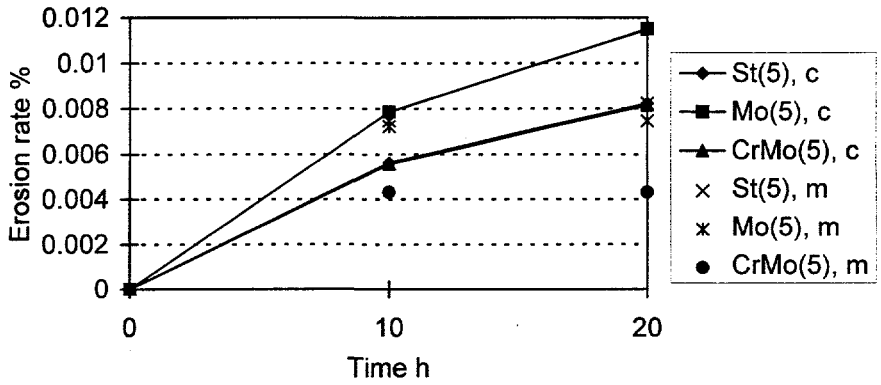

Figure 7.15 Calculated, c, and measured, m, erosion rates in test series CA 4, 5 for the test sleeve number 5

In Figures 7.16 and 7.17 the percentage mass losses of the test sleeves in the centre area of the test channel are presented as a function of time in the test series 2, 5, 8 in the in-line tube bank in different rows. The differences between the calculated and measured values are very small in these figures. In Figures 7.18 and 7.19 the percentage mass losses of the test sleeves in the centre area of the test channel (number 68 in the first row and 77 in the second row) are presented as a function of time in the test series 3, 6, 9 in the staggered tube bank in different rows. The calculated and measured values are close to each other in rows 1, 2, 4 and 6, but differences occur in the rows 3 and 5.

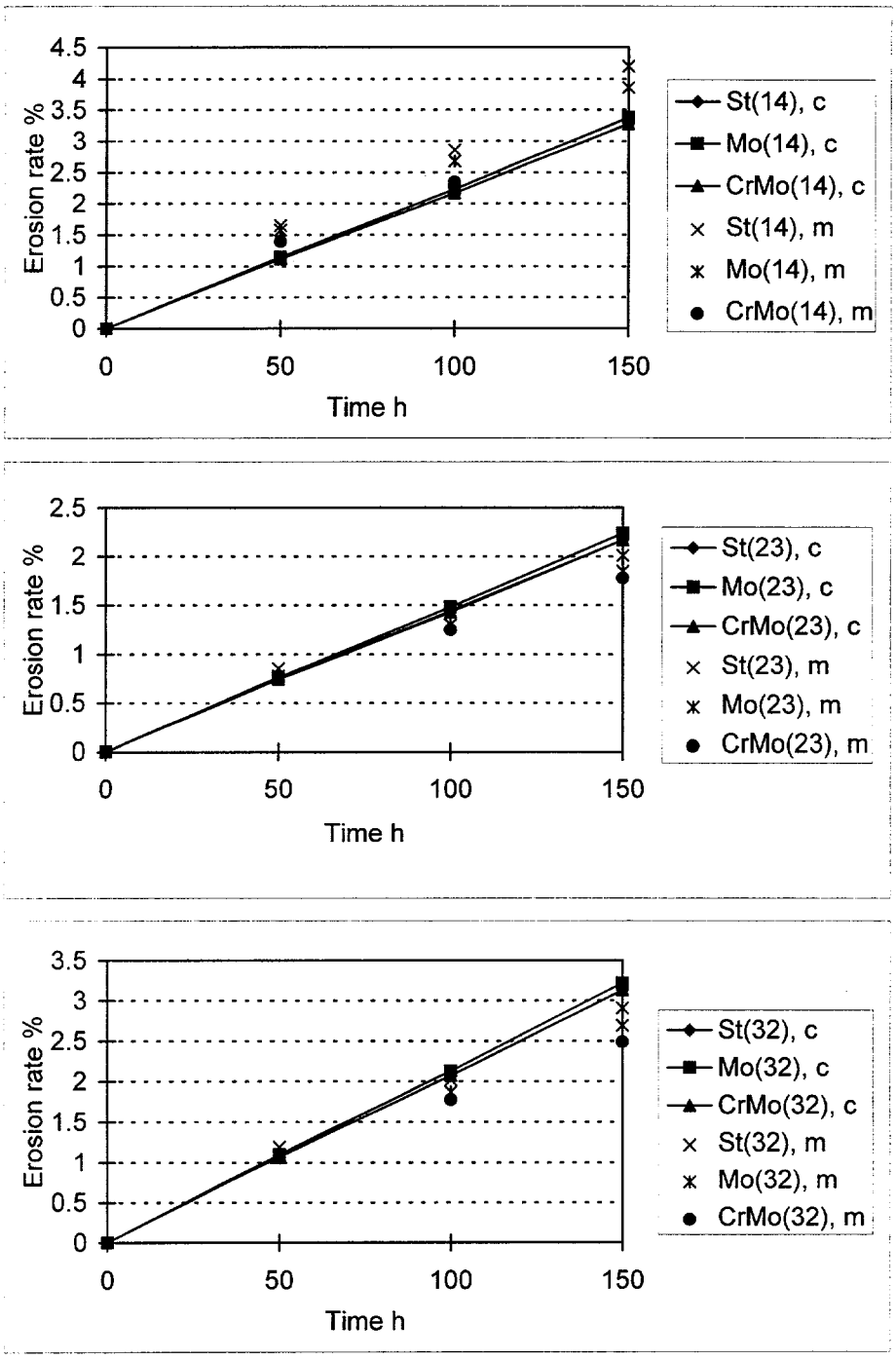

Figure 7.16 Calculated, c, and measured, m, erosion rates in the in-line tube bank for rows 1 to 3

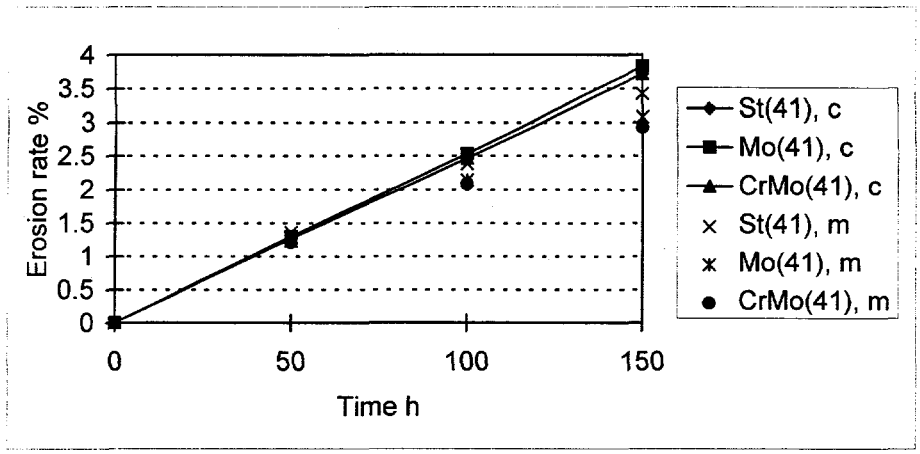

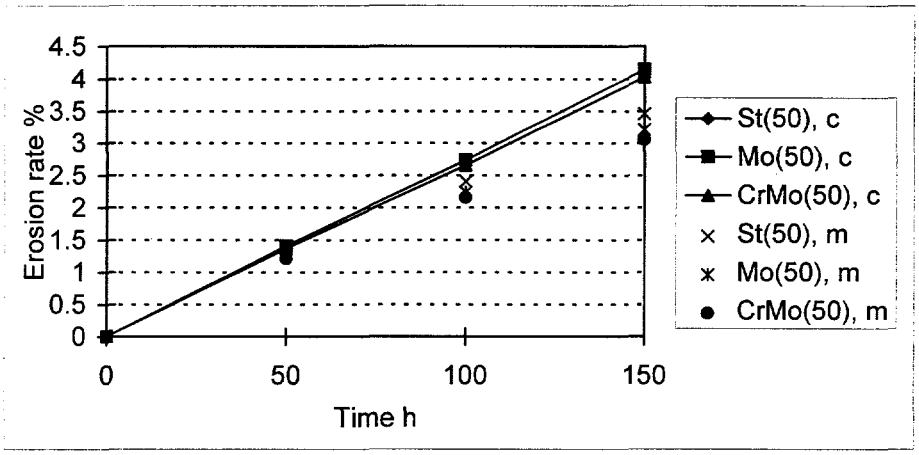

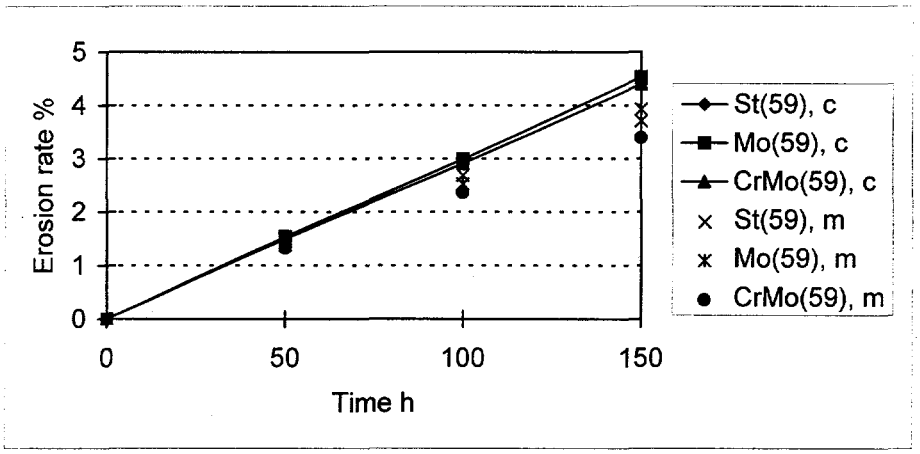

Figure 7.17 Calculated, c, and measured, m, erosion rates in the in-line tube bank for rows 4 to 6

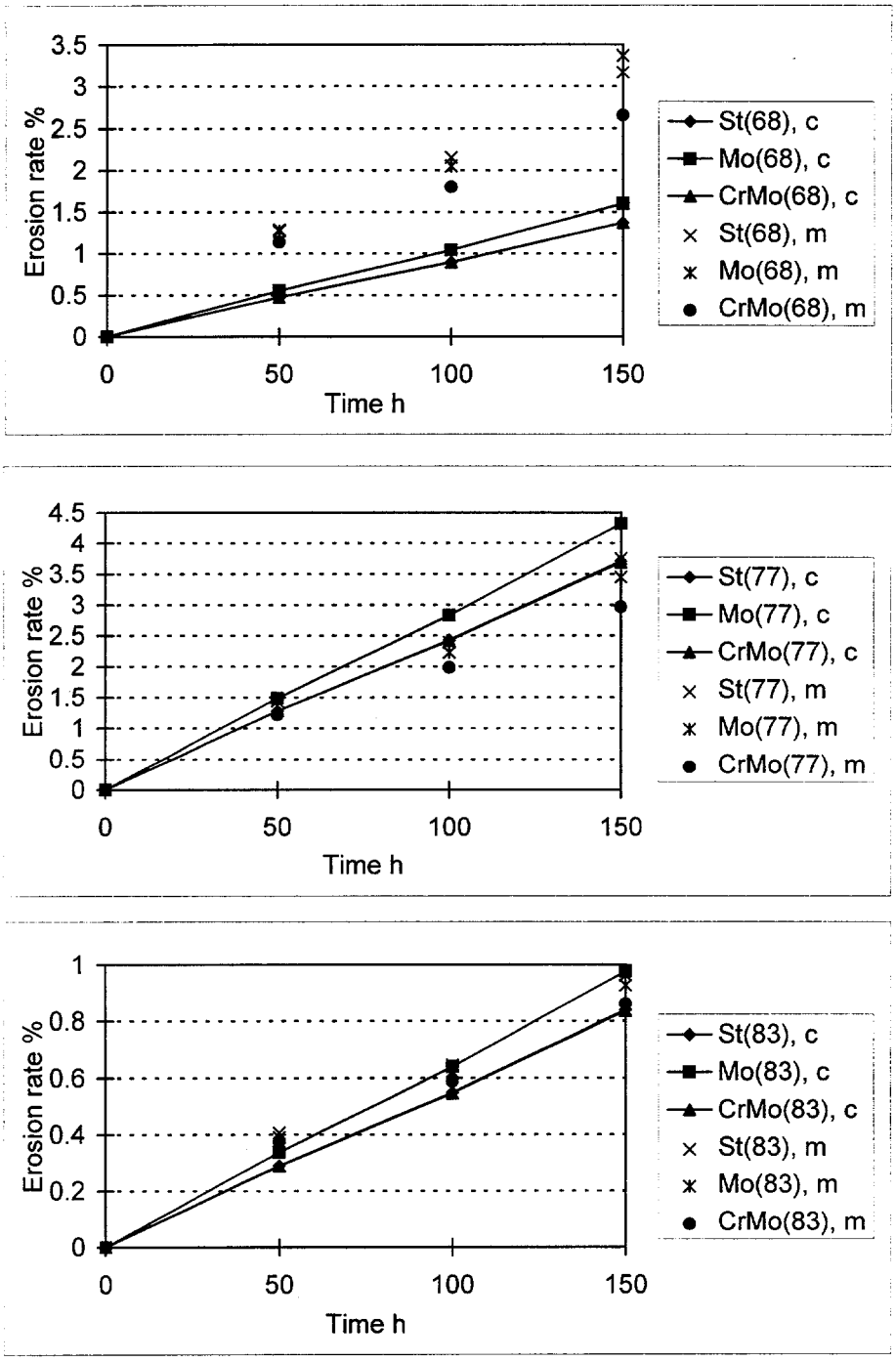

Figure 7.18 Calculated, c, and measured, m, erosion rates in the staggered tube bank for rows 1 to 3

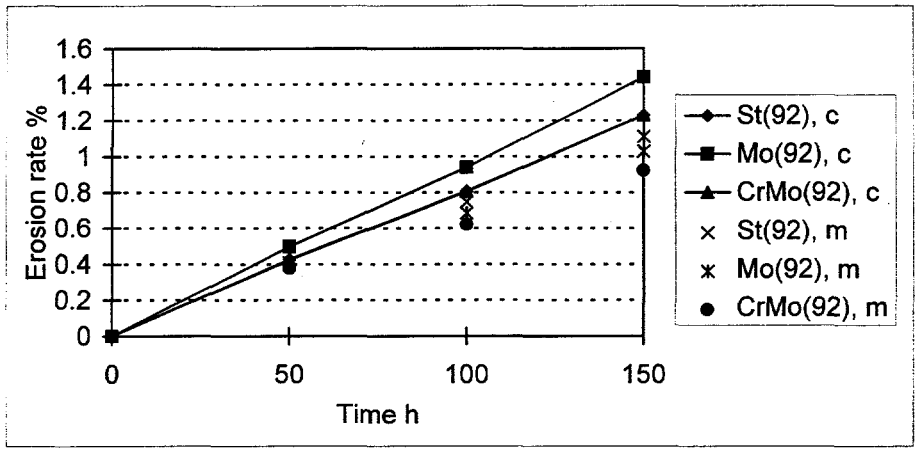

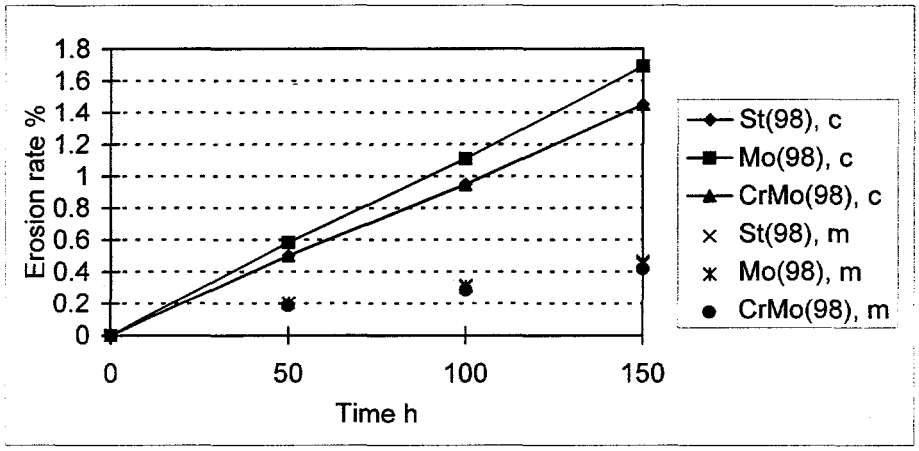

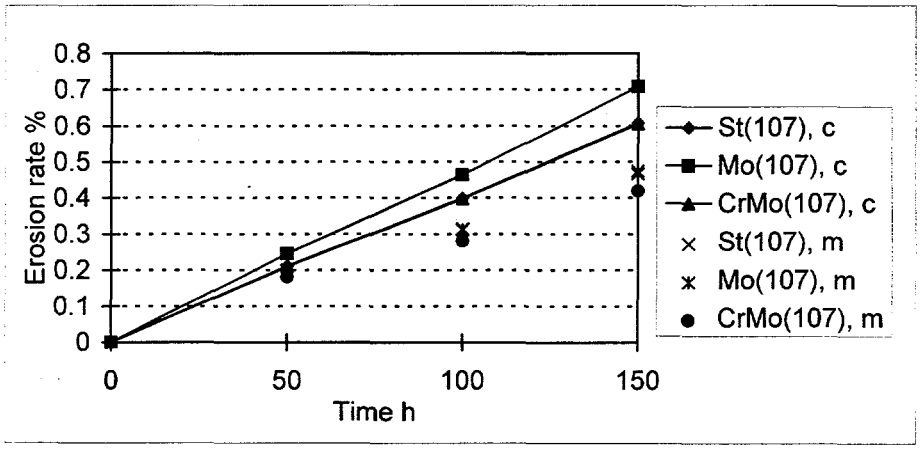

Figure 7.19 Calculated, c, and measured, m, erosion rates in the staggered tube bank for rows 4 to 6

Due to the large number of tests and test sleeves, only a minor part of the measurements are compared here to the calculated values in the figures presented in this chapter. Althought there are differences between the calculated and measured values, it can be seen from the figures that, in most cases, the differences are small and the equations can be used to evaluate the erosion wear in the convective heat exchanger tubes of a steam boiler.

7.3 EVALUATION OF ERRORS

The accuracy of mass measurements of the test sleeves is high compared to the accuracy of diameter or wall thickness measurements. For this reason, mainly mass loss measurements of the test sleeves have been used in the analyses. The diameter and wall thickness loss measurements have been used only when analysing erosion rate as a function of collision angle. The error of the mass loss measurements was evaluated as 0.001 g and the error of diameter and wall thickness loss measurements as 0.01 mm.

The accuracy of the linear regression analyses was evaluated on the basis of the coefficient of determination, the t-value and the residual figure. Standard deviations of coefficients were listed by the regression analysis program. The coefficient of determination should be as high as possible, and in this study only the results of analyses with a coefficient of determination higher than 0.70 were used. The absolute value of t of the parameters should be higher than two and the residuals should be placed randomly above and below the horizontal axis in the figure of the residuals. It has been attempted to meet all these requirements in this study. The standard deviations of the analyses in Chapter 6 are presented in Appendix D.

The errors of the flow parameters in the tests have been evaluated. In the quartz particle tests with the lower particle concentration 20 g/m^3 the particles were ejected into the flow by a screw feeder and the mass flow rate was controlled by weighing the particle material. The error in the mass flow with this device was evaluated as 5 % of the mass flow, that is 1.00 g/s for the mass flow 19.9 g/s, 0.66 g/s for the mass flow 13.3 g/s and 0.43 g/s for the mass flow 8.63 g/s. In tests with the higher particle concentration 375 g/m^3 the particles were ejected into the flow by a hopper feeder. The accuracy of the mass flow when using this particle feeder was evaluated as 15 % of the mass flow, which is 56 g/s for the mass flow 374 g/s, 37 g/s for the mass flow 249 g/s and 24 g/s for the mass flow 162 g/s. The error in the velocity measurements was evaluated to be 3 % of the velocity measurement, that is 0.90 m/s, 0.60 m/s and 0.39 m/s for the velocities 30 m/s, 20 m/s and 13 m/s,

respectively. The velocities used in the tests were the average values of the velocity measurements presented in Figure 4.8.

The error in time measurement was evaluated as 2 hours in all the tests, but 0.5 hours in the short ash particle tests. The error in the particle material parameter a_0 was evaluated to be 5 % of the value of the parameter, and the tube material parameter to be 5 % of the value of the tube material parameter b. The error in the cross-sectional area measurements of the flow channel was evaluated as 1.5 % of the cross-sectional area and the error of the parameter c was evaluated to be 0.75 % of the value of the parameter. The error in the vertical location parameter h was evaluated as 2 % of the value of the parameter. When evaluating errors in erosion wear rate as a function of mass loss per tube area, errors in the density of the tube material, volume and external area of a test sleeve were required. The error of the tube material density was evaluated as being 1 % of the density and the errors of the test sleeve volume and external area were both evaluated as being 2 % of the respective values.

The total error of the erosion calculation formula can be calculated by the Standard VDI 2048 as

$$E_{\Delta m^*} = \pm \sqrt{\sum_{i=1}^{i=n} [\frac{\partial(\Delta m^*)}{\partial x_i} \cdot E_{x_i}]^2} \tag{7.7}$$

where $E_{\Delta m^*}$ is total error of erosion,

n is the number of parameters,

$\frac{\partial(\Delta m^*)}{\partial x_i}$ is the partial derivate of the function and

E_{x_i} is the error of variable x_i.

The relative error of the erosion calculation formula is

$$f = \frac{E_{\Delta m^*}}{\Delta m^*} \tag{7.8}$$

For example, the erosion calculation formula for the three tube construction when using the same dimensions as in the regression analysis in Chapter 6 is

$$\Delta m^* = 8.58 \cdot 10^{-8} \cdot a^{0.687} \cdot b^{0.0915} \cdot w^{3.67} \cdot t^{0.553} \tag{7.9}$$

Particle concentration k can be presented as

$$k = \frac{q_m}{w \cdot A} \tag{7.10}$$

where q_m is particle mass flow
w is the flow velocity at the centre-point of the first tube row
A is the flow area at the centre-point of the first tube row

$$\Rightarrow \Delta m^* = 8.58 \cdot 10^{-8} \cdot a_0^{0.687} \cdot q_m^{0.687} \cdot A^{-0.687} \cdot b^{0.0915} \cdot w^{2.98} \cdot t^{0.553} \tag{7.11}$$

where a_0 is the collision probability times average particle size particle parameter.

The partial derivates can be presented as

$$\frac{\partial(\Delta m^*)}{\partial a_0} = 8.58 \cdot 10^{-8} \cdot (0.687 \cdot a_0^{-0.313}) \cdot q_m^{0.687} \cdot A^{-0.687} \cdot b^{0.0915} \cdot w^{2.98} \cdot t^{0.553} \tag{7.12}$$

$$\frac{\partial(\Delta m^*)}{\partial q_m} = 8.58 \cdot 10^{-8} \cdot a_0^{0.687} \cdot (0.687 \cdot q_m^{-0.313}) \cdot A^{-0.687} \cdot b^{0.0915} \cdot w^{2.98} \cdot t^{0.553} \tag{7.13}$$

$$\frac{\partial(\Delta m^*)}{\partial A} = 8.58 \cdot 10^{-8} \cdot a_0^{0.687} \cdot q_m^{0.687} \cdot (-0.687 \cdot A^{-1.69}) \cdot b^{0.0915} \cdot w^{2.98} \cdot t^{0.553} \tag{7.14}$$

$$\frac{\partial(\Delta m^*)}{\partial b} = 8.58 \cdot 10^{-8} \cdot a_0^{0.687} \cdot q_m^{0.687} \cdot A^{-0.687} \cdot (0.0915 \cdot b^{-0.909}) \cdot w^{2.98} \cdot t^{0.553} \tag{7.15}$$

$$\frac{\partial(\Delta m^*)}{\partial w} = 8.58 \cdot 10^{-8} \cdot a_0^{0.687} \cdot q_m^{0.687} \cdot A^{-0.687} \cdot b^{0.0915} \cdot (2.98 \cdot w^{1.98}) \cdot t^{0.553} \tag{7.16}$$

$$\frac{\partial(\Delta m^*)}{\partial t} = 8.58 \cdot 10^{-8} \cdot a_0^{0.687} \cdot q_m^{0.687} \cdot A^{-0.687} \cdot b^{0.0915} \cdot w^{2.98} \cdot (0.553 \cdot t^{-0.447}) \tag{7.17}$$

The total errors can be calculated in the same way for the in-line tube bank and staggered tube bank equations when all the parameters are included in the observation. The relative total errors were calculated for the dimensionless mass loss values and for the mass losses per tube external area (g/m^2). In Tables 7.5, 7.6 and 7.7, the relative total errors of the analyses are presented.

Table 7.5 Relative total errors of calculation equation for three tube construction

Test series	Relative total error of erosion wear rate as dimensionless mass loss	Relative total error of erosion wear rate as mass loss/tube area
1,4,7	0.14	0.14 (one value 0.15)
10,13,16	0.14	0.14
19,22,25	0.14	0.14
28,31,34	0.10	0.10
37,40,43	0.10	0.10
46,49,52	0.10	0.10
Coal ash 4	0.14	0.14
Coal ash 5	0.14	0.14
Peat ash 1	0.14	0.14
Quartz 1, 2,3	0.14	0.14

Table 7.6 Relative total errors of calculation equation for in-line tube bank

Test series	Relative total error of erosion wear rate as dimensionless mass loss	Relative total error of erosion wear rate as mass loss/tube area
2,5,8	0.13	0.13
11,14,17	0.13	0.13
20,23,26	0.13	0.13
29,32,35	0.10	0.10
38,41,44	0.10	0.10
47,50,53	0.10	0.10

Table 7.7 Relative total errors of calculation equation for staggered tube bank

Test series	Relative total error of erosion wear rate as dimensionless mass loss	Relative total error of erosion wear rate as mass loss/tube area
3	0.12	0.13
6	0.12	0.12
9	0.12	0.12
12,15,18	0.12	0.12
21,24,27	0.12	0.12
30,33,36	0.12	0.12
39,42,45	0.12	0.12
48,51,54	0.12	0.12

8 CONCLUSIONS

8.1 OBSERVATIONS

Erosion testing is difficult because of the long testing periods needed for sufficient erosion rate to be able to be measured. The erosion tests started in 1994 and were finished in 1997. The longest period in the tests was 300 hours. Tests done with the particle materials coal ash and peat ash were short, 10 hours with coal ash and 50 hours with peat ash, compared to the test periods of quartz particles because of great difficulties in the plugging of the transport pipes of the laboratory facility. It would have been possible to install test sleeves in some existing steam boiler, in this way longer test periods could have been achieved. However, the flow parameters could not have been determined as accurately as in the laboratory atmosphere.

The amount of erosion tests is large because of the many parameters which affect erosion rate that were studied. However, the amount of parameters was kept to a minimum. Three different tube constructions were studied: the three tube construction, the in-line tube bank and the staggered tube bank. One tube diameter and transverse or longitude tube spacing was able to be studied in the tests. Two particle concentrations, one low and one very high, and three flow velocities were studied. The erosion rate as a function of time was studied in two three-test series for the three tube construction, and in one three-test series for the in-line and staggered tube bank. Three tube materials were able to be tested at the same time for each test. The particle material coal ash was studied in a test series of two tests and the particle material peat ash in one test in the three tube construction. Quartz particles were used as basic particle material in all tube constructions and with all flow parameters.

Although the number of parameters was limited, the amount of measurements was huge. The total number of test sleeves in the different constructions was 324. The mass losses of the test sleeves were measured in all tests. Six diameter measurements at angles from 0° to 150° and twelve wall thickness measurements at angles from 0° to 330° were done with each test sleeve. In the three tube construction, diameter and wall thickness measurements were done at both ends of the test sleeves. In tests with a very low erosion wear rate, the diameter and wall thickness measurements were not done.

The analysis of the test results has been very timetaking. Without a linear regression analysis program, the analysing would have been virtually impossible. On the other hand, the large amount of measurements makes it easier to form reliable conclusions about the tests.

8.2 CONCLUSIONS AND RECOMMENDATIONS

On the basis of the erosion testing and analysis, conclusions about the erosion wear rate caused by a particulate material on convective heat exchanger tubes can be formed. Erosion rate as a function of particle concentration in the flow was proportional to the particle concentration to the power of 0.69 in the three tube construction, 0.61 in the in-line tube bank and 0.52 in the staggered tube bank. A conclusion can be drawn that the exponent decreases when there are more tube rows and when tubes are installed as staggered instead of in-line. This is because there is more turbulence and interparticle collisions. This decreases the linearity of erosion rate as a function of particle concentration.

Erosion rate as a function of flow velocity on the cross-sectional area at the centre-line of the first tube row was proportional to velocity to the power of 3.7 in the three tube construction, 3.4 in the in-line tube bank and 3.3 in the staggered tube bank. The behaviour of this exponent is similar to that of the concentration exponent. A reason for this behaviour may be the same as for the particle concentration exponents. Erosion rate as a function of time was proportional to the erosion period to the power of 0.55 in the three tube construction, 0.58 in the in-line tube bank and 0.60 in the staggered tube bank. The exponent for time has an opposite behaviour to that of the exponents of particle concentration and velocity with respect to the tube construction.

Erosion wear rates of tube materials 15Mo3 and 10CrMo910 were 95 % and 87 % of the erosion rate of tube material St35.8 from the analyses in Chapter 5. Calculated as the average values of erosion rates from the tests with coal ash and peat ash particles compared to the erosion rate of quartz particles, the result was that the erosiveness of coal ash is 11 % and peat ash 12 % of the erosiveness of quartz particles.

In the in-line tube bank, the erosion rate of different rows compared to the erosion rate of the first row had a minimum value of 65 % in the second row, a value of 95 % in the third row, 110 % in the fourth row, 120 % in the fifth row and 140 % in the sixth row. In the staggered tube bank, the erosion rate of different rows compared to the erosion rate of the first row had a maximum value of 140 % in the second row, a value of 60 % in the third row, 45 % in the fourth row, 110 % in the fifth row and 22 % in the sixth row. The growth of the erosion rate in rows 2 to 6 and the high erosion rate values in rows 4, 5 and 6 in the in-line tube bank can be explained by the growing intensity of the turbulence of the particle flow in the tube bank. The minimum erosion value of the second row is expected because of the shielding effect of the first row. The high local maximum erosion rate in the fifth row in the staggered tube

bank can be explained by the deceleration and separation of the particle flow from the gas flow upon collision with the second row, and the acceleration time needed to get a high enough velocity again to cause erosion takes until row 5. More local maximum values are expected if there were more tube rows. In both of the tube banks, the separation and reunion of the particle and gas flows causes the generation of large eddies and a high intensity of turbulence, which causes a high erosion rate at certain areas or tube rows in a tube bank.

The erosion wear rate of the staggered tube bank was lower than the erosion wear rate of the in-line tube bank in all but the second row. In the first row, the erosion rate of the staggered tube bank was about 80 %, in the second row 180 %, in the third 50 %, in the fourth 30 %, in the fifth 70 % and in the sixth row 10 % of the erosion rate of the in-line tube bank. The staggered tube bank has generally been considered to be more vulnerable to erosion wear than the in-line tube bank because of flow channelling caused by plugging. If plugging is controlled, the erosion rate of the staggered tube bank is lower than that in the in-line tube bank except in the second row.

High erosion wear rates as a function of collision angle between the particle flow and the tube surface occurred at angles of 0°, 30°, 60°, 120°, 150° and 180°, when the tube surface, at an angle of 90°, was faced towards the coming particle flow. The values varied in the different tubes from 50 % to 140 % in the three tube construction, from 50 % to 950 % in the in-line tube bank, and from 15 % to 480 % in the staggered tube bank compared to the erosion rate at an angle of 90° in the respective tubes. The variation of the erosion rate in different tubes and at different angles was very high. Erosion wear rates on the back-sides of the tubes were low in the three tube construction and in the in-line tube bank, except in the second and third row of the in-line tube bank where there was moderate erosion on the back-sides of the tubes, as well. In the staggered tube bank there was moderate erosion on the back-sides of the tubes in the third, fourth and sixth rows.

In the staggered tube bank the erosion rate increased as a function of test sleeve location in the x-direction. The erosion rate on the side tubes of a three tube row was about 230 % of the erosion wear rate of the centre tube, especially in rows 3 and 5. In other constructions a behaviour like this was not observed. The erosion rate as a function of location in the y-direction was about 60 % in the test sleeves near the front and back walls compared to the erosion rate of the test sleeve in the centre area in the three tube construction. In the in-line and staggered tube banks the values were about 95 % and 80 %, respectively.

In this study, one tube diameter and transverse and longitude tube spacing was used in the tests. More knowledge could be acquired by testing different spacings and tube diameters. Also by testing tube banks with more rows, further information could be obtained concerning whether or not the erosion wear rate would increase in subsequent tube rows in the in-line tube bank and if there would be high local erosion wear rates in subsequent tube rows in the staggered tube bank.

REFERENCES

Adams T. Black Liquor Combustion. Huovilainen R., Meuronen V. (eds). Black Liquor Combustion. Lappeenranta, 24-25 Feb. 1988. Lappeenranta. Poltto, palaminen, päästöt -yhteistyö. Lappeenranta University of Technology. Department of Energy Technology. 1988. pp. 1-38. ISSN 07783-5248. ISBN 951-754-434-0.

Agarwal S., Howes M. Erosion-Corrosion of Materials in High-Temperature Environments: Impingement Angle Effects in Alloys 310 and 6B Under Simulated Coal Gasification Atmosphere. J. Materials for Energy Systems, 1986. Vol. 7, No. 4, pp. 370-381.

Bratchikov V. Erosion by Ash of Tubes in a Bundle. Thermal Engineering, 1987. Vol. 34, No. 11, pp. 617-619. (Teploenergetika, 1987. Vol. 34, No. 11, pp. 63-64.)

Dergatshev N. F. Metod issledovanija dvirzhenija pyli v modeljah razlitshnyh apparatov.(A Method to Study The Movements of Dust in Models of Different Devices. In Russian.) Izvestija VTI, 1949. No. 6.

Dergatshev N. F., Zalogin N. G. O dvirzhenija tsthastits zoly v putshke trub. (About The Movements of Ash Particles in Tube Banks. In Russian) Izvestija VTI, 1951. No. 4.

Finnie I. The Mechanism of Erosion of Ductile Metals. Proceedings Third U. S. National Congress of Applied Mechanics. New York. ASME. 1958. pp. 527-532.

Finnie I., Wolak J., Habil Y. Erosion of Metals by Solid Particles. J. Mater., 1967. 2, p. 682.

Foley T., Levy A. The Effect of Heat Treatment on the Erosion Behaviour of Steels. LBL Report No. 13745. Berkeley, California. Lawrence Berkeley Laboratory, University of California. April 1982.

Gat N., Tabakoff W. Effects of Temperature on the Behaviour of Metals Under Erosion of Particulate Matter. Journal of Testing and Evaluation, 1980. Vol. 8, No. 4, pp. 177-186.

Jansson S. Erosion and Erosion-Corrosion in Fluidized Bed Combustor Systems. Levy I (ed.). Proceedings Corrosion-Erosion-Wear of Materials in Emerging Fossil-Energy Systems. Berkeley, California, Jan. 27-29, 1982. National Association of Corrosion Engineers. 1982. pp. 548-561. Conf-820144.

Jianren F., Dadong Z., Kefa C. An Investigation of Tube Erosion by Coal Ash Impaction in CFB Combusters. 1989 International Conference on Fluidized Bed Combustion: FBC-Technology for Today. San Francisco, CA, USA, Apr. 30-May 3, 1989. Vol.1. New York, NY, USA. American Society of Mechanical Engineers. 1989. pp. 551-556. ISBN 0-7918-0308-2.

Kay J. & Nedderman R. Fluid Mechanics and Transfer Processes. Cambridge. Cambridge University Press. 1985. 602 p. ISBN 0-521-303.

Kunii D. & Levenspiel O. Fluidization Engineering. Second Edition. Boston (Mass.). Butterworth Heinemann. 1991. 491 p. ISBN 0-409-90233.

Kuznetsov N. V. Rabochie protsessy i voprosy usovershenstvovaniya konvektivnykh poverkhnostei kotelnykh agregatov. (The Working Processes and the Problems of Improving the Convective Heating Surfaces of Boilers. In Russian) Diss. Moscow. Gosenergoizdat. 1958. 172 p.

Levy A. The erosion of metal alloys and their scales. Levy A. (ed.). Proceedings corrosion-erosion-wear of materials in emerging fossil-energy systems. Berkeley, California, Jan. 27-29, 1982. Washington. National Association of Corrosion Engineers. 1982. pp. 298-376. Conf-820144.

Mansfeld I., Sauermann F., Swirski J. Strahlverschleiss in Dampferzeugen. Energietechnik, 1979. Vol. 29, No. 4, pp. 149-154.

Meuronen V. Höyrykattilan savukaasupuolinen eroosio. (Flue Gas Side Erosion of Steam Boilers. In Finnish.) Licentiate thesis. Lappeenranta. Lappeenranta University of Technology. Department of Energy Technology. 1990. 128 s.

Moilanen A., Nieminen M., Alén R. Polttoaineiden ominaisuudet ja luokittelu. (Properties and Classification of Fuels. In Finnish). Raiko R., Kurki-Suonio I., Saastamoinen J., Hupa M. (eds). Poltto ja palaminen. Jyväskylä. International Flame Research Foundation, Suomen kansallinen osasto. Teknisten tieteiden akatemia. 1995. pp. 87-107. ISBN 951-666-448-2.

National Materials Advisory Board. Erosion Control in Energy Systems. Report of Committee on Conservation of Materials in Energy Systems Through the Reduction of Erosion. Washington D.C. National Academy of Sciences of Academy. 1977. 201 p. Publication NMAB-334.

Raask E. Ash Related Problems in Coal Fired Boilers. Bryers R., Cole S. (eds). Fouling of Heat Exchanger Surfaces Conference. White Haven, PA, 31 Oct.-5 Nov. 1982. Engineering Foundation. 1983. pp. 433-460, 1983. ISBN 0-939204-20-7.

Raask E. Erosion durch Aschepartikeln in kohlegefeuerten Kesselanlagen. (Erosion Caused by Ash Particles in Coal Fired Boilers. In German) VGB Kraftwerkstechnik, 1979. Vol. 59, No. 6, pp. 496-502.

Raask E. Flame Imprinted Characteristics of Ash Relevant to Boiler Slagging, Corrosion, and Erosion. Journal of Engineering for Power, 1982. Vol. 104, Oct. pp. 858-866.

Rao P., Buckley D. Solid Impingement Erosion Mechanisms and Characterization of Erosion Resistance of Ductile Metals. Journal of Pipelines, 1984. No. 4, pp 193-205.

Reid W. The Relation of Mineral Composition to Slagging, Fouling and Erosion During and After Combustion. Progress in Energy and Combustion Science, 1984. Vol. 10, No. 2, pp. 159-175.

Saviharju K., Sjöholm P.-E. Öljykattilalaitoksen käyttö- ja suunnittelutietoa. (The Practice and Management of Oil Fired Boilers. In Finnish) 2. painos. Espoo. Neste. 1989. 230 s. ISSN 0784-5340. ISBN 951-96064-3-2.

Sheldon G., Finnie I. On the Ductile Behaviour of Nominally Brittle Materials During Erosive Cutting. J. Engng. for Industry. Trans. ASME, 88 B, 1966. pp. 387-392.

Shida Y., Fujikawa H. Particle Erosion Behaviour of Boiler Tube Materials at Elevated Temperature. Wear, 1985. Vol. 103, pp. 281-296.

Siitonen P., Mäntylä T., Kettunen P. Korroosio- ja eroosiovauriot turvevoimaloissa. (The Damages Caused by Corrosion and Erosion in Peat Fired Boilers. In Finnish) Report No. 66/1980. Tampere. Tampere University of Technology. 1980. 58 p.

Silén J., Kettunen P. Eroosiokulumista kestävä teräs turvevoimalakäyttöön. (Erosion Resistant Steel for Peat Fired Boilers. In Finnish) Report No. 24/1984. Tampere. Tampere University of Technology. 1984. 41 s.

Singer J. (ed.). Combustion, Fossil Power Systems. Third edition. Windsor. Combustion Engineering. Inc. 1981. 1042 p. ISBN 0-9605974.

Statistics Finland. Energy Statistics, 1994. 1995. Official Statistics of Finland, Energy 1995, 1. 155 p. ISBN 951-727-125-5.

VDI 2048. Messungenauigkeiten bei Abnahmeversuchen, Grundlagen. Ausgabe Juni 1978.

Wall T., Lowe A., Wibberley L., McC. Stewart I. Mineral Matter on Coal and The Thermal Performance of Large Boilers. Progress in Energy and Combustion Science, 1979. Vol. 5, No. 1, pp. 1-29.

Wiederhorn S. Erosion Behaviour of Ceramics. ERDA/NSF Workshop on Ceramics for Energy Applications. Battelle Memorial Institute. Columbus, Ohio, Nov. 24-25, 1975. Washington DC. Institute for Materials Research. National Bureau of Standards. pp. 83-106.

World Energy Council. Survey of Energy Resources, 1995/World Energy Conference. 17 ed. London. World Energy Conference. 1995. 294 p. ISBN 0-946121-11-7.

Wright I. Fireside Corrosion and Fly Ash Erosion in Boilers. Report Summary. Columbus, Ohio. Battelle Columbus Division. 1987. 122 p. EPRI CS-5071. Research Project 2711-1.

Wright I., Herchenroeder R. High-Temperature Erosion-Corrosion of Alloys. Final Report. Columbus, Ohio. Battelle, Columbus Laboratories. 1980. 125 p. CS-1454, Research Project 979-5.

APPENDIX A ELEMENTARY ANALYSES OF COAL AND PEAT ASHES

Element		Coal ash	Peat ash
		Mass percent	Mass percent
Magnesium	Mg	1.38	2.02
Aluminium	Al	17.42	9.02
Silicon	Si	49.30	28.05
Phosphorus	P	0.53	2.33
Sulphur	S	0.62	2.49
Potassium	K	4.17	2.72
Calsium	Ca	11.22	28.86
Titanium	Ti	1.88	0.81
Iron	Fe	13.48	23.70

These analyses don't contain elementary coal.

APPENDIX B RESIDUAL FIGURES OF THE ANALYSES

Analyses of Chapter 5

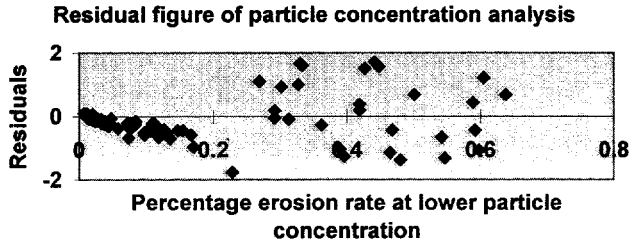

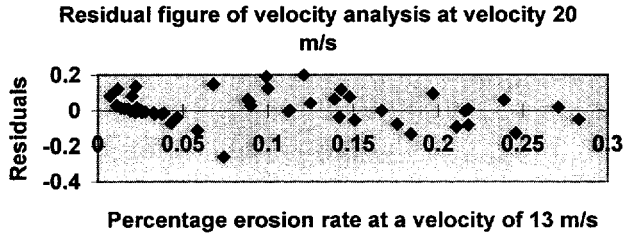

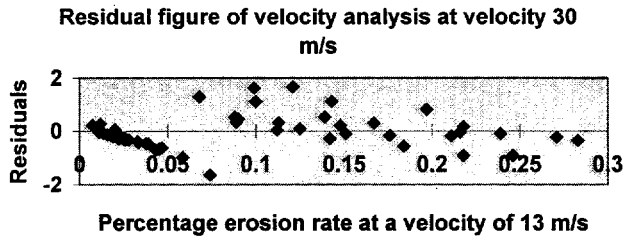

Residual figure of time analysis of tests 1 and 4 at 100 h

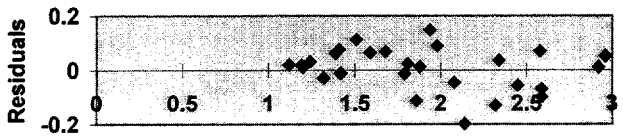

Percentage erosion rate at first 50 h period

Residual figure of time analysis of tests 1 and 7 at 150 h

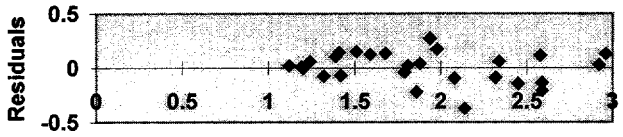

Percentage erosion rate at first 50 h period

Residual figure of time analysis of tests 2 and 5 at 100 h

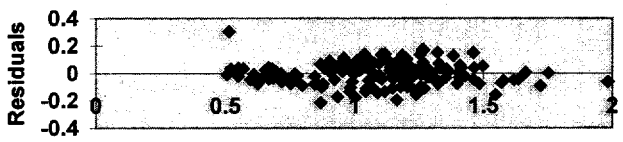

Percentage erosion rate at first 50 h period

Residual figure of time analysis of tests 2 and 8 at 150 h

Percentage erosion rate at first 50 h period

Residual figure of time analysis of tests 3 and 6 at 100 h

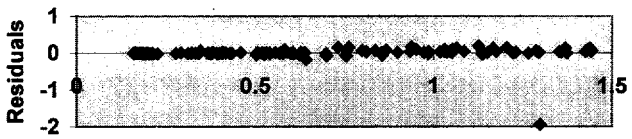

Percentage erosion rate at first 50 h period

Residual figure of time analysis of tests 3 and 9 at 150 h

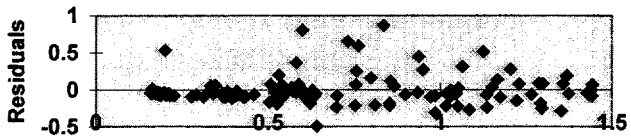

Percentage erosion rate at first 50 h period

Residual figure of time analysis of tests 1 to 6 at 100 h

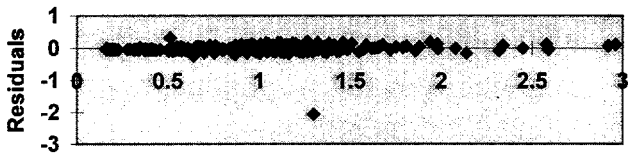

Percentage erosion rate at first 50 h period

Residual figure of time analysis of tests 1, 2, 3 and 7, 8, 9 at 150 h

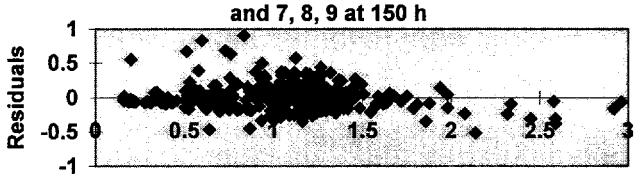

Percentage erosion rate at first 50 h period

Residual figure of time analysis of tests 10 and 13 at 100 h

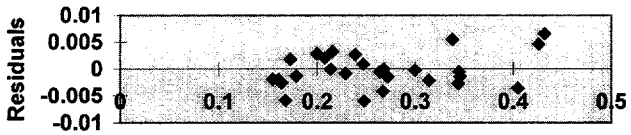

Percentage erosion rate at first 50 h period

Residual figure of time analysis of tests 10 and 16 at 150 h

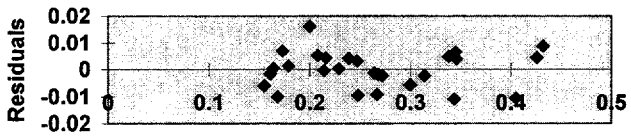

Percentage erosion rate at first 50 h period

Residual figure of analysis of first row erosion rate of in-line tube bank/erosion rate of three tube construction

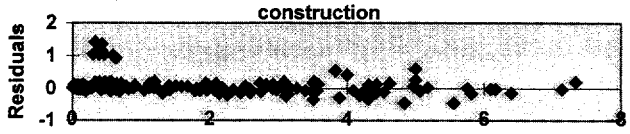

Percentage erosion rate of three tube construction

Residual figure of analysis of first row erosion rate of staggered tube bank/erosion rate of three tube construction

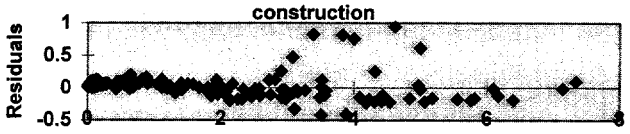

Percentage erosion rate of three tube construction

Residual figure of analysis of erosion rate of staggered tube bank/erosion rate of in-line tube bank, row 1

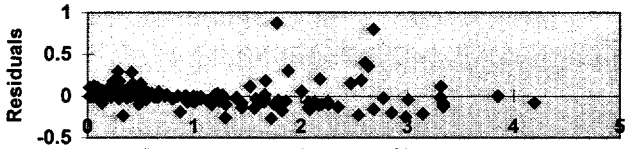

Percentage erosion rate of in-line tube bank

Residual figure of analysis of erosion rate of staggered tube bank/erosion rate of in-line tube bank, row 2

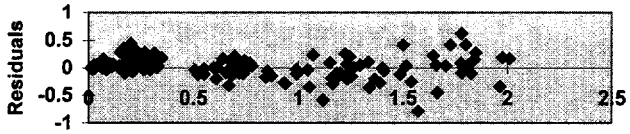

Percentage erosion rate of in-line tube bank

Residual figure of analysis of erosion rate of staggered tube bank/erosion rate of in-line tube bank, row 3

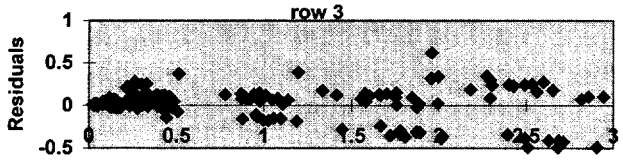

Percentage erosion rate of in-line tube bank

Residual figure of analysis of erosion rate of staggered tube bank/ erosion rate of in-line tube bank, row 4

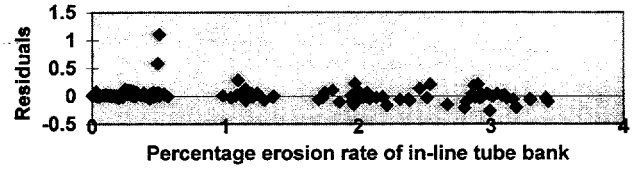

Residual figure of analysis of erosion rate of staggered tube bank/ erosion rate of in-line tube bank, row 5

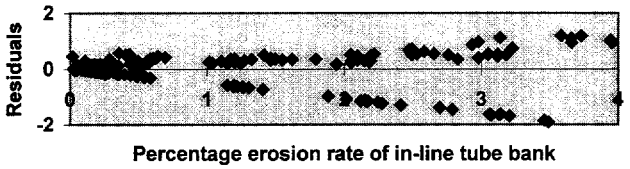

Residual figure of analysis of erosion rate of staggered tube bank/erosion rate of in-line tube bank, row 6

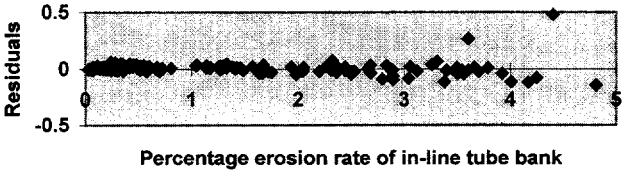

Residual figure of analysis of erosion rate in the first row/average erosion rate, in line-tube bank

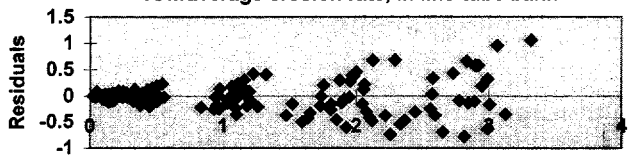

Average erosion rate of different rows, %

Residual figure of analysis of erosion rate of the second row/average erosion rate, in-line tube bank

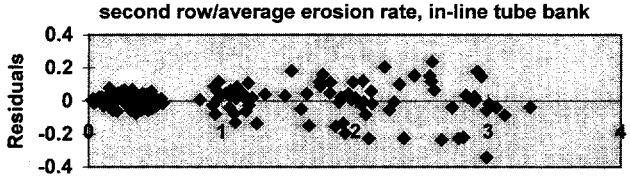

Average erosion rate of different rows, %

Residual figure of analysis of erosion rate in the third row/average erosion rate, in-line tube bank

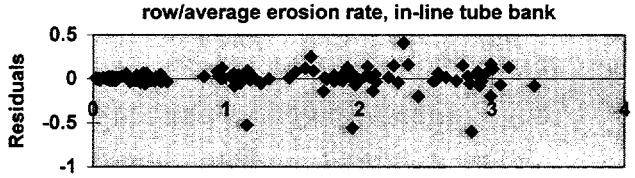

Average erosion rate of different rows, %

Residual figure of analysis of erosion rate in the fourth row/average erosion rate, in-line tube bank

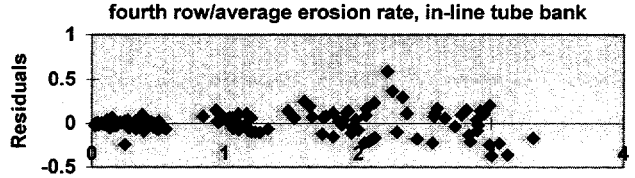

Average erosion rate of different rows, %

Residual figure of analysis of erosion rate in the fifth row/average erosion rate, in-line tube bank

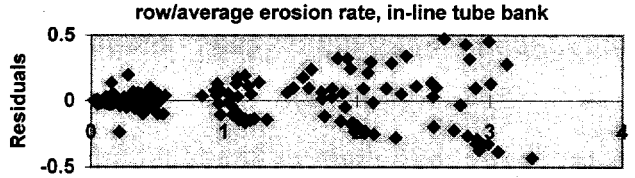

Average erosion rate of different rows, %

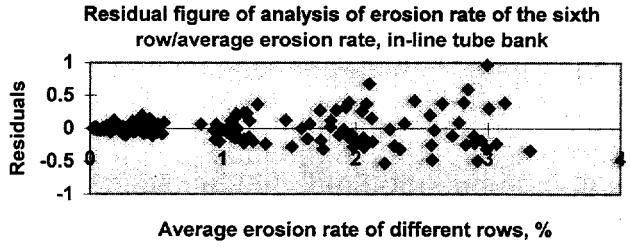
Residual figure of analysis of erosion rate of the sixth row/average erosion rate, in-line tube bank
Residuals
1
0.5
0
-0.5
-1
0
1
2
3
4
Average erosion rate of different rows, %

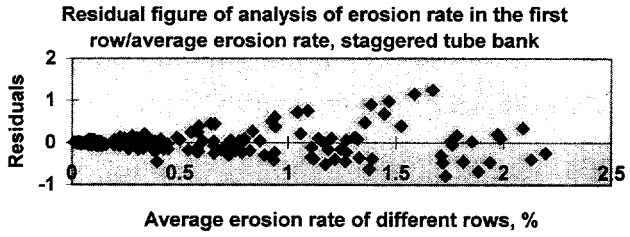
Residual figure of analysis of erosion rate in the first row/average erosion rate, staggered tube bank
Residuals
2
1
0
-1
0
0.5
1
1.5
2
2.5
Average erosion rate of different rows, %

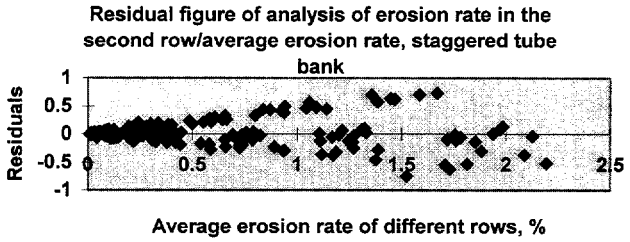
Residual figure of analysis of erosion rate in the second row/average erosion rate, staggered tube bank
Residuals
1
0.5
0
-0.5
-1
0
0.5
1
1.5
2
2.5
Average erosion rate of different rows, %

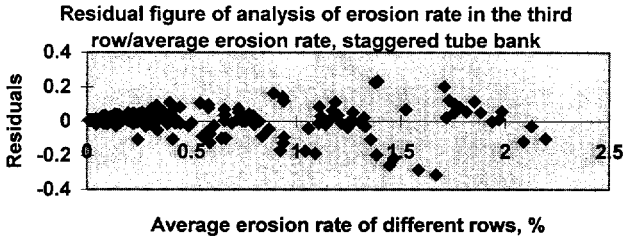
Residual figure of analysis of erosion rate in the third row/average erosion rate, staggered tube bank
Residuals
0.4
0.2
0
-0.2
-0.4
0
0.5
1
1.5
2
2.5
Average erosion rate of different rows, %

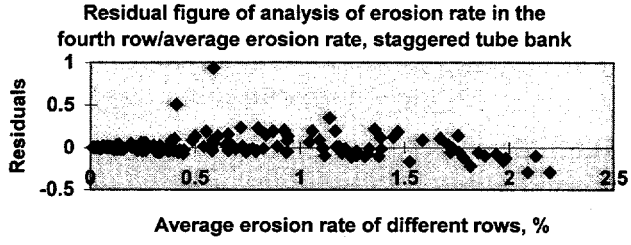
Residual figure of analysis of erosion rate in the fourth row/average erosion rate, staggered tube bank
Residuals
1
0.5
0
-0.5
0
0.5
1
1.5
2
2.5
Average erosion rate of different rows, %

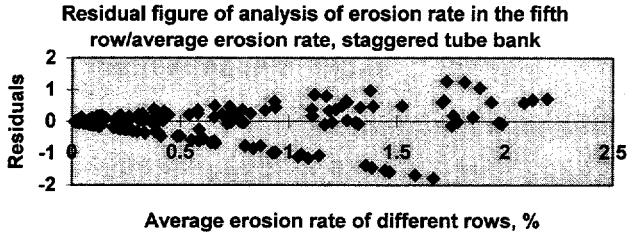
Residual figure of analysis of erosion rate in the fifth row/average erosion rate, staggered tube bank
Residuals
2
1
0
-1
-2
0
0.5
1
1.5
2
2.5
Average erosion rate of different rows, %

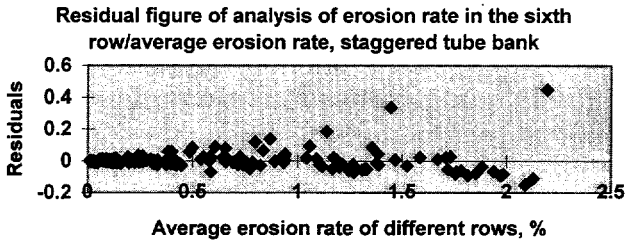
Residual figure of analysis of erosion rate in the sixth row/average erosion rate, staggered tube bank
Residuals
0.6
0.4
0.2
0
-0.2
0
0.5
1
1.5
2
2.5
Average erosion rate of different rows, %

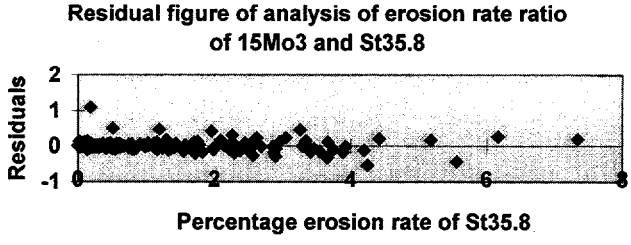
Residual figure of analysis of erosion rate ratio of 15Mo3 and St35.8
Residuals
2
1
0
-1
0
2
4
6
8
Percentage erosion rate of St35.8

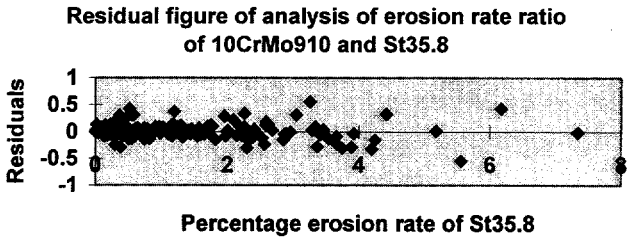
Residual figure of analysis of erosion rate ratio of 10CrMo910 and St35.8
Residuals
1
0.5
0
-0.5
-1
0
2
4
6
8
Percentage erosion rate of St35.8

Analyses of Chapter 6: Equation for three tube construction

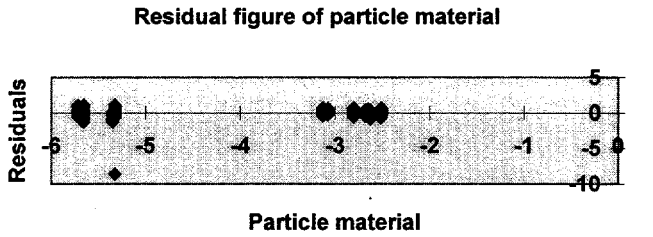

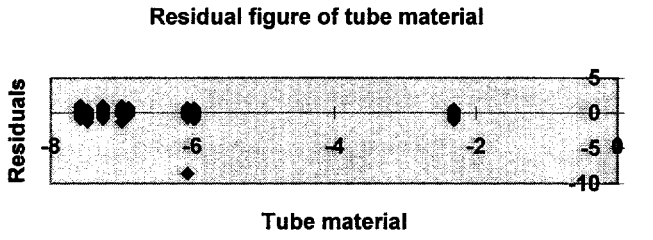

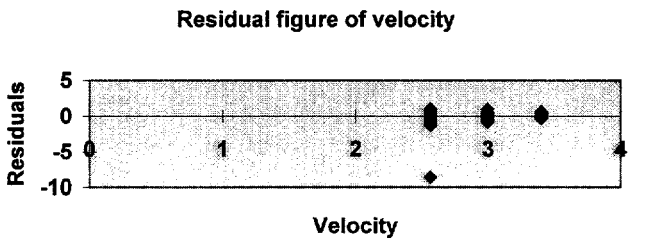

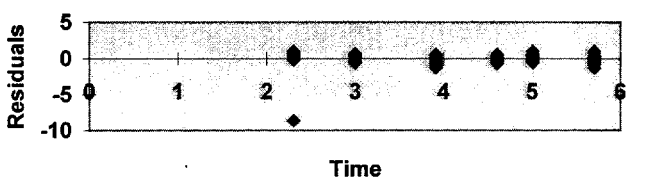

Equation for in-line tube bank

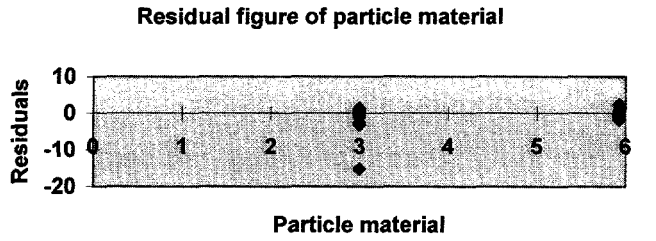

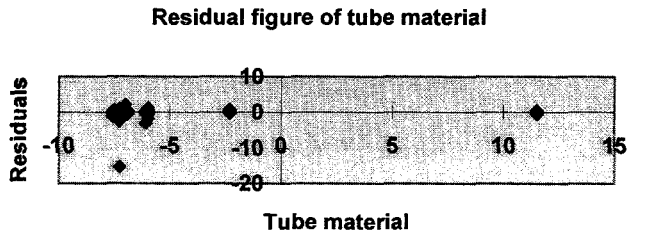

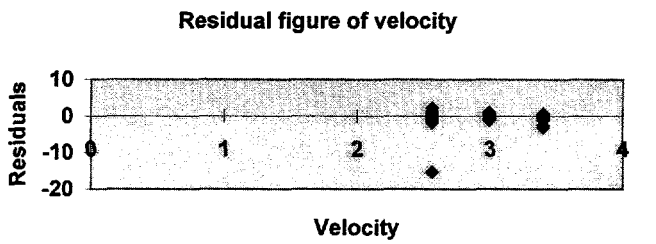

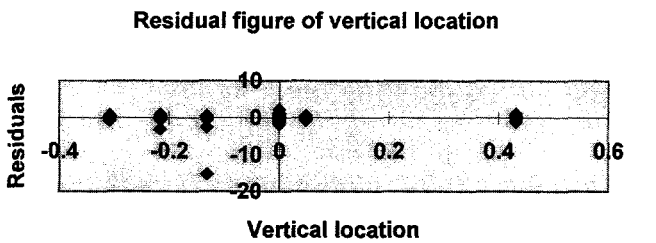

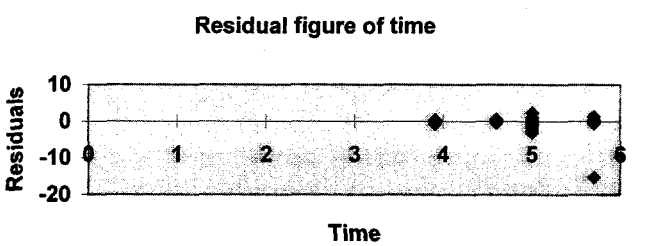

Equation for staggered tube bank

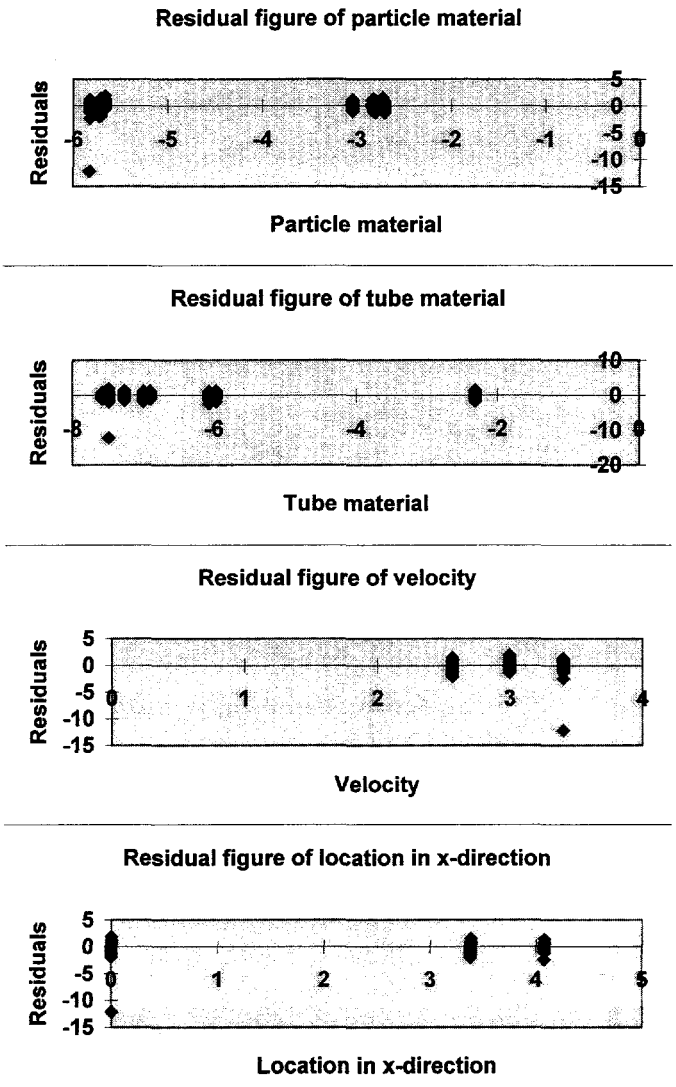

Residual figure of vertical location

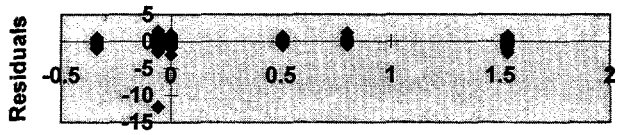

Vertical location

Residual figure of time

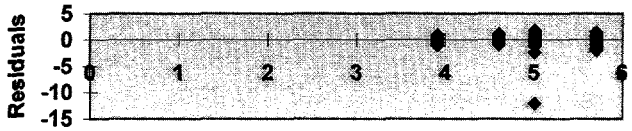

Time

APPENDIX C COEFFICIENTS OF DETERMINATION AND t-VALUES OF ANALYSES IN CHAPTER 5.9

Analyses in Table 5.7

Tube		0°	30°	60°	90°	120°	150°
		CoD/ t-value	CoD/ t-value	CoD/ t-value	CoD/ t-value	CoD/ t-value	CoD/ t-value
1	St35.8	0.89/19	0.95/29	0.94/27	0.98/44	0.98/40	0.93/24
	15Mo3	0.96/30	0.96/33	0.99/56	0.99/57	0.98/51	0.94/27
	10CrMo910	0.92/23	0.97/34	0.98/45	0.98/51	0.99/61	0.95/27
	All materials	0.92/40	0.96/54	0.97/64	0.98/86	0.98/80	0.94/44
2	St35.8		0.97/39	0.96/32	0.98/39	0.98/40	0.96/31
	15Mo3	0.94/26	0.99/62	0.98/51	0.99/67	0.995/87	0.96/35
	10CrMo910	0.89/19	0.97/38	0.98/40	0.94/27	0.96/30	0.90/20
	All materials	0.74/20	0.98/74	0.97/68	0.97/59	0.97/68	0.94/45
3	St35.8	0.74/12	0.84/16	0.91/21	0.88/20	0.93/24	0.92/22
	15Mo3	0.91/21	0.83/16	0.92/23	0.95/31	0.91/21	0.97/35
	10CrMo910	0.83/15	0.88/19	0.78/13	0.93/24	0.92/24	0.94/26
	All materials	0.82/26	0.85/30	0.86/29	0.92/41	0.91/37	0.94/46

Analyses in Table 5.8

Tube	0°	30°	60°	90°	120°	150°	180°
	CoD/ t-value	CoD/ t-value	CoD/ t-value	CoD/ t-value	CoD/ t-value	CoD/ t-value	CoD/ t-value
1	0.73/21	0.87/31	0.91/38	0.88/32	0.92/41	0.80/25	
2		0.89/33	0.91/37	0.89/34	0.92/40	0.84/28	
3			0.83/28	0.88/32	0.75/22	0.85/29	0.71/19

Analyses in Table 5.11

Tube	0°	30°	60°	90°	120°	150°	Row
	CoD/ t-value	CoD/ t-value	CoD/ t-value	CoD/ t-value	CoD/ t-value	CoD/ t-value	
1	0.77/15	0.95/31	0.96/38	0.94/30	0.97/39	0.91/24	1
2	0.93/29	0.92/26	0.97/42	0.95/32	0.97/40	0.97/42	
3	0.87/19	0.86/19	0.97/44	0.97/41	0.96/35	0.91/25	
4	0.95/32	0.94/30	0.89/22	0.71/12		0.85/17	2
5	0.97/44	0.94/30	0.80/16		0.83/16	0.93/26	
6	0.94/31	0.87/19			0.78/14	0.95/35	
7	0.93/27	0.95/33	0.91/24			0.90/23	3
8	0.96/37	0.97/43	0.87/21	0.79/14	0.74/13	0.97/39	
9	0.91/25	0.96/38	0.88/20			0.93/28	
10	0.85/18	0.95/31	0.94/30			0.79/15	4
11	0.92/26	0.96/35	0.90/24	0.74/13	0.79/15	0.83/17	
12	0.97/43	0.97/45	0.75/13			0.88/20	
13	0.95/33	0.94/30	0.89/22	0.76/13	0.78/14	0.91/23	5
14	0.94/30	0.87/20		0.70/12	0.73/12	0.91/24	
15	0.92/25	0.96/39			0.83/17	0.87/19	
16	0.89/22	0.89/21	0.81/16	0.88/20		0.86/19	6
17	0.84/17	0.89/22	0.85/18	0.89/20	0.83/16	0.85/18	
18	0.90/24	0.97/43	0.74/14		0.75/13	0.89/21	

Analyses in Table 5.12

Tube	0°	30°	60°	90°	120°	150°	180°	Row
	CoD/ t-value	CoD/ t-value	CoD/ t-value	CoD/ t-value	CoD/ t-value	CoD/ t-value	CoD/ t-value	
1		0.79/16	0.94/30	0.94/31	0.85/18	0.88/21		1
2		0.92/27	0.95/32	0.84/19	0.93/26	0.78/15	0.83/17	
3			0.87/22	0.84/20	0.93/27	0.79/17	0.78/14	
4	0.84/17	0.89/23				0.75/14		2
5	0.74/13	0.87/21			0.72/13	0.84/18	0.88/20	
6		0.72/12			0.83/17	0.87/22	0.74/13	
7	0.81/16	0.83/18				0.86/19	0.83/18	3
8	0.77/14	0.78/16	0.75/13		0.78/14	0.86/19		
9		0.91/25				0.88/22		
10		0.88/21				0.81/16	0.70/13	4
11	0.72/11	0.86/20	0.87/21	0.74/14		0.75/14	0.84/17	
12		0.90/24		0.71/11		0.83/18	0.71/13	
13	0.84/18	0.91/25	0.74/14			0.89/22	0.70/13	5
14	0.88/21	0.77/15		0.71/12		0.92/27		
15		0.90/24				0.83/18		
16		0.82/18		0.72/12		0.88/22		6
17		0.86/19	0.74/14			0.79/17	0.74/14	
18	0.71/14	0.92/29	0.70/12		0.71/12	0.70/14	0.71/13	

Analyses in Table 5.15

Tube	0°	30°	60°	90°	120°	150°	Row
	CoD/ t-value	CoD/ t-value	CoD/ t-value	CoD/ t-value	CoD/ t-value	CoD/ t-value	
1	0.82/17	0.90/24	0.92/25	0.90/25	0.96/36	0.90/22	1
2	0.83/17	0.95/33	0.95/35	0.95/33	0.97/43	0.97/39	
3	0.91/25	0.89/21	0.94/31	0.88/21	0.92/26	0.98/47	
4	0.88/20	0.72/13	0.90/24	0.97/48	0.85/20	0.76/14	2
5	0.81/16	0.72/13	0.91/24	0.95/36	0.93/30		
6	0.93/30	0.87/20	0.77/13	0.74/12	0.93/27	0.97/46	3
7	0.71/12	0.81/15	0.91/25	0.92/25	0.89/23	0.82/16	
8	0.82/17	0.92/26	0.89/22			0.79/14	
9	0.74/12	0.73/12	0.75/14	0.86/18	0.93/27	0.87/20	4
10			0.94/29	0.87/20	0.86/19		
11	0.80/16	0.77/14		0.77/13	0.92/27	0.98/52	5
12	0.77/13	0.73/12		0.70/11	0.80/14		
13		0.97/49	0.96/38	0.95/34	0.78/15		
14	0.72/12		0.82/15	0.72/13	0.72/12		6
15	0.78/14		0.88/20	0.78/14	0.90/21		

Analyses in Table 5.16

Tube	0°	30°	60°	90°	120°	150°	180°	Row
	CoD/ t-value	CoD/ t-value	CoD/ t-value	CoD/ t-value	CoD/ t-value	CoD/ t-value	CoD/ t-value	
1	0.78/14	0.87/21	0.89/24	0.87/20	0.93/28	0.71/13	0.75/13	1
2		0.87/19	0.79/16	0.92/26	0.87/20	0.82/16		
3			0.80/16	0.81/17	0.79/16	0.81/16		
4			0.94/33	0.94/32				2
5			0.89/22	0.92/30	0.74/17		0.75/14	
6	0.81/17		0.81/15	0.73/12	0.86/20	0.80/18		3
7		0.77/15	0.77/17	0.82/17	0.78/16			
8		0.87/22	0.80/17					
9				0.81/16	0.73/14			4
10		0.75/13	0.79/16		0.72/15			
11				0.70/12	0.87/21	0.96/43		5
12		0.70/11		0.81/15		0.70/11		
13		0.94/34	0.89/26					
14		0.77/14		0.78/15				6
15		0.74/12	0.73/13	0.71/13				

APPENDIX D STANDARD DEVIATIONS OF THE ANALYSES IN CHAPTER 6

	Three tube construction	In-line tube bank	Staggered tube bank
Std. dev. of the whole analysis	0.564	0.530	0.603
Constant	0.309	0.356	0.451
Particle material, ln(a)	0.0208	0.0126	0.0158
Tube material, ln(b)	0.0175	0.00303	0.0118
Velocity, ln(w)	0.0829	0.0569	0.0707
Location in x-direction, ln(c)			0.0121
Location in z-direction, ln(h)		0.0620	0.0316
Time, ln(t)	0.0334	0.0477	0.0601

LAPPEENRANNAN TEKNILLINEN KORKEAKOULU
LAPPEENRANTA UNIVERSITY OF TECHNOLOGY
TIETEELLISIÄ JULKAISUJA
RESEARCH PAPERS

17. Proceedings of the 4th Finnish Mechanics Days, June 5-6, 1991, Lappeenranta, Finland / ed. by Erkki Niemi. 1991. 388 s.

18. International Seminar of Horizontal Steam Generator Modelling March 11-13, 1991, Lappeenranta, Finland. 1991. 181 s.

19. Proceedings of the 3rd Conference on Laser Materials Processing in the Nordic Countries: NOLAMP-3 August 21-22, 1991 Lappeenranta, Finland / ed. by Tapani Moisio. 1991. 228 s.

20. SIERILÄ, PENTTI. Corporate planning, strategies, and critical factors in forest industries:methodology and contents. 1991. U.s. Diss.

21. LAATIKAINEN, MARKKU. Stability of aqueous emulsions of synthetic and extracted wood pitches. 1992. 28 s.

22. SUN, ZHENG. Laser beam welding of austenitic-ferritic dissimilar steel joints. 1992. 87 s. Diss.

23. KOIKKALAINEN, PASI. Neurocomputing systems: formal modeling and software implementation. 1992. 142 s. Diss.

24. PIRTTILÄ, TIMO. Empirical analyses of inventory intensity in the Finnish engineering industry. 1992. 118 s. Diss.

25. KOVANEN, M.A. Monte Carlo study of charged particle behaviour in Tokamak plasmas. 1992. U.s. Diss.

26. KALLAS, JUHA et al. Treatment technology of wastewater containing phenols and phenolic compounds. 1992. 40 s.

27. VAKKILAINEN, ESA K. Offdesign operation of kraft recovery boiler. 1992. 83 s. Diss.

28. LAMPINEN, JOUKO. Neural pattern recognition: distortion tolerance by self-organizing maps. 1992. U.s. Diss.

29. PUUMALAINEN, PERTTI. Paperin laadun ja siihen valmistusprosessissa vaikuttavien tekijöiden on-line mittaukset. 1993. 279 s. Väitösk.

30. Second International Seminar of Horizontal Steam Generator Modelling September 29 - 30, 1992, Lappeenranta, Finland. 1993. 195 s.

31. NYKÄNEN, TIMO. M_K-factor equations and crack growth simulations for fatigue or fillet-welded T-joints. 1993. 198 s. Diss.

32. KOSKINEN, JUKKA TAPIO. Use of population balances and particle size distribution analysis to study particulate processes affected by simultaneous mass and heat transfer and nonuniform flow conditions. 1993. U.s. Diss.

33. TUUNANEN, JARI. Thermal-hydraulic studies on the safety of VVER-440 type nuclear power plants. 1994. U.s. Diss.

34. ZHANG, ZHILIANG. A practical micro-mechanical model-based local approach methodology for the analysis of ductile fracture of welded T-joints. 1994. 151 s. Diss.

35. KÄLVIÄINEN, HEIKKI. Randomized Hough Transform: new extensions. 1994. U.s. Diss.

36. HEIKKONEN, JUKKA. Subsymbolic Representations, Self-Organizing Maps, and Object Motion Learning. 1994. 119 s. Diss.

37. KOSKINEN, JUKKA ANTERO. Knapsack sets for cryptography. 1994. 81 s. Diss.

38. TURUNEN, ESKO. A mathematical study of fuzzy logic; an algebraic approach. 1994. U.s. Diss.

39. JANHUNEN, ANTERO. Toimitustäsmällisyyden suunnittelumenetelmä. 1994. 161 s. Väitösk.

40. LARES-MANKKI, LAURA. Strategy implementation bottlenecks: identification, analysis and removal. 1994. 150 s. Diss.

41. French-Finnish Colloquium on Safety of French and Russian Type Nuclear Power Plants. 1994. 275 s.

42. KORPELA, JUKKA. An analytic approach to distribution logistics strategic management. 1994. U.s. Diss.

43. Third International Seminar on Horizontal Steam Generators October 18-20, 1994, Lappeenranta, Finland. 1995. 413 s.

44. AHOLA, JYRKI. Yrityksen strategiaprosessi: näkökohtia strategisen johtamisen kehittämiseksi konsernlorganisaatiossa. 1995. 235 s., liitt. Väitösk.

45. RANTANEN, HANNU. The effects of productivity on profitability: a case study at firm level using an activity-based costing approach. 1995. 169 s., liitt. Diss.

46. *Optics in Engineering: First Finnish-Japanese meeting Lappeenranta, 12-14th, June 1995 / ed.* by P. Silfsten. 1995. 102 s.

47. HAAPALEHTO, TIMO. Validation studies of thermal-hydraulic code for safety analysis of nuclear power plants. 1995. U.s. Diss.

48. KYLÄHEIKO, KALEVI. Coping with technology: a study on economic methodology and strategic management of technology. 1995. 263 s. Diss.

49. HYVÄRINEN, LIISA. Essays on innovativeness and its evaluation in small and medium-sized enterprises. 1995. U.s. Diss.

50. TOIVANEN, PEKKA. New distance transforms for gray-level image compression. 1996. U.s. Diss.

51. EHSANI, NEDA. A study on fractionation and ultrafiltration of proteins with characterized modified and unmodified membranes. 1996. U.s. Diss.

52. SOININEN, RAIMO. Fracture behaviour and assessment of design requirements against fracture in welded steel structures made of cold formed rectangular hollow sections. 1996. 238 s. Diss.

53. OJA, MARJA. Pressure filtration of mineral slurries: modelling and particle shape characterization. 1996. 148 s. Diss.

54. MARTTILA, ESA. Ilmanvaihdon lämmönsiirtimien teknillinen ja taloudellinen mitoitus. 1996. 57 s. Väitösk.

55. TALONPOIKA, TIMO. Dynamic model of small once-through boiler. 1996. 86 s. Diss.

56. BACKMAN, JARI. On the reversed Brayton cycle with high speed machinery. 1996. 103 s. Diss.

57. ILME, JARNO. Estimating plate efficiencies in simulation of industrial scale distillation columns. 1997. U.s. Diss.

58. NUORTILA-JOKINEN, JUTTA. Choice of optimal membrane processes for economical treatment of paper machine clear filtrate. 1997. U.s. Diss.

59. KUHMONEN, MIKA. The effect of operational disturbances on reliability and operation time distribution of NC-machine tools in FMS. 1997. 133 s., liitt. Diss.

60. HALME, JARKKO. Utilization of genetic algorithm in online tuning of fluid power servos. 1997. 91 s. Diss.

61. MIKKOLA, AKI. Studies on fatigue damage in a hydraulically driven boom system using virtual prototype simulations. 1997. 80 s., liitt. Diss.

63. PIRTTILÄ, ANNELI. Competitor information and competitive knowledge management in a large, industrial organization. 1997. 175 s., liitt. Diss.

LAPPEENRANNAN TEKNILLINEN KORKEAKOULU
MONISTAMO 1997

ISBN 951-764-181-8
ISSN 0356-8210